UNIVERSITY OF CALIFORNIA SAN DIEGO

Engineering efficient and safe *in situ* genome regulation via CRISPR-Cas9 for enabling gene therapies

A dissertation submitted in partial satisfaction of the
requirements for the degree
Doctor of Philosophy

in

Bioengineering

by

Ana María Moreno

Committee in charge:

Professor Prashant Mali, Chair
Professor Pedro Cabrales
Professor Theodore Friedmann
Professor Bruce Hamilton
Professor Yingxiao Wang

2019

The dissertation of Ana María Moreno is approved, and it is acceptable in quality and form for publication on microfilm and electronically:

_____

_____

_____

_____

_____

Chair

University of California San Diego

2019

DEDICATION

Para mis padres, gracias por su apoyo y amor incondicional. Gracias por su dedicación y esfuerzo. Nunca hubiera llegado aquí sin ustedes.

Para mi hermano, gracias por ser un buen ejemplo y siempre estar cerca de mi.

Para mi pareja, por creer en mi y apoyarme en esta nueva etapa que formaremos juntos.

Los amo.

EPIGRAPH

The worst pain a man can suffer:
to have insight into much and power over nothing.
— Herodotus, 5th century BC

TABLE OF CONTENTS

LIST OF FIGURES

LIST OF TABLES

ACKNOWLEDGEMENTS

My PhD journey at UCSD has been an exciting and challenging one, and I have been very blessed to have the support, mentorship, guidance, and generosity of many individuals in this journey. I would like to thank my committee for providing feedback and guidance throughout my PhD. I would also like to acknowledge two fellowships that have supported me during my graduate career—CONACYT and UC Mexus—which allowed me to pursue my dream of obtaining a PhD.

I owe most of my gratitude to my thesis advisor, Dr. Prashant Mali. Thank you for giving me the opportunity to be a part of your research group, for your care, direction, intellect, open mind, and for leading by your example of hard work and scientific rigor. I really enjoyed sharing novel scientific discoveries with you. The Mali Lab would not be the fun, close-knit, and caring group it is without you. Thank you to all the Mali Lab members: Dongxin, Udit, Dhruva, Jasmine, Jessica, Marianna, Hugh, Andrew, Nathan, Amir, Daniella, Michael, and all others for your friendship, emotional support, coffee breaks, conversations in the TC room, positive vibes, and for making my PhD experience a very fun one.

Thank you to my Master's cohort, in particular my dear friends, Sara, Jahir, Shawn, and Harsha. The long-nights studying in the Biomedical Library, Jahir playing the guitar while the rest of us sang, Shawn's salsa dancing, the delicious and heartwarming food from Sara's kitchen, and Harsha's jokes and positive attitude will forever be amazing memories. Thank you for being my family in San Diego and for your friendship. Graduate school would not have been the same without you guys.

I would also like to thank various members of the Bioengineering Department, in particular Dr. Shankar Subramaniam and Dr. Marcos Intaglietta for your support in my transition

from M.S. to PhD. Thank you Jan Lenington for supporting and caring for all the PhD students. Thank you Richard Szubin for always bringing a smile to my face and for your amazing experimental advise. Thank you Haythem Latif for training me and for your patience during my M.S. Thank you Gaby Guzman and for Liz Brunk for being my inspiration as strong female scientists and mothers, I admire you both. Thank you Jose Utrilla for career and advise on dealing with difficult situations. Thank you Kathia Zaleta Rivera for listening and sharing.

I would also like to thank members of UCSD and the Rady School of Business that have mentored and supported me in my path as an entrepreneur. First, I would like to thank Prashant again for believing in me and for your support on our journey of bringing non-opioid solutions to patients with chronic pain. Thank you Vish Krishnan and Ricardo Santos for teaching me business concepts. Thank you Randy Woods for advice in fundraising. I would also like to thank the strong female business mentors that I have had the pleasure of working with: Kim Davis King, Lada Rasochova, Karen Jensen, and Dr. Silvia Mah, thank you for your advice and for dedicating your time to helping female entrepreneurs.

Most importantly, I would like to thank my family: my parents, Francisco Javier and Maria del Carmen, and my amazing brother Eduardo. Without their love and support, I would have never accomplished what I have today. I would also like to thank my cousin (almost sister) Ilse María, and my friend, Alba, for years of friendship and for always being there to celebrate my successes and for lending an ear throughout my failures. I would also like to thank my high school English teacher, Ms. Leggett, for her dedication and continued friendship throughout the years.

Chapter 1 in part is a reprint of the material *Moreno AM, Mali P. Therapeutic Genome Engineering via CRISPR-Cas systems. WIREs Systems Biology and Medicine (2017) 9:e1380.* The dissertation author was the primary author.

Chapter 2 in part is a reprint of the material *Moreno AM, Fu X, Zhu J, Katrekar K, Shih YV, Marlett J, Cabotaje J, Tat J, Naughton J, Lisowski L, Varghese S, Zhang K[#], Mali P[#]. In situ gene therapy via AAV CRISPR-Cas9 mediated targeted gene regulation. Molecular Therapy (2018) 26:1818-1827*. The dissertation author was the primary author.

Chapter 3 in part is from a reprint of the material *Moreno AM[*], Palmer N[*], Aleman F, Chen G, Pla A, Jiang N, Chew WL, Law M, Mali P. Exploring protein orthogonality in immune space: a case study with AAV and Cas9 orthologs. Nature Biomedical Engineering (2019) in press.* The dissertation author was one of the two primary authors.

Chapter 4 in part is from a manuscript that is being prepared for publication *Moreno AM, Mali P. In situ repression of a sodium channel via CRISPR-dCas9 and Zinc-Fingers leads to pain-amelioration.* The dissertation author is the primary author.

VITA

2011	B.S. in Biosystems Engineering, University of Arizona
2011	B.A. in French Literature, University of Arizona
2014	M.S. in Bioengineering, University of California San Diego
2019	Ph.D. in Bioengineering, University of California San Diego

PUBLICATIONS

1. **Moreno AM**, Mali P. *In situ* repression of a sodium channel via CRISPR-dCas9 and Zinc-Fingers leads to pain-amelioration. *In preparation.*

2. **Moreno AM**[*], Palmer N[*], Aleman F, Chen G, Pla A, Jiang N, Chew WL, Law M, Mali P. Exploring protein orthogonality in immune space: a case study with AAV and Cas9 orthologs. Nature Biomedical Engineering (2019) *in press.*

3. **Moreno AM**, Fu X, Zhu J, Katrekar K, Shih YV, Marlett J, Cabotaje J, Tat J, Naughton J, Lisowski L, Varghese S, Zhang K[#], Mali P[#]. *In situ* gene therapy via AAV CRISPR-Cas9 mediated targeted gene regulation. Molecular Therapy (2018) 26:1818-1827.

4. Katrekar D, **Moreno AM**, Chen G, Worlikar A, Mali P, Oligonucleotide conjugated multi-functional adeno-associated viruses. Scientific Reports (2018) 8:3359.

5. **Moreno AM**, Mali P. Therapeutic Genome Engineering via CRISPR-Cas systems. WIREs Systems Biology Medicine (2017) 9:e1380.

CONFERENCE PRESENTATIONS

Moreno AM[*], Palmer N[*], *et al*. (2018) Exploring protein orthogonality in immune space: a case study with AAV and Cas9 orthologs. ASGCT 21st annual meeting, Chicago, Illinois. Poster.

Moreno AM. (2017) Versatile Genome Engineering via CRISPR-Cas Systems. Peptalk, San Diego, California. Oral.

PATENTS

1. Mali P, **Moreno AM**, Palmer N. Engineering CRISPR/Cas9 Immune Stealth. (2018) *WO 2018170015*.
2. Mali P, Katrekar D, **Moreno AM**. CRISPR-Cas genome engineering via modular AAV delivery system. (2018) *WO 2018035503*.

ABSTRACT OF THE DISSERTATION

Engineering efficient and safe *in situ* genome regulation via CRISPR-Cas9 for enabling gene therapies

by

Ana María Moreno

Doctor of Philosophy in Bioengineering

University of California San Diego, 2019

Professor Prashant Mali, Chair

While the genetic and pathogenic basis of human diseases continues to grow, translation is currently bottlenecked by lack of tools and technologies to administer and evaluate corresponding gene-based therapeutics. Consequently, development of safe and efficient *in vivo* gene transfer platforms, coupled with emerging genome and epigenome engineering tools, will transform our ability to target a range of human diseases. In this regard, the holy grail of *in vivo* genome engineering is the ability to achieve the trifecta of: 1) efficient and safe delivery; 2) temporally regulatable and tunable payload delivery; and 3) immune stealth to minimize dosage

& enable re-administration of nucleic acid or protein therapeutics. Towards this, the objective of this dissertation was to develop a platform to enable efficacious *in vivo* genome and epigenome engineering with a focus on enabling *in situ* therapeutic efficacy. The studies in this dissertation are independent bodies of work that explore the optimization and engineering of CRISPR-Cas9 systems to bring these one step closer to their eventual translation into the clinic.

Towards these, I first developed a robust and generalizable platform for *in situ* genome editing and regulation via AAV CRISPR-Cas9. Towards this, I utilized split-Cas9 systems to develop a modular adeno-associated viral (AAV) vector platform for CRISPR-Cas9 delivery to enable the full spectrum of targeted *in situ* gene regulation functionalities, demonstrating robust transcriptional repression (up to 80%) and activation (up to 6-fold) of target genes in cell culture and mice. We also applied our platform for targeted *in vivo* gene-repression-mediated gene therapy for retinitis pigmentosa. Specifically, we engineered targeted repression of Nrl, a master regulator of rod photoreceptor determination, and demonstrated Nrl knockdown mediates *in situ* reprogramming of rod cells into cone-like cells that are resistant to retinitis pigmentosa-specific mutations, with concomitant prevention of secondary cone loss. Furthermore, we benchmarked our results from Nrl knockdown with those from *in vivo* Nrl knockout via gene editing. Taken together, our AAV-CRISPR-Cas9 platform for *in vivo* epigenome engineering enables a robust approach to target disease in a genomically scarless and potentially reversible manner. Additionally, this is the first time that the utility of AAV-KRAB-dCas9 mediated *in situ* gene repression in the context of gene therapy was demonstrated (*Moreno et al., WIREs Systems Biology and Medicine, 2017; Moreno et al., Molecular Therapy, 2018).*

Next, I focused on addressing, arguably the most important hurdle for CRISPR-Cas based gene therapies, which is the interaction of these non-host derived systems with the adaptive

immune system which can lead to neutralization by circulating antibodies and clearance of treated cells by cytotoxic T-lymphocytes. To address this issue, I proposed a new approach: sequential use of orthologous proteins that are orthogonal in immune space. This would, in principle, allow for repeated treatments by thus chosen orthologs without reduced efficacy due to lack of immune cross-reactivity among the proteins. To explore and validate this concept we chose 284 DNA targeting and 84 RNA targeting CRISPR effectors (including Cas9, Cpf1/Cas12a, and Cas13a, b, and c), and 167 Adeno-associated virus (AAV) capsid protein orthologs and developed a pipeline to compare total sequence similarity as well as predicted binding to class I and class II Major Histocompatibility Complex (MHC) proteins. Our MHC binding predictions revealed wide diversity among the set of DNA-targeting Cas orthologs, with 79% of pairs predicted not to elicit cross-reacting immune responses, while no global immune orthogonality among AAV serotypes was observed. We validated the computationally predicted immune orthogonality among three important Cas9 orthologs, from *S. pyogenes*, *S. aureus*, and *C. jejuni* observing cross-reacting antibodies against AAV but not Cas9 orthologs in sera from immunized mice. Finally, to demonstrate the efficacy of multiple dosing with immune orthogonal orthologs, we delivered AAV-Cas9 targeting PCSK9 into BALB/c mice previously immunized against the AAV vector and/or the Cas9 payload, demonstrating that editing efficiency is compromised by immune recognition of either the AAV or Cas9, but, importantly, this effect is abrogated when using immune orthogonal orthologs. Moving forward, we anticipate this framework can be applied to prescribe sequential transient regimens of immune orthogonal protein therapeutics to circumvent pre-existing or induced immunity, and eventually, to rationally engineer immune orthogonality among protein orthologs. (*Moreno, Palmer et al., Nature Biomedical Engineering, in press, 2019).*

Lastly, I then proceeded to integrate the advances accomplished in the previous chapters to enable pain management via *in situ* genome repression. In the US and worldwide, pain is a leading cause of disability, which leads to a diminished quality of life. Patients have come to routinely expect pharmacological management, with the prevalent aggressive approach for managing pain states being based on opiates. While the utility of opiates has made them a mainstay of pain management, there are at least four key reasons supporting the need for new and alternative pain therapeutics: limited efficacy, abuse potential, tolerance after continued exposure, and an enhancement of post-wound pain states. Despite decades of research, broad-acting, longer-lived, non-addictive, and effective drugs for chronic pain remain elusive. Notably, genetic studies have correlated a hereditary loss-of-function mutation in a human Na+ channel isoform – $Na_V1.7$ – with a rare genetic disorder, Congenital Insensitivity to Pain (CIP), which leads to insensitivity to pain without other neurodevelopmental alterations. While an excellent target, the creation of blockers for this site has not led yet to an efficient and safe drug, due to their lack of specificity, leading to unwanted side-effects. Taking advantage of this druggable target in the human genome, the aim of this work was to develop a novel therapeutic regiment via *in situ* $Na_V1.7$ repression to regulate the development and maintenance of impending chronic pain states. In this regard, I demonstrated robust *in vitro* repression using two epigenome engineering tools (KRAB-CRISPR-Cas9 and KRAB-Zinc-Fingers) with ~71% and ~88% repression respectively. To enable pain management, I injected mice intrathecally using the constructs with the highest *in vitro* efficacy and demonstrated robust $Na_V1.7$ repression with a significant improvement in pain response in a carrageenan inflammatory pain model. I demonstrated a 133% improvement in paw withdrawal latency as compared to a negative control (mCherry) and 62% improvement over the positive control (Gabapentin, 100 mg/kg). Taken

together, the use of these *in situ* engineering approaches could thus represent a viable replacement for opioids and a potential therapeutic approach that is tunable and reversible (*Moreno et al., in preparation*).

Together, the advances in these bodies of work, which demonstrate efficacious *in vivo* delivery and gene editing/regulation is a significant step toward their implementation for gene therapeutic applications.

Chapter 1 – Therapeutic genome engineering via CRISPR-Cas systems

1.1 Introduction

Gene therapy entails altering, replacing, or regulating the expression of affected genes to a degree that reverses a diseased phenotypic state. In principle, therapeutic interventions can be effected at two levels: *in vivo* or *ex vivo*. *In vivo* gene therapy involves local or systemic administration of a therapeutic vector, while *ex vivo* approaches involve isolating cells from the human body, such as CD34+ hematopoietic stem cells, application of gene therapy on the isolated cells, followed by re-transplantation of these cells back into the body (Figure 1.1). In this chapter, we review gene therapy in conjunction with gene transfer platforms that encompass both *in vivo* and *ex vivo* targeting modalities, with a focus on therapeutic interventions that directly perturb the genome of host cells.

In this regard, fundamental to enabling gene therapeutics are genome engineering tools that enable the ability to precisely edit or tune the regulation of genomic elements of interest. For instance, for targeted genome editing one harnesses programmable double-stranded breaks to effect precise edits in the genome. Creation of double-stranded breaks (DSBs) can be resolved by the cell via one of two processes: homologous recombination (HR) or nonhomologous end-joining (NHEJ).

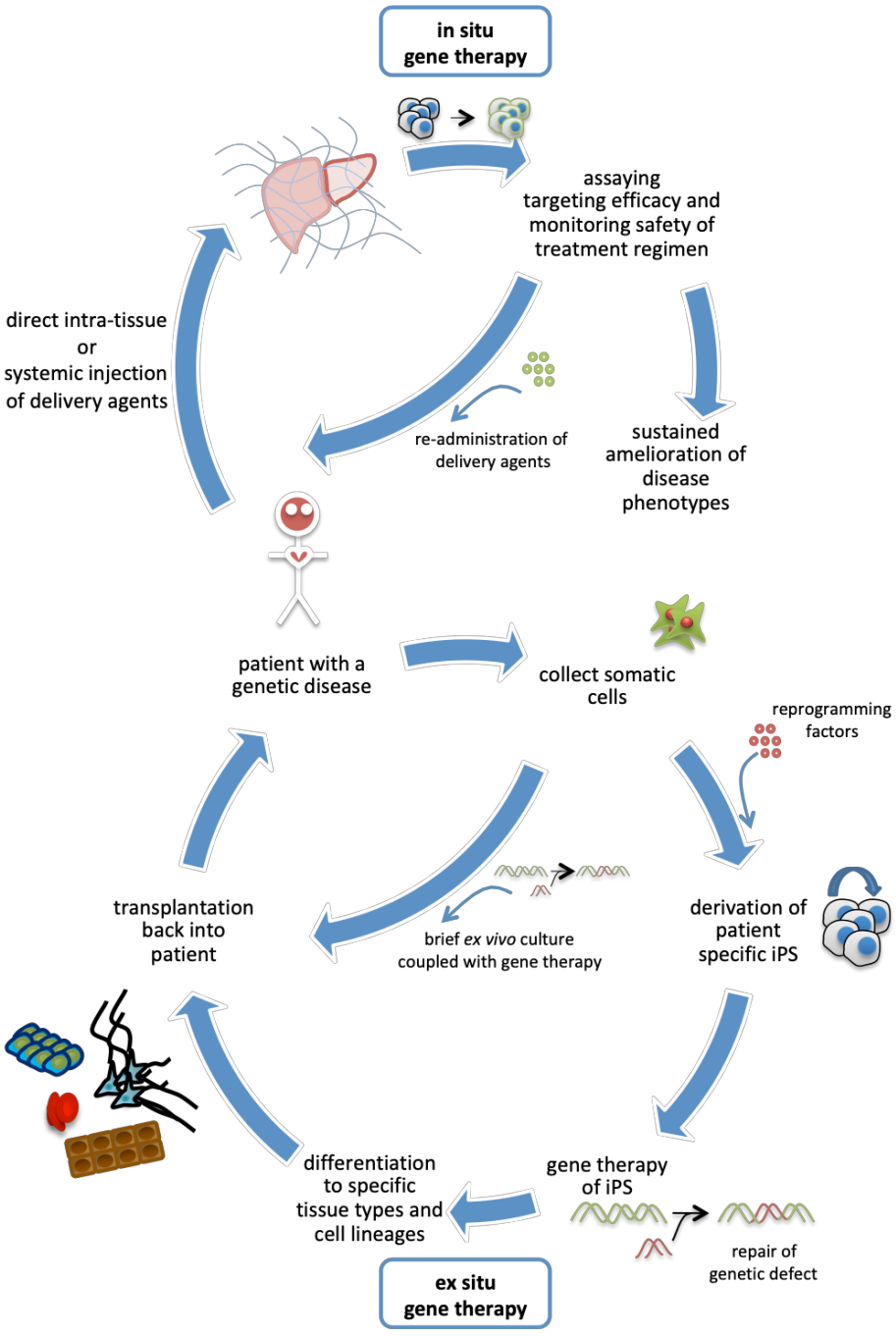

Figure 1.1: Schematic of *in vivo* and *ex vivo* gene therapy modalities. *In vivo* gene therapy involves the direct intra-tissue or systemic injection of delivery agents, followed by assaying of targeting efficacy with close monitoring of safety and efficacy of treatment. In this regard, re-administration of delivery agents might be necessary to achieve therapeutic efficacy. A patient might also be treated via *ex vivo* gene therapy, where patient somatic cells are isolated and either (1) reprogrammed into patient-specific iPSCs, followed by gene therapy of these cells, and which are then differentiated into specific tissue types and cell lineages for transplantation; or (2) edited via *ex vivo* culture coupled with gene therapy (for instance in HSCs).

Whether a cell repairs the break through HR or NHEJ depends on several aspects, including the cell's cycle phase and whether a homologous donor is present or not. Specifically, one can effect HR by providing a synthetic homologous donor to introduce a desired sequence of DNA or to create specific point-mutations [1]. The alternative route for DSB repair is via NHEJ, which unlike HR is active throughout the cell cycle. In NHEJ, an indel (insertion or deletion) or substitution is created. Importantly, if this occurs in a coding exon, the translational reading frame of a gene can be disrupted, which can lead in turn to an inactive or truncated protein [2].

Early genome engineering methods were based on programmable nucleases, such as zinc finger nucleases (ZFNs) and subsequently transcription activator-like effector nucleases (TALENs). ZFNs are comprised of zinc finger proteins (ZFPs), which are DNA binding domains frequently found in eukaryotic transcription factors [3], that are fused to a DNA cleavage domain (typically FokI). The ZFP region of ZFNs typically contains Cys2-His2 fingers, which predominantly interact with nucleotide triplets, and combinations of ZFPs can thus be arranged to recognize a wide range of DNA sequences [4]. ZFNs induce DSBs in a targeted fashion via the DNA-cleavage domains tethered to this engineered sequence. An important advantage of utilizing ZFNs is their specific targeting, which is due to two independent binding events that must occur in order for FokI to dimerize before cleaving DNA [5]. On the other hand, ZFNs are difficult to engineer, requiring a high level of technical expertise [4].

TALENs utilize proteins derived from transcription activator like effector (TALE) repeat domains from bacteria, such as Xanthomonas, which are comprised of highly conserved amino acid repeat domains of 33–35 residues in length, each targeting a single nucleotide, fused in turn to a FokI nuclease [6]. TALENs are easier to engineer than ZFNs and have been observed to similarly induce high efficiency genome editing with limited cytotoxicity [7]. TALENs relative to ZFNs are however significantly larger in size, and also have repetitive sequences which complicates their

construction and incorporation into delivery systems [8]. Furthermore, they have a prokaryotic origin and can potentially elicit a negative immune response. Taken together, ZFNs and TALENs are robust genome engineering systems, but have certain drawbacks such as difficult programmability and/or limited multiplex genome targeting capabilities. A more detailed review on these platforms can be found in Ref 8.

More recently, the emergence of CRISPR-Cas systems has dramatically transformed our ability to target nucleic acids. In comparison to ZFNs and TALENS, CRISPR-Cas systems depend on simple Watson-Crick base-pairing between a RNA guide and a corresponding DNA target site making them remarkably simple to re-engineer. In addition, CRISPR-Cas systems can be utilized for multiplex targeting, which is especially useful when creating disease models or targeting complex diseases in which multiple loci are affected. Their ease of use, coupled with low cost, high efficiency, and broad versatility has resulted in the CRISPR-Cas systems rapidly becoming the genome engineering method of choice. In this chapter, we will focus on this system and provide a brief overview of CRISPR-Cas technologies for genome editing and regulation (Figure 1.2), and also outline the latest advances in CRISPR-Cas mediated *ex vivo* and *in vivo* genome manipulations. We will discuss appropriate delivery approaches for these, and also delineate the current challenges of existing platforms and outline potential applications and areas of further research and development.

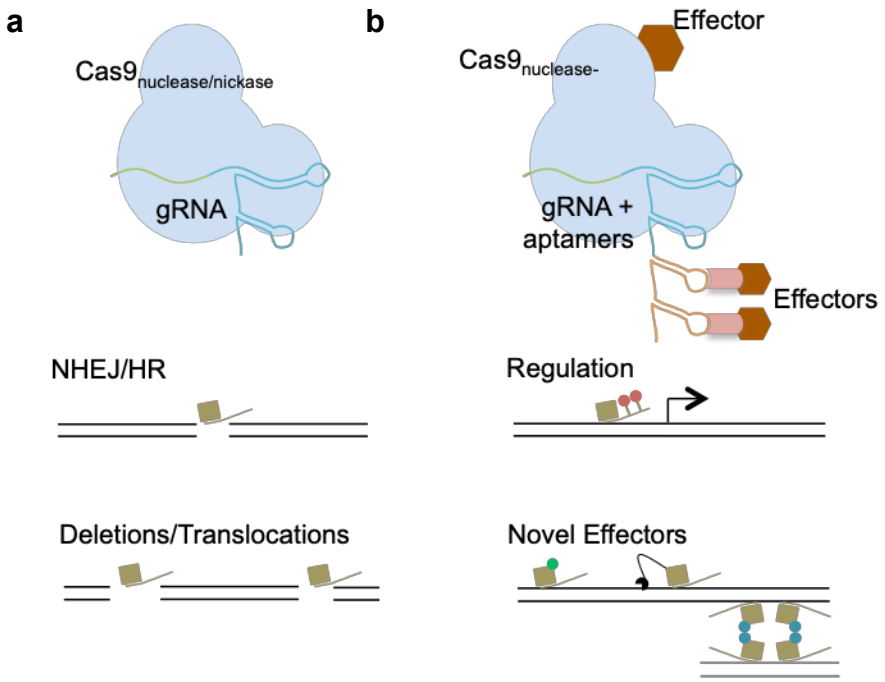

Figure 1.2: The CRISPR-Cas9 genome-engineering toolset. (a) Wild-type Cas9 induces double-stranded DNA breaks, which the cell repairs through either nonhomologous end-joining (NHEJ) or homologous recombination (HR) pathways. A mutated version of Cas9, 'nickase' Cas9, nCas9, is created by mutating one of the two catalytic sites, typically the RuvC domain, which results in engineering of only single stranded breaks. Modifications by Cas9 and nCas9 can used to also engineer genomic deletions or translocations. (b) One can also utilize dead-Cas9, dCas9, with both of its catalytic sites mutated, RuvC and HNH. dCas9 can in turn be tethered to effectors, such as activation or repression domains, to induce targeted genome regulation. In addition, other novel effectors can be utilized, such as fusion to the cytidine-deaminase enzyme for targeted 'base editing' [9].

1.2 CRISPR-Cas9 systems

CRISPR-Cas systems have evolved as adaptive immune defense systems in bacteria and archaea. These systems function in three phases: adaptation, expression, and interference, and typically utilize short RNA to direct degradation of foreign nucleic acids. During adaptation, short pieces of foreign DNA are acquired and integrated as 'spacer' elements into the CRISPR loci. During expression and interference, the CRISPR locus, which consists of acquired 'spacers' separated by repeat regions, is transcribed, which yields a pre-crRNA, which in turn is processed to

generate crRNAs that guide effector nuclease complexes (cas proteins) to disrupt sequences that are homologous to the spacer [10-12]. In type II Cas9 systems, such as that of *Streptococcus pyogenes* Cas9 (SpCas9), pre-crRNAs are processed with the help of a trans-activating crRNA (tracrRNAs), to create a tracrRNA:crRNA:Cas9 complex that induces double-stranded breaks [13]. Notably the tracrRNA and crRNA can be fused to create a single guide RNA (gRNA). This consists of two functional regions: a variable spacer region which guides target loci recognition, and a constant scaffold region which forms hairpin loops to facilitate binding to the Cas9. The variable spacer region is typically a short ~20 bp sequence that is complementary to the target loci, and must be flanked at the 30 end by a conserved protospacer adjacent motif (PAM) sequence, for instance, NGG in SpCas9 [14]. The PAM sequence is necessary for CRISPR-Cas targeting and also crucial for self vs. nonself discrimination [15]. By delivering crRNAs in addition to the Cas9-like effectors, one can thus readily enable programmable genome engineering [16]. Indeed the CRISPR-Cas9 system has now been shown to work in a range of eukaryotic systems [16-18], and has also greatly facilitated our ability to engineer genomes in diverse cell types and organisms (Table 1.1). Some organisms that have been targeted *in vivo* include mice, rats [19], rabbits [20], and also nonhuman primates [21].

Table 1.1: Representative Table of *In vivo* and *Ex Vivo* CRISPR-Cas9 Studies, via a Range of Viral and Nonviral Delivery Methods.

Genes/Disease	Delivery System	Ortholog	Organism	Tissue Type	Ref. Num.
Tet1, Tet2	Injected Embryos	SpCas9	Mice	-	69
P53, Pten	Hydrodynamic injection	SpCas9	Mice	Liver	44
Fah/Tyrosinemia Type I	Hydrodynamic injection	SpCas9	Mice	Liver	22

Table 1.1: Representative Table of *In vivo* and *Ex Vivo* CRISPR-Cas9 Studies, via a Range of Viral and Nonviral Delivery Methods (continued).

Genes/Disease	Delivery System	Ortholog	Organism	Tissue Type	Ref. Num.
Pcsk9	Adenovirus	SpCas9	Mice	Liver	70
NeuN	AAV1/2	SpCas9	Mice	Brain	71
DMD (Duchenne Muscular Dystrophy)	Injected Zygotes	SpCas9	Mice	Muscular Skeletal Tissue	72
X-linked androgen receptor	Injected Embryos	SpCas9 nickase	Mice	-	73
Pten, NKx2-1	Lentiviruses	SpCas9	Mice	Lung	74
Kras, p53, Lkb1	AAV9	SpCas9	Mice	Lung	71
Pcsk9, ApoB	AAV9	SaCas9	Mice	Liver	75
MeCP2/Rett syndrome, Dnmt3a, Dnmt1, Dnmt3b	AAV 1/2	SpCas9	Mice	Brain	76
Pcsk9, ApoB	AAV9	SaCas9	Mice	Liver	28
Apc, Trp53	Hydrodynamic injections	inducible SpCas9	Mice	Intestine/ Thymus	77
Eomes	in utero Electroporation	SpCas9	Mice	Brain	78
DMD	AAV9	SaCas9	Mice	Muscular Skeletal Tissue	79
DMD	AAV8	SaCas9	Mice	Skeletal and Cardiac Muscle	80
DMD	AAV9	SpCas9	Mice	Skeletal and Cardiac Muscle	81
OTC	AAV8	SaCas9	Mice	Liver	31
EGFP	Cationic Liposomes	SpCas9	Mice (Atoh1-GFP)	Ear	82
Ptch1; Trp53, Pten, Nf1	Cationic Polymer	SpCas9	Mice	Brain	83
B2M and CCR5	Electroporation	SpCas9	CD34+ HSCs and CD4+ T cells	HSCs transplanted into NSG mice	84

Notably, one can also engineer nuclease-dead versions of Cas9 (dCas9) via point mutations in the endonuclease domains, HNH and RuvC. This engineered protein retains RNA-guided DNA binding activity but lacks endonuclease activity [42,43]. dCas9 coexpressed with a gRNA can be utilized for gene repression as it interferes with transcriptional elongation, RNA polymerase binding, or transcription factor binding [44]. Additionally, dCas9 can also be fused to effector domains and be programmed to enable diverse genome engineering functionalities such as gene repression (via KRAB fusions [43]), or gene activation, (such as via fusions of VP64, Rta, and P65 or combinations thereof) [45], and furthermore for targeted chromatin modulation by acetylation or methylation via fusions of methyltransferase (DNMT3A) and acetyltransferase (p300) [46,47]. Another strategy is to fuse dCas9 to a multimeric tag such as 'Suntag,' which comprises of a repeating peptide array which can in turn recruit multiple copies of effector domains [48]. A primary drawback of utilizing dCas9 for permanent gene activation or repression is that it needs to be continuously expressed, whereas nuclease-Cas9 can enable irreversible changes in the genome, even with limited expression. Because of this, a patient would necessitate repeat treatments of dCas9. However, an advantage to utilizing dCas9 for genome activation over traditional methods is that one can activate/repress genes in a multiplexed manner, which could be beneficial for complex diseases that have multiple loci involved, or one could target genes that are otherwise difficult to edit. Additionally, since dCas9 lacks endonuclease activity, there is no permanent change to the genome [49] and thus off-target effects can also be avoided by using this system.

The CRISPR-Cas toolset has also been rapidly expanding with characterization of several new Cas9-like proteins. For instance, recently a class 2 type V CRISPR-Cas system, Cpf1, (CRISPR from *Prevotella* and *Francisella* 1), has been shown to effect robust *in vitro* genome editing in human cells [50]. Some differences between Cpf1 and other Cas9 proteins is that it does not require an additional trans-activating crRNA (tracrRNA) [51], and that it creates a 4–5 nt

staggered dsDNA break distal to its Trich PAM, which could thus expand the range of potential targetable genomic sites. A recent paper compared the specificity and efficiency of Cpf1 with Cas9. They first tested four Cpf1 orthologs, and found *Acidaminococcus sp. BV3L6* (AsCpf1) and *Lachnospiraceae bacterium N D2006* (LbCpf1) to be the most efficient. They then went on to compare the frequency of targeted mutations by LbCPf1, AsCpf1, and SpCas9 at ten chromosomal target sites, each containing two PAM sequences, one recognized by Cpf1 (50-TTTN-30) and the other recognized by SpCas9 (50-NGG-30). They discovered that Cpf1 is a less efficient endonuclease than SpCas9 in some human cell lines, but is highly specific [52]. Notably, mutant mice have also been generated by injecting crRNAs with Cpf1 (AsCpf1 and/or LbCpf1) mRNA into fertilized eggs and do not exhibit overt off-target effects [53].

1.3 Delivery Approaches

To realize the versatility of CRISPR-Cas systems in genome engineering applications, appropriate delivery systems for the same will be critical. In fact, a key technological barrier to gene-based therapies has been the development of efficient and safe delivery systems. Towards this, both viral and nonviral methods have been utilized, with most vectors utilized in gene therapy clinical trials being engineered viruses, and below we discuss these technologies in the context of delivery of CRISPR-Cas for gene therapy (Table 1.2).

Table 1.2: Methods of Gene Therapy Delivery.

Mode of Delivery	Duration of Expression	Risk of genomic Integration	Immunogenicity[#]
Retro-viruses	Long term	Yes (observed oncogenecity)	Low
Lenti-viruses	Long term	Yes (low oncogenecity)	Low
Adenoviruses	Medium term	Low	High

Table 1.2: Methods of Gene Therapy Delivery (continued).

Mode of Delivery	Duration of Expression	Risk of genomic Integration	Immunogenicity[#]
Adeno-associated viruses	Medium term	Low	Low
Mini-circle Plasmids	Short term	Low	Low
Conventional Plasmids	Transient	Low	Low
Proteins	Transient	No	Under evaluation
RNA	Transient	No	Low
Nanoparticles/biomaterials	Transient	Low	Under evaluation
Liposomes	Transient	Low	Under evaluation

Some key factors distinguishing current delivery methods are outlined: duration of expression, risk of genomic integration (which can lead to oncogenicity), and immunogenicity (which is especially important if repetitive gene therapy treatments are required). Observed efficiency of genome targeting is also a function of innate properties of the target cells, in particular the mitotic state [38,58,113], and ability to efficiently deliver the genome engineering effectors [58,113]. [#]Immunogenicity is also a function of the delivery payload.

1.3.1 Viral Delivery Systems

Viral vectors, such as retroviruses, lentiviruses, adenoviruses, and adeno-associated viruses (AAVs) have naturally evolved to transduce mammalian cells efficiently, and consequently have been a preferred format for gene delivery over the past few decades. These vector systems can in turn be broadly divided into two major classes, those whose genome integrates into the host chromatin, such as retroviruses and lentiviruses, and those that persist inside the host nucleus or cytoplasm, such as adenoviruses, AAVs, sindbis, and sendai viruses [54]. Each of these systems however come with certain tradeoffs, for instance, retroviral integration into the host chromosome can lead to increased frequency of random mutagenesis and oncogene activation [55], but corresponding delivery systems are also best suited for long-term stable expression of their payloads. Thus nature of the application often governs choice of the delivery chassis and below we highlight some prominent viral systems relevant to CRISPR-Cas.

A preferred viral delivery system for gene therapy is AAVs. These have been widely utilized for gene therapy due to their overall safety, mild immune response, long-term transgene

expression, high-infection efficiency, and are now already being used in clinical trials [56]. A primary drawback of AAVs, however, is that they have a limited packaging capacity of around 4.7 kb, making it difficult to deliver large Cas9-like effector proteins such as the *Streptococcus pyogenes* Cas9 (SpCas9), with a size of around 4.2 kb, a single gRNA, and other components necessary for effective transcription [57.58]. In order to overcome this packaging issue, distinct solutions have been suggested. For instance, smaller Cas9 orthologs, such as *Straphylococcus aureus* Cas9 (SaCas9), with ~3.3 kb has been successfully packaged into a single AAV [32], and another small ortholog, *Streptococcus thermophilus* (St1Cas9) with ~3.3 kb [59,60] could also potentially be packaged into a single AAV. However, a potential issue with smaller orthologs is it that they require more complex PAM sequences: SaCas9 recognizes the 5'-NNGRRT-3' PAM and St1Cas9 recognizes the 5'-NNAGAAW-3' PAM, which restricts the range of targetable sequences [32]. Moreover, these orthologs are not all equally robust. To circumvent this issue, the PAM sequence can be engineered utilizing structural information, such as been done in *Francisella novicida* FnCas9, in which its PAM 5'-NGG-3' was altered to a more relaxed 50-YG-30 PAM [61]. In another study, SpCas9 was modified to recognize alternative PAM sequences via bacterial directed evolution, structural information, and combinatorial design [62]. Alternatively truncated SpCas9 proteins have been designed [63,64] utilizing the SpCas9 crystal structure [65], however these do not retain the robustness of their wild-type counterpart. In an elegant study to circumvent this, a split-Cas9 system was recently designed which takes advantage of inteins from *Nostoc punctiforme*. This design utilizes a two-vector system where each half of Cas9 is fused to a corresponding split-intein moiety, and upon co-expression intein mediated trans-splicing occurs and the full SpCas9 protein is reconstituted [66]. Additionally, some other studies have also utilized a dual-AAV system, where one AAV is utilized to deliver the sgRNA and the other to deliver the SpCas9 [38,67]. The drawback to these dual-AAV systems, however, is that both AAVs must be

delivered to the same cell to elicit an effect, thereby decreasing the efficiency or alternatively entailing the use of significantly higher viral titers. In summary, while AAVs are a preferred mode of delivery for Cas9-gRNA agents, further studies on serotype engineering and Cas9 orthologs must be done to deliver all desired components and fusions thereof efficaciously.

Another versatile delivery system relevant to CRISPR-Cas are lentiviruses, which have also been widely utilized for gene therapy. Lentiviruses, originally adapted from HIV-1, are highly potent viral vectors due to their broad tropism, their large cargo capacity (9.7 kb), and the fact that they can infect post-mitotic cells [68]. Lentiviruses can thus be readily utilized to deliver Cas9 and other components necessary for genome editing via a single construct [69]. Additionally, the tropism of lentiviruses can be easily altered by the addition of envelope proteins targeting distinct cell surface receptors. This pseudotyping is ideal for transducing certain cell types or tissues that are otherwise difficult to transduce. Lentiviruses have also been widely utilized for *ex vivo* gene therapy, specifically in hematopoietic stem cells (HSCs) and T lymphocytes (T cells). In a recent review, some relevant genetic therapy clinical trials were highlighted in which lentiviruses were safely utilized to treat Wiskot-Aldrich syndrome, β-Thalassaemia, and various T-cell immunotherapy for cancer [70]. Additionally, some *in vivo* studies utilizing CRISPR-Cas systems have also demonstrated robust gene editing (Table 1.1). It should be noted nevertheless that while lentiviruses are preferred due to their high efficiency of delivery and long-term expression of payload, their genomic integration, however, is unfavorable due to its potential mutagenic effects, or silencing/ activation of neighboring loci [71]. In this regard the newest generation of integrase-deficient lentivirus vectors (IDLV), which carry mutations in the integrase and viral LTRs greatly reduce the risk of insertional mutagenesis, however these do not completely eliminate this risk [72-74]. Additionally, immunogenicity is still a risk [75]. Furthermore, the consequences of Cas9 integration into the genome by lentiviruses are not yet fully understood, and although advances in

lentiviruses have been made [76], there may still be risks of having a nuclease integrate into the genome. Lentiviruses, however, could be utilized for the delivery of nuclease-deficient dCas9, or nonintegrating versions of lentiviruses may be utilized for hit-and-run nuclease applications.

1.3.2 Nonviral Delivery Systems

Complementary to the viral systems are a host of nonviral delivery systems that have been developed over the past few decades. These include methods utilizing nanoparticles such as cationic nanocarriers [39], liposomes, and polymeric materials. An advantage to these systems is their overall safety, low immune response, large loading capacity, and general ease of production. On the other hand, nonviral methods utilized to deliver DNA have to surpass many physical barriers imposed by the cell to efficiently deliver genomes to the cell [77]. However, given the nearly complete control over their synthesis and constituents, one could potentially engineer nanoparticles or polymeric materials to target diseased cells specifically, for instance by coating them with ligands that are specific to receptors on target or diseased cells, as has been done for drug delivery and imaging [78].

In this context, both Cas9 and gRNA are anionic, which allows their ready integration into cationic liposomes or polymers as a delivery system [79]. Correspondingly there have been several recent studies utilizing nanoparticles for CRISPR-Cas9 delivery. For instance, a recent study developed bioreducible lipid nanoparticles to deliver Cas9-sgRNA *in vitro* with genome efficiencies of 70% [80]. Additionally, a Cas9:gRNA targeting EGFP complex was delivered *in vivo* to Atoh1-GFP mice ear hair cells via cationic lipids, enabling up to 20% editing rates [39]. This study demonstrated that by modifying protein charges of Cas9-sgRNA complexes, one can successfully deliver these via cationic lipids. Additionally, due to the fact that the Cas9–sgRNA complex is delivered as a protein, with a short half-life, the risk of potential offtarget effects can be

significantly reduced [81]. These approaches thus have huge potential for utilization in gene therapy applications. Another alternative approach commonly used for delivery is hydrodynamic injections – these are high volume injections (8–10% body weight of mice) delivered into the vasculature at high speeds (5–7 seconds), to enable the delivery of naked DNA or siRNA. Hydrodynamic injections delivering CRISPRCas9 have since been utilized in several *in vivo* CRISPR-Cas9 studies targeting the liver [23,24]. Hydrodynamic injections, however, are not considered to be clinically feasible due to the potential damage these inflict on the liver and the heart [82].

1.4 Challenges and Future Directions

While CRISPR-Cas systems have been widely utilized for genome engineering, several key challenges must to be addressed before these tools can be utilized for efficacious gene therapy. For instance, an important challenge for in vivo CRISPR-Cas therapy is the ability to achieve immune stealth in order to minimize dosage and enable re-administration of nucleic acid or protein therapeutics. Classic immunosuppression for the duration of treatment is one option, but this will be less useful for long-term genome regulatory modifications. Therefore, the delivery vector of choice must be capable of high transduction efficiency while avoiding immune responses of both of the delivery system and the CRISPR payload. In this regard, Table 1.2 describes the distinct delivery systems, both viral and nonviral, and their known immunogenicity and levels of payload expression. For example, although adenoviruses (Ad) or retroviruses have the advantage of a high packaging capacity, their high immunogenicity may lead to unwanted side effects [83,84]. A study found that inflammatory cytokines and chemokines were activated by Kupffer cells in the liver and MARCO+ macrophages in the spleen in as early as ten minutes post intravenal injection of adenoviruses in mice [85]. On the other hand, AAVs have lower immunogenicity in comparison,

but have a small packaging limit. Although viruses are a preferred delivery system due to their efficacy in infecting cells and tissues, the low immunogenicity of nonviral vectors, such as nanoparticles could be a preferred method in the future. Nonviral vectors, however, require further engineering to improve levels of transduction and transient expression in vivo [86,87]. It is important to note that not only is the immune response an important consideration for delivery systems, but for the CRISPR-Cas9 payload as well. For instance, Cas9 is a foreign prokaryotic protein, and could potentially elicit a strong immune response. A recent study demonstrated that Cas9 indeed evokes cellular and humoral immune responses, with Cas9-specific antibodies elicited post exposure [88]. Therefore, if a patient were to necessitate repetitive treatments, CRISPR-Cas efficacy might be reduced by the body's immune response.

Yet another important challenge to overcome is specificity, or reducing off-target genomic effects. Specifically, in order to conduct safe clinical treatments, off-target mutations must be reduced in order to avoid perturbation of areas of the genome with unknown effects. Various groups have correspondingly characterized SpCas9 specificity [89–91] and several strategies to improve Cas9 specificity have been reported, including minimizing the amount of Cas9 in the cell [89,92], utilizing a nickase Cas [9,43,93] and utilizing dCas9 fused to a FokI nuclease domain [94,95]. An important factor that can contribute to reducing off-target effects is also the design of gRNAs. Studies on the specificity of SpCas9 have demonstrated that mismatches between gRNA and target DNA can be tolerated [43,57,89,95]. Moreover, the farther mismatches are from the PAM sequence, the more tolerated that they are [57,91]. Additionally, several *in silico* methods have been developed to design gRNAs [96–99] including easily accessible online sources, for example, Benchling (http://benchling.com), which detail the number of mismatches each gRNA will have, in order to aid the design of the optimal gRNAs for genome engineering. Importantly, one also needs to balance gRNA activity with specificity. For example research has indicated that guanine rich

gRNA sequences, specifically close to the PAM sequence, are favorable, while cytosines are unfavorable [99]. Furthermore, truncated gRNAs of ~17 nt have been shown to have lower off-target effects than a ~20 nt gRNA [100]. Another strategy that has been utilized to increase specificity is using a nickase version of Cas9. Briefly, SpCas9 creates double stranded breaks through two catalytic domains: RuvC and HNH domains. By editing one of these two domains, one can create a nickase, which only creates a single-strand break. By designing two gRNAs, one in the sense and one in the antisense direction, one can then create targeted double-stranded breaks. Since two gRNAs are involved, the probability of off-target effects is greatly reduced, as off-target single nicks are typically repaired scarlessly by the cell [43,101]. Another alternative is to utilize an engineered Cas9, such as the high-fidelity Cas9 (SpCas9-HF1) [102] or 'enhanced specificity' SpCas9 (eSpCas9) [103]. The SpCas9-HF1 was engineered based on the hypothesis that there is excess energy between the SpCas9–gRNA complex and the DNA target, and that disrupting the Cas9–target DNA interactions might minimize off-target effects. To this effect, an SpCas9 with the four amino acid mutations, N497A, R661A, Q695A, and Q926A, deemed SpCas9-HF1, reduced off-target effects, while maintaining on-target activity [102]. In another study, the eSpCas9 was rationally designed based on the crystal structure of SpCas9, with the hypothesis that disrupting positive charges between the domains that are involved in stabilizing the nontarget DNA strand, will weaken nontarget binding. Correspondingly they disrupted interactions between SpCas9 and the nontarget DNA strand by neutralizing the positive charges between these domains. Their results demonstrated reduced off-target activity while maintaining on-target activity [103]. In addition to Cas9 engineering, one can also deliver Cas9 as a protein instead of as a vector, since reducing the temporal pulse of Cas9 expression can greatly reduce off-target effects [81]. Finally, one can also utilize genetic circuits to enable temporal control of Cas9, such as small molecule regulated approaches [33,104–108]. In addition to temporal control, tissue-specific expression, or spatial

control, is another important challenge. Here tissue-specific promoters can be utilized [109,110]. Additionally, one can engineer targeted integrations at a specific locus, for example, the albumin locus, which leads not only to high transgene expression, but also is tissue specific to the liver [111]. Moreover, by engineering viral vectors to target specific tissues, the input titers utilized could be minimized, which in turn could also potentially minimize the immunogenic response. One can therefore decrease the chance of off-target effects (genomic and tissue specific) by effective design of gRNA, and spatiotemporal control of Cas9 or gRNA expression.

Finally, basic science insights into the mechanisms of DNA repair will also be critical: specifically biasing HR versus NHEJ outcomes is a major challenge that needs to be addressed. This is critical since for safe gene repair one needs to enable primarily HR events with essentially no concurrent NHEJ events (which could instead mutagenize the target region of interest). This aspect is further complicated by the fact that the majority of the human body is post-mitotic and correspondingly HR machinery and hence activity is significantly diminished. Inspiration for new technologies to address this may come from nature, for instance in *E. coli* the lambda red system can be harnessed to enable DSB independent recombineering [112], or by coopting transposase or recombinase mediated approaches. On the other hand, growing mechanistic insights into underlying pathways will also be critical. Indeed in a pioneering study, investigation of the mechanism for suppression of HR in G1 phase deduced that the mechanisms which inhibit HR in G1 include suppression of DNA-end resection coupled with a block in recruitment of BRCA2 to DNA sites with damage, and leveraging this knowledge the authors were able to create conditions to stimulate HR in G1 [113]. In another strategy, Cas9 was controlled in a cell-cycle temporal manner by fusing its N-terminal to human Geminin, converting it into a substrate for APC/Cdh1, the E3 ubiquitin ligase complex, thereby regulating Cas9 expression to S/G2/M phases, by degrading Cas9 in the G1 phase [114]. Another interesting recent approach here was to inhibit NHEJ by targeting of the DNA

ligase IV enzyme with the inhibitor Scr7 [115]. Alternatively, as indicated earlier one can also forego HR/NHEJ pathways altogether. A recent paper developed 'base editing,' which enables point mutations without relying on innate HR/NHEJ pathways. This method utilizes dCas9 fused to a cytidine deaminase enzyme, that mediates direct conversion of cytidine to uridine [9]. In another study, the interaction of Cas9–sgRNA complex with the target DNA was harnessed in a clever approach. The authors while measuring the Cas9 dissociation rates found that both Cas9 and dCas9 dissociate very slowly from their target. Upon investigating the release of DNA target post-cleavage closely, they observed that Cas9 held tightly to one of the two strands of the duplex, leaving the other free to anneal to complementary ssDNA. They then tested ssDNA donors and confirmed that single stranded DNA that was complementary to the released strand supported higher frequencies of gene editing, and that one could thereby systematically increase HR frequencies by tailoring the orientation, polarity, and length of the donor ssDNA to match the properties of the Cas9–DNA complex [116].

1.5 Conclusion

Taken together, we believe that with the rapid progress in genome engineering toolsets based on CRISPR-Cas systems, coupled with the development of new generation of viral and nonviral delivery approaches will spur many new gene therapeutic applications. As outlined earlier, several important challenges need to be surmounted towards enabling safe and efficient gene therapy. For instance, studies need to be performed to better understand Cas9 immunogenicity. Additionally, finding the ideal delivery system for CRISPR-Cas systems with the optimal packaging limit, and efficiency also need to be taken into consideration. Finally, finding ways of eliminating NHEJ and boosting HR efficiency will further increase our abilities to target human

disease, including in adults. In addition, discovery of new Cas9-like proteins from diverse organisms might further expand our toolset towards addressing some of the current challenges. We foresee that further development of CRISPR-Cas systems will eventually pave the way for gene therapeutic applications.

1.6 Acknowledgements

This work was completed with generous support from the Burroughs Wellcome Fund, the March of Dimes Foundation, the Kimmel Foundation, and a graduate fellowship from CONACYT and the University of California Institute of Mexico and the United States.

Chapter 1 in part is a reprint of the material *Moreno AM, Mali P. Therapeutic Genome Engineering via CRISPR-Cas systems. WIREs Systems Biology and Medicine (2017) 9:e1380.* The dissertation author was the primary author.

1.7 References

1. Sung P, Klein H. Mechanism of homologous recombination: mediators and helicases take on regulatory functions. Nat Rev Mol Cell Biol 2006, 7:739–750.

2. Lieber MR. The mechanism of double-strand DNA break repair by the nonhomologous DNA end-joining pathway. Annu Rev Biochem 2010, 79:181–211.

3. Wolfe SA, Nekludova L, Pabo CO. DNA recognition by Cys2His2 zinc finger proteins. Annu Rev Biophys Biomol Struct 2000, 29:183–212.

4. Urnov FD, Rebar EJ, Holmes MC, Zhang HS, Gregory PD. Genome editing with engineered zinc finger nucleases. Nat Rev Genet 2010, 11:636–646.

5. Carroll D. Genome engineering with zinc-finger nucleases. Genetics 2011, 188:773–782.

6. Joung JK, Sander JD. TALENs: a widely applicable technology for targeted genome editing. Nat Rev Mol Cell Biol 2012, 14:49–55.

7. Chen S, Oikonomou G, Chiu CN, Niles BJ, Liu J, Lee DA, Antoshechkin I, Prober DA. A large-scale in vivo analysis reveals that TALENs are significantly more mutagenic than ZFNs

generated using context dependent assembly. Nucleic Acids Res 2013, 41:2769–2778.

8. Gaj T, Gersbach CA, Barbas CF 3rd. ZFN, TALEN and CRISPR/Cas-based methods for genome engineering. Trends Biotechnol 2013, 31:397–405.

9. Komor AC, Kim YB, Packer MS, Zuris JA, Liu DR. Programmable editing of a target base in genomic DNA without double-stranded DNA cleavage. Nature 2016, 533:420–424.

10. Wiedenheft B, Sternberg SM, Doudna JA. RNA guided genetic silencing systems in bacteria and archaea. Nature 2012, 482:331–338.

11. Horvath P, Barrangou R. CRISPR/Cas, the immune system of bacteria and archaea. Science 2010, 327:167–170.

12. Barrangou R, Fremaux C, Deveau H, Richards M, Boyaval P, Moineau S, Romero DA, Horvath P. CRISPR provides acquired resistance against viruses in prokaryotes. Science 2007, 315:1709–1712.

13. Deltcheva E, Chylinski K, Sharma CM, Gonzales K, Chao Y, Pirzada ZA, Eckert MR, Vogel J, Charpentier E. CRISPR RNA maturation by transencoded small RNA and host factor RNase III. Nature 2011, 471:602–607.

14. Jinek M, Chylinski K, Fonfara I, Hauer M, Doudna JA, Charpentier E. A programmable dual-RNA guided DNA endonuclease in adaptive bacterial immunity. Science 2012, 337:816–821.

15. Marraffini LA, Sontheimer EJ. Self versus non-self discrimination during CRISPR RNA-directed immunity. Nature 2010, 463:568–571.

16. Jinek M, East A, Cheng A, Lin S, Doudna JA. RNA programmed genome editing in human cells. Elife 2013, 2:e00471.

17. Mali P, Yang L, Esvelt KM, Aach J, Guell M, DiCarlo JE, Norville JE, Church GM. RNA-guided human genome engineering via Cas9. Science 2013, 339:823–826.

18. Cong L, Ran FA, Cox D, Lin S, Barretto R, Habib N, Hsu PD, Wu X, Jiang W, Marraffini LA, Zhang F. Multiplex genome engineering using CRISPR/Cas systems. Science 2013, 339:819–823.

19. Li D, Qiu Z, Shao Y, Chen Y, Guan Y, Liu M, Li Y, Gao N, Wang L, Lu X, et al. Heritable gene targeting in the mouse and rat using a CRISPR-Cas system. Nat Biotechnol 2013, 31:681–683.

20. Yang D, Xu J, Zhu T, Fan J, Lai L, Zhang J, Chen YE. Effective gene targeting in rabbits using RNA guided Cas9 nucleases. J Mol Cell Biol 2014, 6:97–99.

21. Niu Y, Shen B, Cui Y, Chen Y, Wang J, Wang L, Kang Y, Zhao X, Si W, Li W, et al.

Generation of gene-modified cynomolgus monkey via Cas9/RNA mediated gene targeting in one-cell embryos. Cell 2014, 156:836–843.

22. Wang H, Yang H, Shivalila CS, Dawlaty MM, Cheng AW, Zhang F, Jaenisch R. One-step generation of mice carrying mutations in multiple genes by CRISPR/Cas-mediated genome engineering. Cell 2013, 153:910–918.

23. Xue W, Chen S, Yin H, Tammela T, Papagiannakopoulos T, Joshi NS, Cai W, Yang G, Bronson R, Crowey DG, et al. CRISPR-mediated direct mutation of cancer genes in the mouse liver. Nature 2014, 514:380–384.

24. Yin H, Xue W, Chen S, Bogorad RL, Benedetti E, Grompe M, Koteliansky V, Sharp PA, Jacks T, Anderson DG. Genome editing with Cas9 in adult mice corrects a disease mutation and phenotype. Nat Biotechnol 2014, 32:551–553.

25. Ding Q, Strong A, Patel KM, Ng SL, Gosis BS, Regan SN, Cowan CA, Rader DJ, Musunuru K. Permanent alteration of PCSK9 with in vivo CRISPR-Cas9 genome editing. Circ Res 2014, 15:488–492.

26. Platt RJ, Chen S, Zhou Y, Yim MJ, Swiech L, Kempton HR, Dahlman JE, Parnas O, Eisenhaure TM, Jovanovic M, et al. CRISPR-Cas9 knockin mice for genome editing and cancer modeling. Cell 2014, 159:440–455.

27. Long C, McAnally JR, Shelton JM, Mireault AA, Bassel-Duby R, Olson EN. Prevention of muscular dystrophy in mice by CRISPR/Cas9–mediated editing of germline DNA. Science 2014, 345:1184–1188.

28. Shen B, Zhang W, Zhang J, Zhou J, Wang J, Chen L, Wang L, Hodgkins A, Iyer V, Huang X, et al. Efficient genome modification by CRISPR-Cas9 nickase with minimal off-target effects. Nat Methods 2014, 11:399–402.

29. Sánchez-Rivera FJ, Papagiannakopoulos T, Romero R, Tammela T, Bauer MR, Bhutkar A, Joshi NS, Subbaraj L, Bronson RT, Xue W, et al. Rapid modeling of cooperating genetic events in cancer through somatic genome editing. Nature 2014, 516:428–431.

30. Heckl D, Kowalczyk MS, Yudovich D, Belizaire R, Puram RV, McConkey ME, Thielke A, Aster JC, Regev V, Ebert BL. Generation of mouse models of myeloid malignancy with combinatorial genetic lesions using CRISPR-Cas9 genome editing. Nat Biotechnol 2014, 32:941–946.

31. Swiech L, Heidenreich M, Banerjee A, Habib N, Li Y, Trombetta J, Sur M, Zhang F. In vivo interrogation of gene function in the mammalian brain using CRISPR-Cas9. Nat Biotechnol 2015, 33:102–106.

32. Ran FA, Cong L, Yan WX, Scott DA, Gootenberg JS, Kriz AJ, Zetsche B, Shalem O, Wu X, Makarova KS, et al. In vivo genome editing using Staphylococcus aureus Cas9. Nature 2015, 520:186–191.

33. Dow LE, Fisher J, O'Rourke KP, Muley A, Kastenhuber ER, Livshits G, Tschaharganeh DF, Socci ND, Lowe SW. Inducible in vivo genome editing with CRISPR-Cas9. Nat Biotechnol 2015, 33:390–394.

34. Kalebic N, Taverna E, Tavano S, Wong FK, Suchold D, Winkler S, Huttner WB, Sarov M. CRISPR/Cas9-induced disruption of gene expression in mouse embryonic brain and single neural stem cells in vivo. EMBO Rep 2016, 17:338–348.

35. Tabebordbar M, Zhu K, Cheng JK, Chew WL, Widrick JJ, Yan WX, Maesner C, Wu EY, Xiao R, Ran FA, et al. In vivo gene editing in dystrophic mouse muscle and muscle stem cells. Science 2016, 351:407–411.

36. Nelson CE, Hakim CH, Ousterout DG, Thakore PI, Moreb EA, Castellanos Rivera RM, Madhavan S, Pan X, Ran FA, Yan WX, et al. In vivo genome editing improves muscle function in a mouse model of Duchenne muscular dystrophy. Science 2016, 351:403–407.

37. Long C, Amoasii L, Mireault AA, McAnally JR, Li H, Sanchez-Ortiz E, Bhattacharyya S, Shelton JM, Bassel-Duby R, Olson EN. Postnatal genome editing partially restores dystrophin expression in a mouse model of muscular dystrophy. Science 2016, 351:400–403.

38. Yang Y, Wang L, Bell P, McMenamin D, He Z, White J, Yu H, Xu C, Morizono H, Musunuru K, et al. A dual AAV system enables the Cas9-mediated correction of a metabolic liver disease in newborn mice. Nat Biotechnol 2016, 34:334–338.

39. Zuris JA, Thompson DB, Shu Y, Guilinger JP, Bessen JL, Hu JH, Maeder ML, Joung JK, Chen ZY, Liu DR. Cationic lipid-mediated delivery of proteins enables efficient protein-based genome editing in vitro and in vivo. Nat Biotechnol 2015, 33:73–80.

40. Zuckermann M, Hovestadt V, Knobbe-Thomsen CB, Zapatka M, Northcott PA, Schramm K, Belic J, Jones DTW, Tschida B, Moriarity B, et al. Somatic CRISPR/Cas9-mediated tumour suppressor disruption enables versatile brain tumour modelling. Nat Commun 2015, 6:7391.

41. Mandal PK, Ferreira LM, Collins R, Meissner TB, Boutwell CL, Friesen M, Vrbanac V, Garrison BS, Stortchevoi A, Bryder D, et al. Efficient ablation of genes in human hematopoietic stem and effector cells using CRISPR/Cas9. Cell Stem Cell 2014,
15:643–652.

42. Gilbert LA, Larson MH, Morsut L, Liu Z, Brar GA, Torres SE, Stern-Ginossar N, Brandman O, Whitehead EH, Doudna JA, et al. CRISPR-mediated modular RNA-guided regulation of transcription in eukaryotes. Cell 2013, 154:442–451.

43. Mali P, Aach J, Stranges PB, Esvelt KM, Moosburner M, Kosuri S, Yang L, Church GM, et al. CAS9 transcriptional activators for target specificity screening and paired nickases for cooperative genome engineering. Nat Biotechnol 2013, 31:833–838.

44. Qi LS, Larson MH, Gilbert LA, Doudna JA, Weissman JS, Arkin AP, Lim WA. Repurposing

CRISPR as an RNA-guided platform for sequence specific control of gene expression. Cell 2013, 152:1173–1183.

45. Chavez A, Scheiman J, Vora S, Pruitt BW, Tuttle M, Iyer EPR, Lin S, Kiani S, Guzman CD, Wiegand DJ, et al. Highly efficient Cas9-mediated transcriptional programming. Nat Methods 2015, 12:326–328.

46. Hilton IB, D'Ippolito AM, Vockley CM, Thakore PI, Crawford GE, Reddy TE, Gersbach CA. Epigenome editing by a CRISPR-Cas9-based acetyltransferase activates genes from promoters and enhancers. Nat Biotechnol 2015, 33:510–517.

47. Vojta A, Dobrinic P, Tadic V, Bockor L, Korac P, Julg B, Klasic M, Zoldoš V. Repurposing the CRISPR-Cas9 system for targeted DNA methylation. Nucl Acids Residues 2016, 44:5615–5628.

48. Tanenbaum ME, Gilbert LA, Qi LS, Weissman JS, Vale RD. A protein-tagging system for signal amplification in gene expression and fluorescence imaging. Cell 2014, 159:635–646.

49. Gilbert LA, Horlbeck MA, Adamson B, Villalta JE, Chen Y, Whitehead EH, Guimaraes C, Panning B, Ploegh HL, Bassik MC, et al. Genome-scale CRISPR mediated control of gene repression and activation. Cell 2016, 159:647–661.

50. Zetsche B, Gootenberg JS, Abudayyeh OO, Slaymaker IM, Makarova KS, Essletzbichler P, Volz SE, Joung J, van der Oost J, Regev A, et al. Cpf1 is a single RNA-guided endonuclease of a class 2-CRISPR-Cas system. Cell 2015, 163:759–771.

51. Fonfara I, Richter H, Bratovic M, Rhun AL, Charpentier E. The CRISPR-associated DNA-cleaving enzyme Cpf1 also processes precursor CRISPR RNA. Nature 2016, 532:517–521.

52. Kim D, Kim J, Hur JK, Been KW, Yoon SH, Kim JS. Genome-wide analysis reveals specificities of Cpf1 endonucleases in human cells. Nat Biotechnol 2016, 34:863–868.

53. Kim Y, Cheong S, Lee JG, Lee S-W, Lee MS, Baek IJ, Sung YH. Generation of knockout mice by Cpf1-mediated gene targeting. Nat Biotech 2016, 34:808–810.

54. Thomas CE, Ehrhardt A, Kay MA. Progress and problems with the use of viral vectors for gene therapy. Nat Rev Genet 2003, 4:346–358.

55. Anson DS. The use of retroviral vectors for gene therapy-what are the risks? A review of retroviral pathogenesis and its relevance to retroviral vector mediated gene delivery. Genet Vaccines Ther 2004, 2:9.

56. Mingozzi F, High KA. Therapeutic in vivo gene transfer for genetic disease using AAV: progress and challenges. Nat Rev Genet 2011, 12:341–355.

57. Hsu PD, Lander ES, Zhang F. Development and applications of CRISPR-Cas9 for genome engineering. Cell 2014, 157:1262–1278.

58. Mali P, Esvelt KM, Church GM. Cas9 as a versatile tool for engineering biology. Nat Methods 2013,10:957–963.

59. Deveau H, Barrangou R, Garneau JE, Labonté J, Fremaux C, Boyaval P, Romero DA, Horvath P, Moineau S. Phage response to CRISPR-encoded resistance in Streptococcus thermophilus. J Bacteriol 2008, 190:1390–1400.

60. Horvath P, Romero DA, Coûte-Monvoisin AC, Richards M, Deveau H, Moineau S, Boyaval P, Fremaux C, Barrangou R. Diversity, activity, and evolution of CRISPR loci in Streptococcus thermophilus. J Bacteriol 2008, 190:1401–1412.

61. Hirano H, Gootenberg JS, Horii T, Abudayyeh OO, Kimura M, Hsu PD, Nakane T, Ishitani R, Hatada I, Zhang F, Nishimasu H, Nureki O. Structure and engineering of Francisella novicida Cas9. Cell 2016, 164:950–961.

62. Kleinstiver BP, Prew MS, Tsai SQ, Topkar VV, Nguyen NT, Zheng Z, Gonzales AP, Li Z, Peterson RT, Yeh JR, Aryee MJ, Joung JK. Engineered CRISPR-Cas9 nucleases with altered PAM specificities. Nature 2015, 523:481–485.

63. Zetsche B, Volz SE, Zhang F. A split-Cas9 architecture for inducible genome editing and transcription modulation. Nat Biotechnol 2015, 33:139–142.

64. Wright AV, Sternberg SH, Taylor DW, Staahl BT, Bardales JA, Kornfeld JE, Doudna JA. Rational design of a split-Cas9 enzyme complex. *Proc Natl Acad Sci USA* 2015, 112:2984–2989.

65. Nishimasu H, Ran FA, Hsu PD, Konermann S, Shehata SI, Dohmae N, Ishitani R, Zhang F, Nureki O. Crystal structure of Cas9 in complex with guide RNA and target DNA. *Cell* 2014, 156:935–949.

66. Truong DJ, Kuhner K, Kuhn R, Werfel S, Engelhardt S, Wurst W, Ortiz O. Development of an intein-mediated split—Cas9 system for gene therapy. *Nucleic Acids Res* 2015, 43:6450–6458.

67. Hung SS, Chrysostomou V, Li F, Lim JK, Wang JH, Powell JE, Tu L, Daniszewski M, Lo C, Wong RC, et al. AAV-mediated CRISPR/Cas gene editing of retinal cells. *Invest Ophthalmol Vis Sci* 2016, 57:3470–3476.

68. Naldini L, Blömer U, Gallay P, Ory D, Mulligan R, Gage FH, Verma IM, Trono D. In vivo gene delivery and stable transduction of nondividing cells by a lentiviral vector. *Science* 1996, 272:263–267.

69. Shalem O, Sanjana NE, Hartenian E, Shi X, Scott DA, Mikkelsen TS, Heckl D, Ebert BL, Root DE, Doench JG, et al. Genome-scale CRISPR-Cas9 knock- out screening in human cells. *Science* 2014, 343:84–87.

70. Naldini L. Gene therapy returns to centre stage. *Nature* 2015, 526:351–360.

71. White MK, Hu W, Khalili K. The CRISPR/Cas9 genome editing methodology as a weapon against human viruses. *Discov Med* 2015, 19:255–262.

72. Wanisch K, Yáñez-Muñoz RJ. Integration-deficient lentiviral vectors: a slow coming of age. *Mol Ther* 2009, 17:1316–1332.

73. Miyoshi H, Blömer U, Takahashi M, Gage FH, Verma IM. Development of a self-inactivating lentivirus vector. *J Virol* 1998, 72:8150–8157.

74. Philippe S, Sarkis C, Barkats M, Mammeri H, Ladroue C, Petit C, Mallet J, Serguera C. Lentiviral vectors with a defective integrase allow efficient and sustained transgene expression in vitro and in vivo. *Proc Natl Acad Sci USA* 2006, 103:17684–17689.

75. Rothe M, Modlich U, Schambach A. Biosafety challenges for use of lentiviral vectors in gene therapy. *Curr Gene Ther* 2013, 13:453–468.

76. Persons DA. Lentiviral vector gene therapy: effective and safe? *Mol Ther* 2010, 18:861–862.

77. Yin H, Kanasty RL, Eltoukhy AA, Vegas AJ, Dorkin JR, Anderson DG. Non-viral vectors for gene-based therapy. *Nat Rev Genet* 2014, 15:541–555.

78. Koo OM, Rubinstein I, Onyuksel H. Role of nano- technology in targeted drug delivery and imaging: a concise review. *Nanomed Nanotechnol Biol Med* 2016, 1:193–212.

79. Wang L, Fangfei L, Dang L, Liang C, Wang C, He B, Liu J, Li D, Wu X, Xu X, et al. In vivo delivery systems for therapeutic genome editing. Int J Mol Sci 2016, 17:626.

80. Wang M, Zuris JA, Meng F, Rees H, Sun S, Deng P, Han Y, Gao X, Pouli D, Wu Q, et al. Efficient deliv- ery of genome-editing proteins using bioreducible lipid nanoparticles. Proc Natl Acad Sci USA 2016, 113:2868–2873.

81. Kim S, Kim D, Cho SW, Kim J, Kim JS. Highly efficient RNA-guided genome editing in human cells via delivery of purified Cas9 ribonucleoproteins. Genome Res 2014, 24:1012–1019.

82. Bonamassa B, Hai L, Liu D. Hydrodynamic gene delivery and its applications in pharmaceutical research. Pharm Res 2011, 28:694–701.

83. Hacein-Bey-Abina S, Garrigue A, Wang GP, Soulier J, Lim A, Morillon E, Clappier E, Caccavelli L, Delabesse E, Beldjord K, et al. Insertional oncogenesis in 4 patients after retrovirus-mediated gene therapy of SCID-X1. J Clin Investig 2008, 118:3132–3142.

84. Yang Y, Nunes FA, Berencsi K, Furth EE, Gönczöl E, Wilson JM. Cellular immunity to viral antigens limits E1-deleted adenoviruses for gene therapy. Proc Natl Acad Sci USA 1994, 91:4407–4411.

85. Di Paolo NC, Miao EA, Iwakura Y, Murali-Krishna K, Aderem A, Flavell RA, Papayannopoulou T, Shayakhmetov DM. Virus binding to a plasma mem- brane receptor triggers interleukin-1α-mediated proinflammatory macrophage response in vivo. Immunity 2009, 31:110–121.

86. Katsumi A, Emi N, Abe A, Hasegawa Y, Ito M, Saito H. Humoral and cellular immunity to an encoded protein induced by direct DNA injection. Hum Gene Ther 1994, 5:1335–1339.

87. Pickering JG, Jekanowski J, Weir L, Takeshita S, Losordo DW, Isner JM. Liposome-mediated gene transfer into human vascular smooth muscle cells. Circulation 1994, 89:13–21.

88. Chew WL, Tabebordbar M, Cheng JKW, Mali P, Wu EY, Ng AHM, Zhu K, Wagers AJ, Church GM. A multifuncitonal AAV-CRISPR-Cas9 and its host reponse. Nat Methods 2016, 13:868–874.

89. Hsu PD, Scott DA, Weinstein JA, Ran FA, Konermann S, Agarwala V, Li Y, Fine EJ, Wu X, Shalem O, et al. DNA targeting specificity of RNA- guided Cas9 nucleases. Nat Biotechnol 2013, 31:827–832.

90. Pattanayak V, Lin S, Guilinger JP, Ma E, Doudna JA, Liu DR. High-throughput profiling of off-target DNA cleavage reveals RNA-programmed Cas9 nuclease specificity. Nat Biotechnol 2013, 31:839–843.

91. Fu Y, Foden JA, Khayter C, Maeder ML, Reyon D, Joung JK, Sander JD. High-frequency off-target mutagenesis induced by CRISPR-Cas nucleases in human cells. Nat Biotechnol 2013, 31:822–826.

92. Ran FA, Hsu PD, Lin CY, Gootenberg JS, Konermann S, Trevino A, Scott DA, Inoue A, Matoba S, Zhang Y, et al. Double nicking by RNA- guided CRISPR Cas9 for enhanced genome editing specificity. *Cell* 2013, 154:1380–1389.

93. Tsai SQ, Wyvekens N, Khayter C, Foden JA, Thapar V, Reyon D, Goodwin MJ, Aryee MJ, Joung JK. Dimeric CRISPR RNA-guided FokI nucleases for highly specific genome editing. *Nat Biotechnol* 2014, 32:569–576.

94. Guilinger JP, Thompson DB, Liu DR. Fusion of catalytically inactive Cas9 to FokI nuclease improves the specificity of genome modification. *Nat Biotechnol* 2014, 32:577–582.

95. Zhang XH, Tee LY, Wang XG, Yang SH. Off-target effects in CRISPR/Cas9-mediated genome engineering. *Mol Ther Nucl Acids* 2015, 4:e264.

96. Xie S, Shen B, Zhang C, Huang X, Zhang Y. sgRNA- cas9: a software package for designing CRISPR sgRNA and evaluating potential off-target cleavage sites. *PLoS One* 2014, 9:e100448.

97. Bae S, Park J, Kim JS. Cas-OFFinder: a fast and versatile algorithm that searches for potential off-target sites of Cas9 RNA-guided endonucleases. *Bioinfor- matics* 2014, 30:1473–1475.

98. Cradick TJ, Qiu P, Lee CM, Fine EJ, Bao G. COS- MID: a web-based tool for identifying and validating CRISPR/Cas off-target sites. *Mol Ther Nucl Acids* 2014, 3:e214.

99. Moreno-Mateos MA, Beaudoin JD, Fernandez JP, Mis EK, Khokha MK, Giraldez AJ. CRISPRscan: designing highly efficient sgRNAs for CRISPR-Cas9 targeting in vivo. *Nat Methods* 2015, 12:982–988.

100. Fu Y, Sander JD, Reyon D, Cascio VM, Joung JK. Improving CRISPR-Cas nuclease specificity using truncated guide RNAs. *Nat Biotechnol* 2014, 32:279–284.

101. Cho SW, Kim S, Kim JM, Kim JS. Targeted genome engineering in human cells with the Cas9 RNA- guided endonuclease. *Nat Biotechnol* 2013, 31:230–232.

102. Kleinstiver BP, Pattanayak V, Prew MS, Tsai SQ, Nguyen NT, Zheng Z, Joung JK. High-fidelity CRISPR–Cas9 nucleases with no detectable genome-wide off-target effects. *Nature* 2016, 529:490–495.

103. Slaymaker IM, Gao L, Zetsche B, Scott DA, Yan WX, Zhang F. Rationally engineered Cas9 nucleases with improved specificity. *Science* 2016, 351:84–88.

104. Tsai SQ, Zheng Z, Nguyen NT, Liebers M, Topkar VV, Thapar V, Wyvekens N, Khayter C, lafrate AJ, Le LP, et al. GUIDE-seq enables genome-wide profiling of off-target cleavage by CRISPR-Cas nucleases. *Nat Biotechnol* 2015, 33:187–197.

105. Singh R, Kuscu C, Quinlan A, Qi Y, Adli M. Cas9- chromatin binding information enables more accurate CRISPR off-target prediction. *Nucleic Acids Res* 2015, 43:e118.

106. Frock RL, Hu J, Meyers RM, Ho YJ, Kii E, Alt FW. Genome-wide detection of DNA double-stranded breaks induced by engineered nucleases. Nat Biotechnol 2015, 33:179–186.

107. Hendel A, Fine EJ, Bao G, Porteus MH. Quantifying on-and off-target genome editing. Trends Biotechnol 2015, 33:132–140.

108. Kim D, Bae S, Park J, Kim E, Kim S, Yu HR, Hwang J, Kim JI, Kim JS. Digenome-seq: genome-wide profiling of CRISPR-Cas9 off-target effects in human cells. Nat Methods 2015, 12:237–243.

109. Lee JH, Park IH, Gao Y, Li JB, Li Z, Daley GQ, Zhang K, Church GM. A robust approach to identifying tissue-specific gene expression regulatory variants using personalized human induced pluripotent stem cells. PLoS Genet 2009, 5:e1000718.

110. Yoshioka S, Fujii W, Ogawa T, Sugiura K, Naito K. Development of a mono-promoter-driven CRISPR/ Cas9 system in mammalian cells. Sci Rep 2015, 5:18341.

111. Sharma R, Anguela XM, Doyon Y, Wechsler T, DeKelver RC, Sproul S, Paschon DE, Miller JC, Davidson R, Shivak D. In vivo genome editing of the albumin locus as a platform for protein replacement therapy. *Blood* 2015, 126:1777–1784.

112. Ellis HM, Yu D, DiTrizio T, Court DL. High efficiency mutagenesis, repair, and engineering of chromosomal DNA using single-stranded oligonucleotides. Proc Natl Acad Sci USA 2001, 98:6742–6746.

113. Orthwein A, Noordermeer SM, Wilson MD, Landry S, Enchev RI, Sherker A, Munro M, Pinder J, Salsman J, Dellaire G, et al. A mechanism for the suppression of homologous recombination in G1 cells. Nature 2015, 528:422–426.

114. Gutschner T, Haemmerle M, Genovese G, Draetta GF, Chin L. Post-translational regulation of Cas9 during G1 enhances homology-directed repair. Cell Rep 2016, 14:1555–1566.

115. Maruyama T, Dougan SK, Truttman MC, Bilate AM, Ingram JR, Ploegh HL. Increasing the efficiency of precise genome editing with CRISPR-Cas9 by inhibition of nonhomologous end joining. Nat Biotechnol 2015, 33:538–542.

116. Richardson CD, Ray GJ, DeWitt MA, Curie GL, Corn JE. Enhancing homology-directed genome editing by catalytically active and inactive CRISPR-Cas9 using asymmetric donor DNA. Nat Biotechnol 2016, 34:339–344.

Chapter 2 – *In situ* Gene Therapy via AAV-CRISPR-Cas9-Mediated Targeted Gene Regulation

2.1 Abstract

Development of efficacious *in vivo* delivery platforms for CRISPR-Cas9 based epigenome engineering will be critical to enable the ability to target human diseases without permanent modification of the genome. Towards this, we utilized split-Cas9 systems to develop a modular adeno-associated viral (AAV) vector platform for CRISPR-Cas9 delivery to enable the full spectrum of targeted *in situ* gene regulation functionalities, demonstrating robust transcriptional repression (up to 80%) and activation (up to 6-fold) of target genes in cell culture and mice. We also applied our platform for targeted *in vivo* gene repression mediated gene therapy for retinitis pigmentosa (RP). Specifically, we engineered targeted repression of *Nrl*, a master regulator of rod photoreceptor determination, and demonstrated *Nrl* knockdown mediates *in situ* reprogramming of rod cells into cone-like cells that are resistant to RP-specific mutations, with concomitant prevention of secondary cone loss. Furthermore, we benchmarked our results from *Nrl* knockdown, with those from *in vivo Nrl* knockout via gene editing. Taken together, our AAV-CRISPR-Cas9 platform for *in vivo* epigenome engineering enables a robust approach to target disease in a genomically scarless and potentially reversible manner.

2.2 Introduction

The recent advent of RNA-guided effectors derived from clustered regularly interspaced short palindromic repeats (CRISPR)–CRISPR-associated (Cas) systems has transformed our ability to engineer genomes[1–11]. In addition to gene editing, CRISPR-Cas9 can also be utilized for transcriptional regulation, in which catalytically inactivated "dead" Cas9 (dCas9) can be fused to transcriptional effectors to activate or repress gene expression[12–16]. Applications of these systems for gene therapy, coupled with the growing knowledge of the genetic and pathogenic basis of disease, are likely to have great impact.

Realizing the full potential for CRISPR based *in situ* genome and epigenome engineering entails the development of corresponding safe and efficient gene transfer platforms. In this regard, a range of novel viral and non-viral based approaches have been developed for *in vitro* and *in vivo* delivery of CRISPRs[17–26]. Here we develop a CRISPR delivery platform using adeno-associated viruses (AAVs), since they are the preferred vectors for gene transfer due to their mild immune response, low toxicity, long-term transgene expression, and favorable safety profile[27,28]. Although advantageous as delivery vectors, AAVs suffer from a limited packaging capacity (~4.7 kb). This limited capacity does not typically accommodate the payload requirements of delivering a dCas9, the associated guide RNA (gRNA), and also dCas9-fused effector domains for epigenome engineering. To overcome this limitation, utilizing recent split-Cas9 systems that use two AAV vectors for CRISPR-Cas9 delivery[29–32], we leveraged the resulting packaging capacity in each to engineer and optimize a broader range of genome regulation functionalities, including multiplex targeting via single or dual-gRNA delivery.

We applied this system to target retinitis pigmentosa (RP) in a mouse model of the disease. RP is an inherited retinal dystrophy affecting ~1 in every 4000 individuals in the general population

and is characterized by progressive degeneration of rod photoreceptor cells in the retina, followed by deterioration and death of cone photoreceptor cells[33,34]. Affected patients with RP bear mutations in over 200 causative genes[35], which limits the potential effectiveness of conventional gene therapy strategies. Additionally, targeted gene repair typically relies on endogenous homologous recombination machinery, which is usually diminished in activity in post-mitotic cells. Correspondingly, in this study, we utilized a therapeutic *in situ* cellular reprogramming strategy to overcome these challenges in both gene therapy and endogenous tissue regeneration, by aiming to switch a mutation-sensitive cell type to a functionally related cell type resistant to that mutation. Specifically, we targeted *Nrl*, a master regulator of rod versus cone photoreceptor determination, which activates *Nr2e3*, a transcription factor that represses transcription of multiple cone-specific genes[36]. Consistent with this, transgenic strategies in mice have demonstrated that knockdown of rod photoreceptor determinant *Nrl* in adult rod cells results in reprogramming of rods into cone-like cells resistant to rod photoreceptor RP-specific mutations, with prevention of secondary cone loss[35]. Recent work has also demonstrated that in adult rod cells, *in situ* genome-editing of rod photoreceptor determinant *Nrl* results in reprogramming of rods into cone-like cells that are resistant to rod photoreceptor RP-specific mutations, as well as prevention of secondary cone loss[37,38]. Building on these studies, we conducted targeted *in situ Nrl* gene repression in the mouse retina to determine whether we could reprogram rods into cone-like cells in a genomically scarless manner. We also benchmarked these results with those obtained via Cas9 based gene editing of *Nrl*.

2.3 Materials and Methods

2.3.1 Vector design and construction

See "*Chapter S1: Supplementary Notes: Description of effectors"* for annotated sequence information on the modules used for the AAV vector constructions. Split-Cas9/dCas9 AAV vectors were constructed by sequential assembly of corresponding gene blocks (IDT) into a custom synthesized rAAV2 vector backbone. gRNA sequences were inserted into NCas9 or dNCas9 plasmids by cloning oligonucelotides (IDT) encoding spacers into AgeI cloning sites via Gibson assembly.

2.3.2 Guide RNA (gRNA) designs

Editing gRNAs were designed utilizing the *in silico* tool: MIT CRISPR Design and Broad Institute CRISPRko (https://portals.broadinstitute.org/gpp/public/analysis-tools/sgrna-design). Regulation gRNAs were designed utilizing an *in silico* tool to predict gRNAs[57].

2.3.3 Mammalian cell culture

All HEK293T cells were grown in Dulbecco's Modified Eagle Medium (10%) supplemented with 10% FBS and 1% Antibiotic-Antimycotic (ThermoFisher Scientific) in an incubator at 37 °C and 5% CO_2 atmosphere. HEK 293T cells were plated in 24-well plates for AAV transductions. Hematopoietic stem cells expressing CD34 (CD34+ cells) were grown in serum free StemSpan™ SFEM II with StemSpan™ CD34+ Expansion Supplement (10X) (all from StemCell Technologies). CD34+ cells were plated in 96-well plates for AAV transductions.

2.3.4 Production of AAVs

AAV8 was utilized for *in vivo* studies in the liver, AAV2-Y444F was used for *in situ* studies in the eye, AAV6 was utilized for *in vitro* studies in CD34+ cells, AAV-DJ was utilized for *in vitro* studies in HEK293T cells.

Large-scale production: Virus was either prepared by the Gene Transfer, Targeting and Therapeutics (GT3) core at the Salk Institute of Biological Studies (La Jolla, CA), or in house utilizing the GT3 core protocol. Briefly, AAV2/8, AAV2/2-Y444F, AAV2/6, AAV2/DJ virus particles were produced using HEK293T cells via the triple transfection method and purified via an iodixanol gradient[58]. Confluency at transfection was between 80% and 90%. Media was replaced with pre-warmed media 2 hours before transfection. Each virus was produced in 5 x 15 cm plates, where each plate was transfected with 7.5 μg of pXR-capsid (pXR-8, pXR-2-Y444F, pXR-6, pXR-DJ), 7.5 of μg recombinant transfer vector, and 22.5 μg of pAd5 helper vector using PEI (1μg/μL linear PEI in 1xDPBS pH 4.5, using HCl) at a PEI:DNA mass ratio of 4:1. The mixture was incubated for 10 minutes at RT and then applied dropwise onto the media. The virus was harvested after 72 hours and purified using an iodixanol density gradient ultracentrifugation method. The virus was then dialyzed with 1 x PBS (pH 7.2) supplemented with 50 mM NaCl and 0.0001% of Pluronic F68 (Thermo Fisher) using 100kDA filters (Millipore), to a final volume of ~1 mL and quantified by qPCR using primers specific to the ITR region, against a standard (ATCC VR-1616). *AAV-ITR-F: 5'-CGGCCTCAGTGAGCGA-3' and AAV-ITR-R: 5'-GGAACCCCTAGTGATGGAGTT-3'.*

Small-scale production: Small-scale AAV preps were prepared using 6-well plates containing HEK293T cells, which were co-transfected with 0.5 μg pXR-capsid, 0.5 μg recombinant transfer vector, and 1.5 μg pAd5 helper vector using PEI. The cells and supernatant were harvested

after 72 hours, and the crude extract was utilized to transduce HEK293T cells in 24 well plates. Small-scale production virus was utilized to generate data from Figure 2.1 and Figure S1.1.

2.3.5 Lipid-Mediated Cell Transfections

One day prior to transfection, HEK293T cells were seeded in a 24-well plate at a cell density of 1–2E+5 cells per well. 0.5 µg of each plasmid was added to 25 µl of Opti-MEM medium, followed by addition of 25 µl of Opti-MEM containing 2 µl of Lipofectamine 2000. The mixture was incubated at room temperature for 15 min and then added to the cells. The entire solution was added to the cells in a 24-well plate and mixed by gently swirling the plate. Media was changed after 24 hours, and the plate was incubated at 37°C for 72 h in a 5% CO_2 incubator. Cells were harvested, spun down and frozen at -80°C.

2.3.6 T7E1 assay

To examine the efficacy of the *Nrl* gRNAs, we performed T7E1 assay in immortalized mouse fibroblasts. Briefly, cells were transfected with pAAV-U6-gRNA and hCas9 (Addgene 41815) using Lipofectamine 2000 (ThermoFisher). Two days after transfection, the cells were harvested and genomic DNA was extracted with DNeasy Blood & Tissue kit (QIAGEN), and a T7E1 (NEB) assay was done following manufacturer's instructions. Primers to amplify genomic regions are listed as following: NRL-F: ACCTCTCTCTGCTCAGTCCC; NRL-R: GACATGCTGGGCTCCTGTC. The cleavage frequency was calculated from the proportion of cut bands intensity to total bands intensity.

2.3.7 Animal AAV Injections

All animal procedures were performed in accordance with protocols approved by the Institutional Animal Care and Use Committee (IACUC) of the University of California, San Diego and adhered to the ARVO Statement for the Use of Animals in Ophthalmic and Vision Research. All mice were acquired from Jackson labs. AAV injections were done in adult C57BL/6J mice (10 weeks) through tail-vein injections using 5E+11 vg/mouse of each split-Cas9 (total virus of 1E+12 vg/mouse), or in rd10, NRL-EGFP, and C57BL/6J neonates (P7) through subretinal injections as previously described[59,60] using ~1E+10 vg/mouse of each split-Cas9 (total virus of ~2E+10). For subretinal injections, approximately 0.3µl AAV2-Y444F was introduced into the subretinal space using a pulled angled glass pipette controlled by a FemtoJet (Eppendorf). The left eyes were uninjected for within-animal controls. Experimental mice were anesthetized with an intraperitoneal injection of a mixture of ketamine and xylazine. Pupils were dilated with 1% topical tropicamide. Subretinal injection was performed under direct visualization using a dissecting and a glass micropipette (internal diameter 50~75 µm). 1µl of AAV mixture was injected into the subretinal space through a small scleral incision. A successful injection was judged by creation of a small subretinal fluid bleb. Fundus examination was performed immediately following injection, and mice showing any sign of retinal damage such as bleeding were excluded from final animal counts.

2.3.8 Doxycycline administration

Mice transduced with pAAV inducible-Cas9 vectors were given IP injections of 200 mg Doxycyline in 10 mL 0.9% NaCl with 0.4 mL of 1N HCl, three times a week for four weeks.

2.3.9 Optokinetic nystagmus (OKN) tests

Visual acuity testing of all animals was conducted at 5 weeks after injection with an optomotor testing apparatus as previously reported[61]. Briefly, a virtual reality chamber was created with four computer monitors facing into a square. A virtual cylinder, covered with a vertical sine wave grating, was drawn and projected onto the monitors using software running on a Java application. The animal was placed on a platform within a clear cylinder (diameter ~30 cm) in the center of the square. A video camera situated above the animal provided real-time video feedback on another computer screen. From the mouse's point of view, the monitors appeared as large windows through which the animals viewed the rotating cylinder. Each mouse was placed on the platform in a quiet environment before the test until it became accustomed to the test conditions with minimal movement. The virtual stripe cylinder was set up at the highest level of contrast (100%, black 0, white 255, illuminated from above 250 cd/m^2), with the number of stripes starting from 4 per screen (2 black and 2 white). The test began with 1 min of clockwise rotation at a speed of 13. (The baseline value is 10, at which the bars move 1 pixel/cycle. Values less than 10 delay the cycle by X*100 ms, with a minimum value of 1). An unbiased observer tracked and recorded the head movements of the mouse. The test was then repeated with 1 min of counterclockwise rotation. The data were measured by cycles/degree (c/d) and expressed as mean ± s.e.m. with comparison using a t-test statistical analysis. A p value <0.05 was considered statistically significant.

2.3.10 Histology

Mice were humanely sacrificed by CO_2. Eyeballs were dissected, marked with the injection site and fixed in 4% PFA. Cornea, lens, and vitreous were removed from each eye without disturbing the retina. The remaining retina containing eyecup was infiltrated with 30% sucrose and

embedded in OCT compound. Horizontal frozen sections were cut on a cryostat. Care was taken to obtain retinal sections from control and experimental groups along comparable points along the dorsal-ventral axis. Retinal cross-sections were prepared for histological evaluation by immunofluorescence staining.

2.3.11 Immunofluorescence

Retinal cryosections were rinsed in PBS and blocked in 0.5% Triton X-100 and 5% BSA in PBS for 1 hour at room temperature, followed by an overnight incubation in primary antibodies at 4°C. After three washed in PBS, sections were incubated with secondary antibody. Cell nuclei were counterstained with DAPI (49,6-diamidino-2-phenylindole). The following antibodies were used: mouse anti-Rhodopsin monoclonal antibody (Abcam ab3267), rabbit anti-Opsin polyclonal antibody (Millipore AB5405), rabbit anti-Cone Arrestin polyclonal antibody (Millipore AB15282). The following secondary antibodies, Alexa Fluor-488 or 555-conjugated anti-mouse or rabbit immunoglobulinG (IgG) (Invitrogen) were used at a dilution of 1:500. Sections were mounted with Fluoromount-G (Southern Biotech) and coverslipped. Images were captured using Olympus FV1000 confocal microscope.

2.3.12 Gene expression analysis and RT-qPCR

RNA from cells was extracted using RNeasy kit (Qiagen, 74104), from liver using RNeasy Plus Universal Kit (Qiagen, 73442) and from eyeballs using AllPrep DNA/RNA Mini Kit (Qiagen, 80204). cDNA was synthesized from RNA using Protoscript II Reverse Transcriptase Kit (NEB, E6560L). Real-time PCR (qPCR) reactions were performed using the KAPA SYBR Fast qPCR Kit (Kapa Biosystems, KK4601), with gene specific primers (Table S1.2) in technical triplicates and in

biological triplicates. Relative mRNA expression was calculated using the comparative CT (ΔΔCT) method and normalized to β–actin or GAPDH. Mean fold change and standard deviation were calculated using Microsoft Excel.

2.3.13 Genomic DNA extraction and NGS preps

Genomic DNA from cells and tissues was extracted using DNeasy Blood and Tissue Kit (Qiagen, 69504), according to the manufacturer's protocol. Next generation sequencing libraries were prepared as follows. Briefly, 4-10 μg of input whole liver gDNA was amplified by PCR with primers that amplify 150 bp surrounding the sites of interest (Table S.1.2) using KAPA Hifi HotStart PCR Mix (Kapa Biosystems, KK2602). PCR products were gel purified (Qiagen, 28704), and further purified (Qiagen PCR Purification Kit, 28104) to eliminate byproducts. Library construction was done with NEBNext Multiplex Oligos for Illumina kit (NEB, E7335S). 10-25 ng of input DNA was amplified with indexing primers. Samples were then purified and quantified using a qPCR library quantification kit (Kapa Biosystems, KK4824). Samples were then pooled and loaded on an Illumina Miseq (150 bp paired-end run or 150 single-end run) at 4nM concentrations. Data analysis was performed using CRISPR Genome Analyzer[40].

2.3.14 ELISA

Levels of serum *Afp* were measured using the alpha-fetoprotein (Afp) mouse ELISA kit (Abcam ab210905) according to manufacturer's guidelines. First, 50 μL of 2 μg/mL Capture Antibody was added to each well of a 96-well of a high bind microplate (ab210903). The plates were sealed and incubated overnight at 4°C on a plate rocker. The plates were manually washed three times with 350 μL of 1X Wash Buffer (ab206977). To reduce non-specific binding, the plates

were blocked by adding 300 µL of 1X Blocking Buffer (ab210904) to each well. The plates were then sealed and incubated at RT for 2 hours. Plates were washed as described above. The Afp protein standards were diluted in 1X Blocking Buffer (ab210904) and prepared for a two-fold diluted standard curve. Samples were diluted 1:20 in 1X Blocking Buffer (ab210904), 50 µL of sample and standard (in duplicates) were added onto the plates and allowed to bind for 2 hours. Plates were washed as described above. Then, 50 µL of 0.5 µg/mL of Detector Antibody was added to each well and incubated for 1 hour at RT. The plates were washed as described above. HRP-Streptavidin solution (ab20901) was added to each well at a 1:7500 dilution and incubated at RT for 1 hour. Plates were washed as described above. Then, 100 µL of TMB Substrate was added to each well and incubated until optimal blue density was obtained. Finally, 100 µL of stop solution was added to each well. The absorbance was immediately determined on a microplate reader (BioRad iMark) at a wavelength of 450 nm.

2.4 Results

2.4.1 *In vitro* and *in vivo* genome editing via a dual-AAV split-Cas9 system

We first confirmed that split-Cas9 constructs delivered as AAVs were functional *in vitro* and *in vivo*. Expression cassettes of split-*Streptococcus pyogenes* (SpCas9) and gRNA were delivered via a dual-AAV vector system (Figure S1.1). The first AAV contains a gRNA driven by a human RNA polymerase III promoter, U6, and a N-terminal Cas9 (NCas9) fused to an N-intein driven by a CMV promoter, as well as a polyadenylation (polyA) signal[39]. The second AAV cassette contains a CMV driven C-terminal Cas9 (CCas9) fused to a C-intein as well as a polyA signal. We confirmed targeted genome editing through next-generation sequencing (NGS)[40] across two distinct cell types *in vitro* (Figure S1.1), notably also observing robust AAV6 mediated editing

in human CD34+ hematopoietic stem cells. We additionally confirmed *in vivo* genome editing in adult C57BL/6J mice injected with 5E+11 vg/split-Cas9/mouse through the tail-vein (Figure S1.1).

As a hit and run approach suffices for genome editing and is preferable over long-term nuclease expression, we next engineered small-molecule inducibility[32,41,42] of *in vivo* CRISPR-Cas9 editing activity. Specifically, we engineered one AAV construct to bear a minimal CMV promoter with a tetracycline response element (TRE) up-stream of the C-Intein-CCas9 fusion, while the other bore a full length CMV promoter that drives expression of the N-Intein-NCas9 fusion and a tet-regulatable-activator (tetA). The binding of tetA to the TRE, upon doxycycline addition, allows for inducible expression of the CCas9 and thereby temporal regulation of genome editing (Figure S1.1). We confirmed robust functioning of this system both *in vitro* and *in vivo* (Figure S1.1). Taken together these studies confirmed the functionality of the dual-AAV split-Cas9 format for CRISPR-Cas9 delivery.

2.4.2 *In vitro and in vivo* genome regulation via a dual-AAV split-dCas9 system

Next, to engineer targeted genome repression and activation, we utilized a dead split-Cas9 (dCas9) protein and its fusion to repression and activation domains (specifically a KRAB and a VP64+rTA (VR) domain respectively) (Figure 2.1)[12,14–16,43]. Utilizing the dual-AAV strategy enabled us to package these additional effector domains without exceeding the viral packaging capacity. We confirmed functionality via *in vitro* experiments in HEK293T cells targeting *CXCR4* for repression and *RHOX1* for activation utilizing the AAV-DJ serotype, with control non-targeting virus (equal viral titers). For *in vivo* AAV delivery, we performed tail vein injections at titers of 5E+11 vg/split-dCas9/mouse using the AAV8 serotype, and harvested mice livers 4 weeks post-

injection. We achieved 80% *in vivo* repression at the *Cd81* locus (n=4, p<0.0001), and over 2-fold *in vivo* activation at the *Afp* locus (n=4, p=0.0117). Taken together, we confirmed targeted gene repression and activation, as assayed via quantitative RT-qPCR, in both *in vitro* and *in vivo* scenarios and across multiple genomic loci (Figures 2.1).

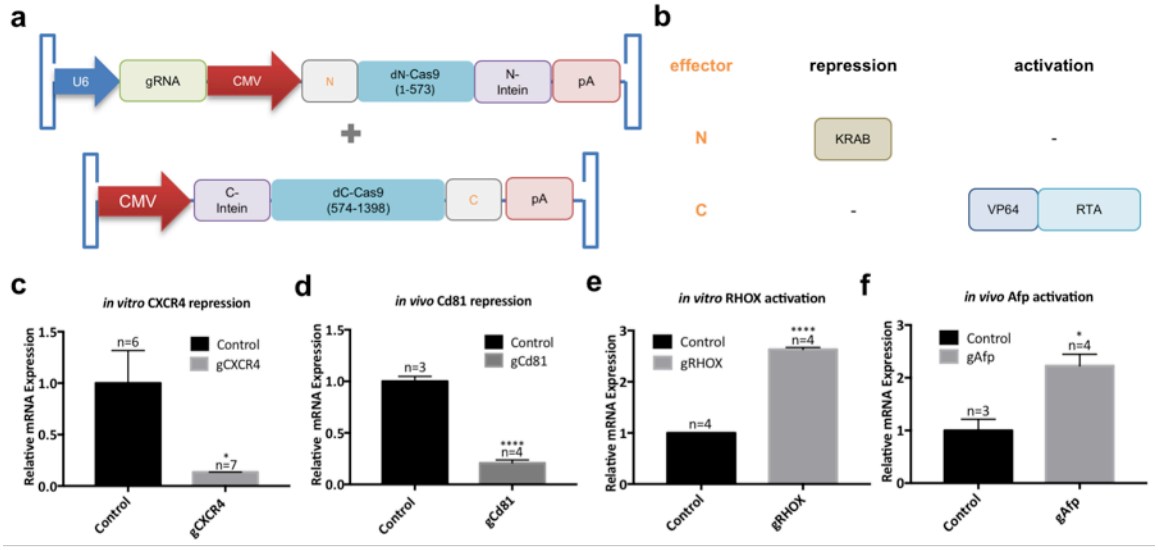

Figure 2.1: Versatile genome regulation via a modular dual-AAV split-dCas9 system. (a) Schematic of intein-mediated split-dCas9 pAAVs for genome regulation. **(b)** Approach for modular usage of effector cassettes to enable genome repression via a KRAB-dCas9 repressor fusion protein, and genome activation via a dCas9-VP64-RTA fusion protein. **(c)** In vitro CXCR4 repression in HEK293T cells utilizing two spacers targeting the CXCR4 locus, as determined by RT-qPCR. Controls consist of a gRNA targeting the AAVS1 locus. (n=3; error bars are s.e.m.; Student's t-test; p=0.0127). **(d)** In vivo Cd81 repression in adult mice livers utilizing two spacers targeting the Cd81 locus, as determined by RT-qPCR. Control mice received non-targeting AAV8 virus at the same titers, 5E+11 vg/split-dCas9/mouse. (n=4; error bars are s.e.m.; Student's t-test; p<0.0001). **(e)** In vitro RHOX activation in HEK293T cells utilizing two spacers targeting the RHOX locus, as determined by RT-qPCR. Controls consist of a gRNA targeting the AAVS1 locus. (n=3; error bars are s.e.m.; Student's t-test; p<0.0001). **(f)** In vivo Afp activation in adult mice livers utilizing two spacers targeting Afp locus, as determined by RT-qPCR. Control mice received non-targeting AAV8 virus at the same titers, 5E+11 vg/split-dCas9/mouse. (n=4; error bars are s.e.m.; Student's t-test; p=0.0117).

To see if we could further improve targeted genome regulation, we screened additional repression and activation domains by taking advantage of the modular vector designs of our dual-AAV-CRISPR platform (Figure 2.2). Specifically, for our activation system, we evaluated coupling

of additional VP64 or P65 domains onto the N-terminal of the dCas9 vector (dNCas9). The additional domains indeed yielded enhanced activation of a target locus (*ASCL1*) in HEK293T cells, with a ~17-fold higher activation with VP64 (n=3, p=0.0387) and ~23-fold higher activation with P65 (n=3, p=0.0069) (Figure 2.2), implying that tethering of a VP64 or P65 domain on the N-terminal in addition to the existing VP64-RTA on the C-terminal led to improved gene activation. We further confirmed this improved architecture *in vivo* in mice, observing over 6-fold activation at the *Afp* locus (n=4, p=0.0271) (Figure 2.2). In addition, to evaluate the *in vivo* kinetics of CRISPR-based gene regulation, we performed a time-course ELISA on mice injected with 5E+11 vg/split-dCas9/mouse of AAV8 VP64-dCas9-VR-Afp, which were bled weekly for 10 weeks. Control mice received equal titers of a non-targeting AAV8 virus. We observed that *Afp* activation peaks at week 6, with a 19 ng/mL concentration of *Afp* in the blood, from a baseline of 3.8 ng/mL (calculated based on an *Afp* protein standard curve) (Figure 2.2).

Figure 2.2: Domain optimization for AAV-CRISPR regulation. (a) Taking advantage of the extra space in the split-dCas9 system, additional activation domains were fused onto the C-terminal, and additional repression domains were fused onto the N-terminal. **(b)** Domain optimization for AAV-CRISPR activation (left panel): Activity of multiple N-terminal domain fusions: VP64 and P65 were evaluated and notably addition of a VP64 domain yielded ~17-fold higher gene expression, and addition of P65 yielded ~23-fold higher expression after transfection. (n=3; error bars are s.e.m.; one-way ANOVA; p=0.0387 and p=0.0069, respectively; HEK293T cells; locus: *ASCL1*). Based on this, a VP64 activation domain was added onto the dNCas9 vector and the *in vivo Afp* activation experiments were repeated in mice (right panel) receiving 5E+11 vg/split-dCas9/mouse of AAV8 split-VP64-dCas9-VR-Afp. Control mice received non-targeting AAV8 virus at the same titers, 5E+11 vg/split-dCas9/mouse. Mice were harvested at week 4. A >6-fold activation of *Afp* was observed with the additional VP64 domain. (n=4; error bars are s.e.m.; Student's *t*-test; p=0.0271). **(c)** To determine the *in vivo* kinetics of CRISPR activation, C57BL/6J mice were injected with 5E+11 vg/split-dCas9/mouse of AAV8 split-VP64-dCas9-VR-Afp and were bled weekly. Control mice received non-targeting AAV8 virus at the same titers, 5E+11 vg/split-dCas9/mouse. *Afp* concentrations were calculated based on *Afp* protein standard curve. *Afp* concentration peaked at week 6, at ~19.2 ng/mL compared to a baseline of ~3.8 ng/mL, showing a ~5-fold increase in *Afp* concentration. (n=6; error bars are s.e.m.; two-way ANOVA with Dunnett's multiple comparisons post-hoc test). **(d)** Domain and guide RNA optimization for AAV-CRISPR repression: activity of multiple C-terminal domain fusions: KRAB, DNA methyltransferase (DNMT3A or DNMT3L), and FOG1 were evaluated, however, no significant additional repression in transient repression assays was observed. Higher repression was observed when utilizing two gRNAs. (n=3; error bars are s.e.m.; HEK293T cells; locus: *CXCR4*).

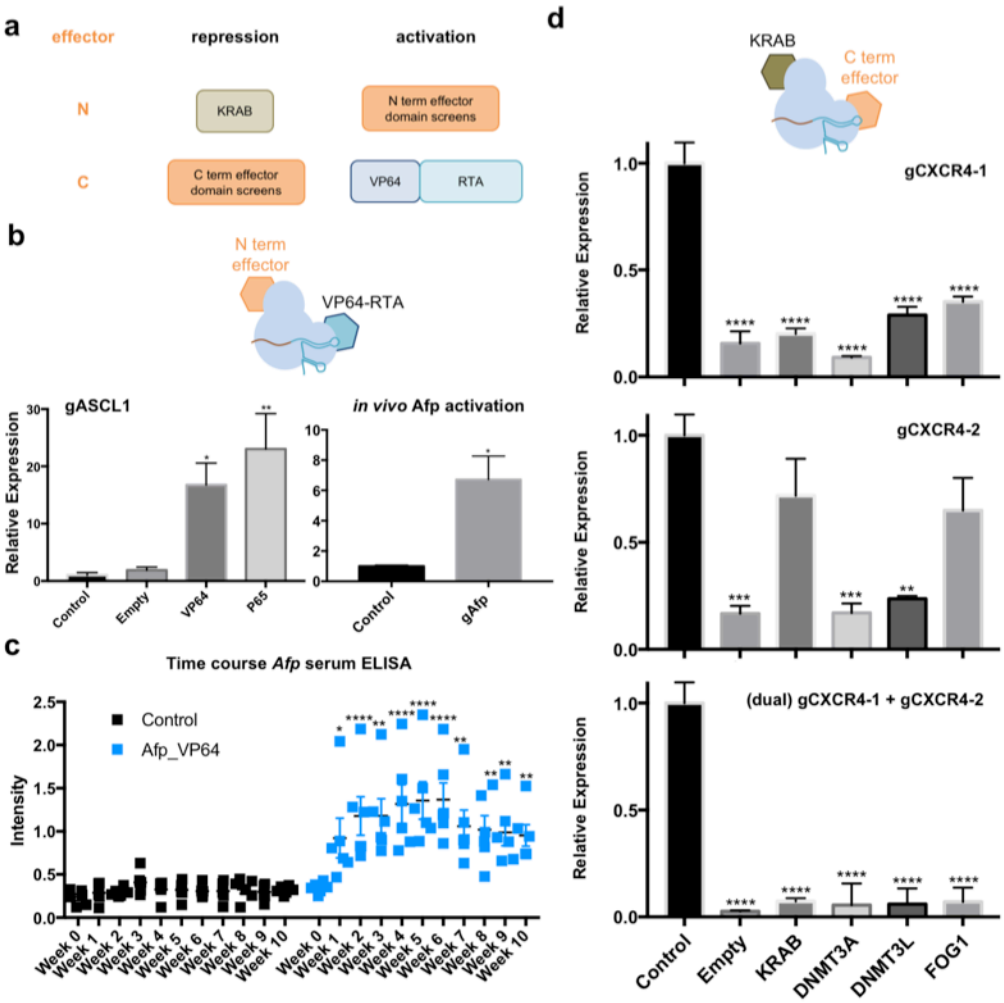
a
effector
repression
activation
N
KRAB
N term effector domain screens
C
C term effector domain screens
VP64
RTA
b
N term effector
VP64-RTA
gASCL1
Relative Expression
Control
Empty
VP64
P65
in vivo Afp activation
Control
gAfp
c
Time course Afp serum ELISA
Control
Afp_VP64
Intensity
Week 0
Week 1
Week 2
Week 3
Week 4
Week 5
Week 6
Week 7
Week 8
Week 9
Week 10
d
KRAB
C term effector
gCXCR4-1
gCXCR4-2
(dual) gCXCR4-1 + gCXCR4-2
Relative Expression
Control
Empty
KRAB
DNMT3A
DNMT3L
FOG1

Next, we focused on optimizing targeted gene repression. While dCas9 alone can cause repression as it can halt RNA polymerase progression by steric hindrance when targeted downstream of the transcription start site (TSS), or can competitively interfere with transcription factor binding when targeted to promoter regions or regulatory elements[12,44,45], KRAB-dCas9 has been shown to be more potent for gene silencing than dCas9 alone[45–47]. To determine whether we could further improve the repression system, we evaluated fusions of additional KRAB, DNA methyltransferase domains (DNMT3A or DNMT3L)[48,49], or FOG1[50] onto the C-terminal of the dCas9 vector (dCCas9), and also the use of single versus dual-gRNAs. To avoid repeat sequences in the AAV that can compromise vector stability and viral titers, we utilized a human U6 promoter and a mouse U6 promoter to drive each individual gRNA, and also used non-homologous trans-activating small RNA (tracrRNA) sequences[51]. However, we did not observe an increase in repression with the addition of repression domains, implying that a single KRAB domain suffices for our transient repression assays in HEK293T cells, but the use of dual-gRNAs consistently yielded enhanced gene repression (Figure 2.2, Figure S1.2).

2.4.3 *In situ* cellular reprogramming of rod photoreceptors

Having established a robust *in vivo* genome regulation system, we next focused on applying the same in a therapeutically relevant mouse model of disease, specifically focusing on retinitis pigmentosa (RP). For these studies we utilized a AAV2 mutant containing a tyrosine to phenylalanine substitution (Y444F) due to its high retinal transduction efficiency[52]. To further boost gene targeting, we utilized a dual-gRNA approach per above. We designed corresponding Cas9-based editing (split-Cas9-Nrl), and dCas9-based repression system (split-KRAB-dCas9-Nrl) where the KRAB repressor domain is fused to the N-terminal of the dCas9 protein (Figure 2.3). We first delivered the split-Cas9-Nrl vectors into mouse embryonic fibroblasts (MEFs) and assessed gene

editing rates through a T7E1 assay, which cuts mismatched dsDNA, and confirmed editing rates of about ~25% (Figure S1.3).

Figure 2.3: Dual-AAV split-dCas9 repression strategy rescues retinal function in rd10 mice. **(a)** Schematic of AAV construction for split-Cas9-Nrl gene editing vectors. To avoid repeat sequences in the AAV, a human U6 promoter and a mouse U6 promoter were utilized to drive each individual gRNA. **(b)** Approach for modular usage of effector cassettes to enable genome repression via a split-KRAB-dCas9-Nrl repressor. **(c)** Target sequences for *Nrl* genome editing and repression. PAM sequences are underlined. **(d)** Immunofluorescence analysis of $mCAR^+$ cells in rd10 mouse retina treated with AAV-split-Cas9-Nrl or AAV-split-KRAB-dCas9-Nrl. Mice were treated at P7 and harvested at P50. Rhodopsin, green; mCAR, Red; DAPI, blue. **(e)** Quantification of $mCAR^+$ cells in rd10 mice retina treated with AAV-split-Cas9-Nrl or AAV-split-KRAB-dCas9-Nrl. Results are shown as mean ± s.e.m. (*$p<0.05$. Student's *t*-test, n=3). **(f)** Increased ONL thickness in rd10 mice retina treated with AAV-split-Cas9-Nrl and AAV-split-KRAB-dCas9-Nrl. ONL, outer nuclear layer. Results are shown as mean ± s.e.m. (*$p<0.05$. Student's *t*-test, n=3). **(g)** Quantification of b wave amplitude in AAV-split-Cas9-Nrl and AAV-split-KRAB-dCas9-Nrl injected, and un-injected rd10 mice. Results are shown as mean ± s.e.m. (*$p<0.05$. Paired student's *t*-test, n=3). **(h)** Quantification of visual acuity in rd10 mouse retina treated with AAV-split-Cas9-Nrl and AAV-split-KRAB-dCas9-Nrl. Results are shown as mean ± s.e.m. (*$p<0.05$. Student's *t*-test, n=3)

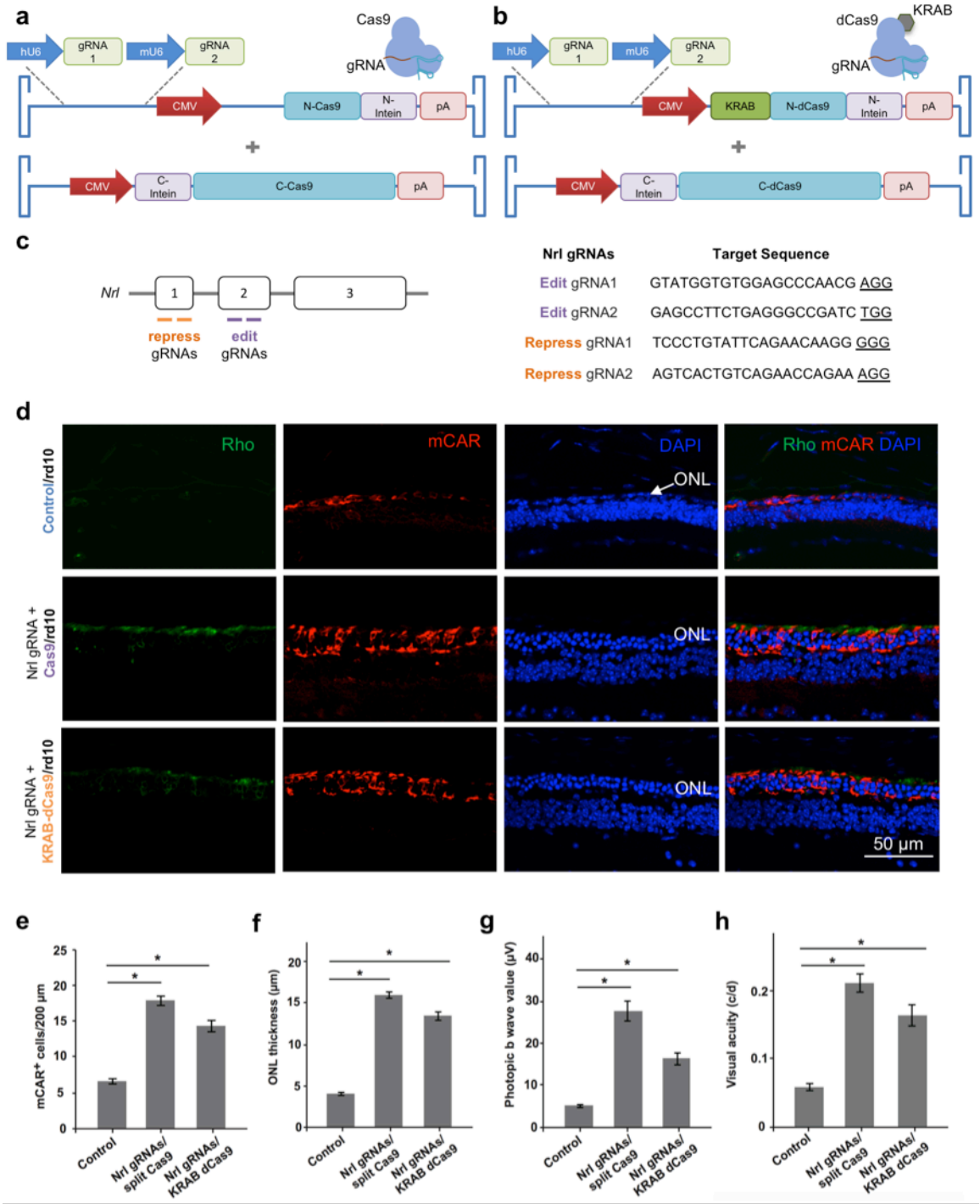
a
hU6
gRNA 1
mU6
gRNA 2
CMV
N-Cas9
N-Intein
pA
C-Intein
C-Cas9
Cas9
gRNA
b
KRAB
N-dCas9
C-dCas9
dCas9
c
Nrl
repress gRNAs
edit gRNAs
Nrl gRNAs
Target Sequence
Edit gRNA1 GTATGGTGTGGAGCCCAACG AGG
Edit gRNA2 GAGCCTTCTGAGGGCCGATC TGG
Repress gRNA1 TCCCTGTATTCAGAACAAGG GGG
Repress gRNA2 AGTCACTGTCAGAACCAGAA AGG
d
Rho
mCAR
DAPI
Rho mCAR DAPI
ONL
Control/rd10
Nrl gRNA + Cas9/rd10
Nrl gRNA + KRAB-dCas9/rd10
50 µm
e
mCAR+ cells/200 µm
f
ONL thickness (µm)
g
Photopic b wave value (µV)
h
Visual acuity (c/d)
Control
Nrl gRNAs/ split Cas9
Nrl gRNAs/ KRAB dCas9

We next used quantitative RT-qPCR to measure the relative expression levels of photoreceptor-specific genes in reprogrammed retinas and controls. We confirmed down-regulation of *Nrl*, with simultaneous upregulation of cone specific genes, i.e. *Arr3, Opnlmw, PDE6C, GNAT2* (Figure S1.3). To assay rod reprogramming into cone-like cells, we transduced transgenic Nrl-EGFP mice bearing GFP-labeled rod photoreceptor cells, with 2E+10 vg/split-Cas9/mouse of AAV-split-Cas9 or 2E+10 vg/split-dCas9/mouse of AAV-split-KRAB-dCas9 systems targeting *Nrl* into the subretinal space at postnatal day 7 (P7). These were then sacrificed for histology at P30 via flash-freezing, sectioning, and staining of retinas for a cone marker, cone arrestin (mCAR). We indeed observed a reprogrammed photoreceptor phenotype with both our split-Cas9-Nrl and split-KRAB-dCas9-Nrl *in vivo,* with a decrease in Nrl-GFP+ rod photoreceptors (Figure S1.3) and an increase in the number of mCAR positive cells (Figure S1.3). We next repeated the above experiments in normal wild-type C57BL6 mice. Consistent with the results in Nrl-EGFP transgenic mice, we again observed a reprogrammed photoreceptor phenotype in the retina, characterized by a significant increase in the number of mCAR and mOpsin positive cells (Figure S1.3). Taken together, the above experiments confirmed the efficacy of our dual-AAV-CRISPR platform in engineering *in situ* cellular reprogramming of retinal rod cells.

2.4.4 Prevention of photoreceptor degeneration in a RP mouse model

Next, to validate our approach in a RP mouse model, we targeted *Nrl* in rd10 mice, a model of autosomal recessive RP. These mice carry a spontaneous mutation of the rod-phosphodiesterase gene, and exhibit rod degeneration around P18. By P60, rods are no longer detectable, with accompanying cone photoreceptor degeneration[53]. To assess if conversion of rods to cones is sufficient to reverse degeneration and rescue visual function, we subretinally injected split-Cas9-Nrl or split-KRAB-dCas9-Nrl in rd10 mice at P7. While untreated eyes had sparsely distributed

photoreceptor cell nuclei in the outer nuclear layer (ONL), split-Cas9-Nrl or split-KRAB-dCas9-Nrl treated eyes had ~2-3 layers of ONL, indicating that the treatment prevented photoreceptor degeneration and preserved ONL (Figure 2.3). To determine the effect of the treatment on cone physiological function and visual acuity, we also measured optic kinetic nystagmus (OKN) to quantify visual acuity 6 weeks after injection (P50). All eyes treated with split-KRAB-dCas9-Nrl had improved visual function as indicated by significantly higher visual acuity (Figure 2.3). Taken together, our split-KRAB-dCas9 AAV system thus paves the way for fine control of *in situ* gene expression for gene therapy of RP, and importantly also enables a scarless approach for *in vivo* genome engineering.

2.5 Discussion

Collectively, our integrated AAV-CRISPR delivery platform provides a facile and robust method to edit and regulate the expression of endogenous genes via Cas9 and dCas9 based effectors. In recent work, others and we have demonstrated the use of AAV-split-Cas9s[29,30]. Here, we establish a modular vector architecture whereby we also couple dCas9 and several transcriptional regulators with ease, thereby engineering the full spectrum of genome editing and regulation (both activation and repression) functionalities. This system has several advantages, including the utilization of a split-Cas9 system, which due to the limited cargo capacity of AAVs (~4.7kb), is an optimal approach to enable desired genome engineering applications. Additionally, one can utilize desired accessory elements of interest to optimize transcription of the payloads. We show that our AAV-CRISPR system can be utilized to achieve a high level of *in vivo* transcriptional repression (up to 80%) (Figure 2.1) and *in vivo* transcriptional activation (up to 6 fold increase)

(Figure 2.1), as well as for editing *in vitro* in HEK293T cells and CD34+ HSCs, and *in vivo* in C57BL/6J mice (Figure S1.1).

Furthermore, we demonstrated for the first time the utility of AAV-KRAB-dCas9 mediated *in situ* gene repression in the context of gene therapy, specifically, to prevent vision loss in a mouse model of retinitis pigmentosa (rd10 mice) (Figure 2.3). With our approach, we demonstrate reprogramming of rod to cone-like cell fate, with rescue of visual function, by targeted inactivation or repression of *Nrl*. Gene targeting efficiency was significantly improved with our dual-gRNA strategy. Using our cellular reprogramming approach, we demonstrate significant rescue and preservation of cone function. However, this approach may also reduce rod photoreceptor number and function, and therefore lead to night blindness. Nonetheless, studies have indicated that RP patients are willing to tolerate night blindness, as it is considered an acceptable risk given the potential for significant restoration of cone function, and therefore of daylight vision. Furthermore, as RP in advanced stages of the disease eventually leads to loss of both rods and cones, and therefore to legal blindness, this reprogramming strategy would represent an attractive therapeutic approach.

We note that secondary cone degeneration and death in RP may be due to toxic factors released from dying rods that damage cones, or to an unfavorable environment from ONL collapse that cannot maintain sufficient structural or physiological support for cones. It can be hypothesized that the preservation of rod cell bodies may thus provide the requisite support necessary to prevent secondary cone death. Indeed, *Gnat1*$^{-/-}$ knockout mice, which have severe rod dysfunction, have cones with near normal histology and function without significant rod degeneration or ONL collapse[54,55]. In fact, our current study showed increased ONL thickness in eyes treated with AAV-split-Cas9-Nrl and AAV-split-KRAB-dCas9-Nrl. Moving forward it will however be important to perform long-term studies in the mice to determine the effects of prolonged *Nrl* repression. As such,

an advantage of using a repression based system via the dual AAV-split-KRAB-dCas9 is that this strategy provides a potentially reversible approach for gene therapy, with no risk of mutagenesis due to the inactivation of the Cas9 nuclease activity[12,15]. In addition, recessive mutations in *NRL* can cause retinal degeneration, which is why an *in vivo* gene repression (versus gene editing) of *Nrl* to rescue cone degeneration is advantageous given the deleterious long-term effects of *Nrl* ablation.

An additional advantage of utilizing this system is that one can also potentially multiplex gene activation or repression[56], which could be beneficial for complex diseases that have multiple loci involved. Additionally, genes that are typically difficult to edit could also be readily accessed through the dCas9 system. Finally, since dCas9 lacks endonuclease activity, and there is no permanent change to the genome, off-target effects that can lead to oncogenesis can also be avoided. We also note some potential limitations of our system: utilizing a split-Cas9 system will have reduced targeting efficiency as both components, CCas9 and NCas9, have to be co-delivered to the target cell of interest to reconstitute Cas9 activity. Additionally, since dCas9 does not enable a permanent change to the genome, multiple treatments might be necessary. We however expect that with steady improvements in techniques for localized tissue-specific delivery and optimization of AAV production, these aspects will be progressively addressed.

Taken together, we believe that our CRISPR-dCas9 mediated *in situ* cellular reprogramming approach represents a promising strategy in the prevention of tissue degradation and restoration of normal tissue function, and points to an important approach towards the treatment of human diseases in a gene and mutation independent context. We also anticipate our programmable multi-functional AAV based synthetic delivery platform, through its ready programmability in CRISPR effector incorporation, will have broad utility in basic science and translational applications.

2.6 Acknowledgements

We thank Dr. Pedro Cabrales for help and advice with mouse work, and Derek Gao for help with Illumina MiSeq runs. We thank Hugh Chen, Sherina Malkani, Atharv Worlikar and Neha Shah in the Mali lab for help with molecular biology experiments and viral productions, and Udit Parekh for help with the manuscript.

We acknowledge generous support of this study by UCSD Institutional Funds, the Burroughs Wellcome Fund (1013926), the March of Dimes Foundation (5-FY15-450), the Kimmel Foundation (SKF-16-150), and NIH grants (R01HG009285, RO1CA222826, RO1GM123313). A.M. acknowledges a graduate fellowship from CONACYT and UCMEXUS.

Chapter 2 in part is a reprint of the material *Moreno AM, Fu X, Zhu J, Katrekar K, Shih YV, Marlett J, Cabotaje J, Tat J, Naughton J, Lisowski L, Varghese S, Zhang K[#], Mali P[#]. In situ gene therapy via AAV CRISPR-Cas9 mediated targeted gene regulation. Molecular Therapy (2018) 26:1818-1827*. The dissertation author was the primary author.

2.7 References

1. Charpentier, E and Doudna, JA (2013). Rewriting a genome. *Nature* **495**: 50–51.

2. Hwang, WY, Fu, Y, Reyon, D, Maeder, ML, Tsai, SQ, Sander, JD, Peterson RT, Yeh JR, Joung JK (2013). Efficient genome editing in zebrafish using a CRISPR-Cas system. *Nat Biotechnol* **31**: 227–229.

3. Li, D, Qiu, Z, Shao, Y, Chen, Y, Guan, Y, Liu, M, Li, Y, Gao, N, Wang, L, Lu, X, Zhao, Y, Liu, M (2013). Heritable gene targeting in the mouse and rat using a CRISPR-Cas system. *Nat Biotech* **31**: 681–683.

4. Mali, P, Esvelt, KM and Church, GM (2013). Cas9 as a versatile tool for engineering biology. *Nat Methods* **10**: 957–963.

5. Mali, P, Yang, L, Esvelt, KM, Aach, J, Guell, M, DiCarlo, JE, Norvile, JE, Church, GM

(2013). RNA-guided human genome engineering via Cas9. *Science* **339**: 823–6.

6. Nakayama, T, Fish, MB, Fisher, M, Oomen-Hajagos, J, Thomsen, GH and Grainger, RM (2013). Simple and efficient CRISPR/Cas9-mediated targeted mutagenesis in Xenopus tropicalis. *Genesis* **51**: 835–843.

7. Zhang, XH, Tee, LY, Wang, XG, Huang, QS and Yang, SH (2015). Off-target Effects in CRISPR/Cas9-mediated Genome Engineering. *Mol Ther Nucleic Acids* **4**: e264.

8. Shan, Q, Wang, Y, Li, J, Zhang, Y, Chen, K, Liang, Z, Zhang, K, Liu, J, Xi, JJ, Qiu, JL, Gao, C (2013). Targeted genome modification of crop plants using a CRISPR-Cas system. *Nat Biotech* **31**: 686–688.

9. Yang, D, Xu, J, Zhu, T, Fan, J, Lai, L, Zhang, J, Chen, YE (2014). Effective gene targeting in rabbits using RNA-guided Cas9 nucleases. *J. Mol. Cell Biol.* **6**: 97–99.

10. Yu, Z, Ren, M, Wang, Z, Zhang, B, Rong, YS, Jiao, R, Gao, G (2013). Highly efficient genome modifications mediated by CRISPR/Cas9 in Drosophila. *Genetics* **195**: 289–291.

11. Dicarlo, JE, Norville, JE, Mali, P, Rios, X, Aach, J and Church, GM (2013). Genome engineering in Saccharomyces cerevisiae using CRISPR-Cas systems. *Nucleic Acids Res.* **41**: 4336–4343.

12. Qi, LS, Larson, MH, Gilbert, LA, Doudna, JA, Weissman, JS, Arkin, AP, Lim, WA (2013). Repurposing CRISPR as an RNA-guided platform for sequence-specific control of gene expression. *Cell* **152**: 1173–1183.

13. Chavez, A, Scheiman, J, Vora, S, Pruitt, BW, Tuttle, M, P R Iyer, E, Lin, S, Kiani, S, Guzman, CD, Wiegand, DJ, Ter-Ovanesyan D, Braff, JL, Davidsohn, N, Housden BE, Perrimon, N, Weiss, R, Aach, J, Collins JJ, Church GM (2015). Highly efficient Cas9-mediated transcriptional programming. *Nat Meth* **12**: 326–328.

14. Hilton, IB, D'Ippolito, AM, Vockley, CM, Thakore, PI, Crawford, GE, Reddy, TE, Gersbach, CA (2015). Epigenome editing by a CRISPR-Cas9-based acetyltransferase activates genes from promoters and enhancers. *Nat. Biotechnol.* **33**: 510–7.

15. Mali, P, Aach, J, Stranges, PB, Esvelt, KM, Moosburner, M, Kosuri, S, Yang, L, Church, GM (2013). CAS9 transcriptional activators for target specificity screening and paired nickases for cooperative genome engineering. *Nat. Biotechnol.* **31**: 833–8.

16. Maeder, ML, Linder, SJ, Cascio, VM, Fu, Y, Ho, QH and Joung, JK (2013). CRISPR RNA-guided activation of endogenous human genes. *Nat Methods* **10**: 977–979.

17. Niu, Y, Shen, B, Cui, Y, Chen, Y, Wang, J, Wang, L, Kang, Y, Zhao, Z, Wei, S, Wei, L, Peng Ziang, A, Zhou, J, Guo, X, Bi, Y, Si, C, Hu, B, Dong, G, Wang, H, Zhou, Z, Li, T, Tan T, Pu, X, Wang, F, Ji, S, Zhou, Q, Huang, X, Ji, W, Sha, J (2014). Generation of gene-modified cynomolgus monkey via Cas9/RNA-mediated gene targeting in one-cell embryos.

Cell **156**: 836–843.

18. Su, S, Hu, B, Shao, J, Shen, B, Du, J, Du, Y, Zhou, J, Yu, L, Zhang, L, Chen, F, Sha, H, Cheng, L, Meng, F, Zou, Z, Huang, X (2016). CRISPR-Cas9 mediated efficient PD-1 disruption on human primary T cells from cancer patients. *Sci. Rep.* **6**: 20070.

19. Yin, H, Song, C-Q, Dorkin, JR, Zhu, LJ, Li, Y, Wu, Q, Park, A, Yang, J, Suresh, S, Bizhanova, A, Gupta, A, Bolukbasi, MF, Walsh, S, Bogorad, RL, Gao, G, Weng, Z, Dong, Y, Kotellansky, V, Wolfe, SA, Langer, R, Xue, W, Andersong, DG (2016). Therapeutic genome editing by combined viral and non-viral delivery of CRISPR system components in vivo. *Nat. Biotechnol.* **34**: 328–333.

20. Yin, H, Xue, W, Chen, S, Bogorad, RL, Benedetti, E, Grompe, M, Koteliansky, V, Sharp, PA, Jacks, T, Anderson, DG (2014). Genome editing with Cas9 in adult mice corrects a disease mutation and phenotype. *Nat. Biotechnol.* **32**: 551–553.

21. Zuris, JA, Thompson, DB, Shu, Y, Guilinger, JP, Bessen, JL, Hu, JH, Maeder, ML, Joung, JK, Chen, ZY, Liu, DR (2015). Cationic lipid-mediated delivery of proteins enables efficient protein-based genome editing in vitro and in vivo. *Nat Biotech* **33**: 73–80.

22. Xu, L, Park, KH, Zhao, L, Xu, J, El Refaey, M, Gao, Y, Zhu, H, Ma, J, Han, R (2016). CRISPR-mediated genome editing restores dystrophin expression and function in mdx mice. *Mol. Ther.* **24**: 564–569.

23. Ran, FA, Cong, L, Yan, WX, Scott, DA, Gootenberg, JS, Kriz, AJ, Zetsche, B, Wu, X, Makarova, KS, Koonin, EV, Sharp, PA, Zhang, F (2015). In vivo genome editing using Staphylococcus aureus Cas9. *Nature*. **9**:186-91.

24. Long, C, Amoasii, L, Mireault, AA, McAnally, JR, Li, H, Sanchez-Ortiz, E, Bhattacharyya, S, Shelton, JM, Bassel-Duby, R, Olson, EN (2015). Postnatal genome editing partially restores dystrophin expression in a mouse model of muscular dystrophy. *Science* **351**: aad5725.

25. Tabebordbar, M, Zhu, K, Cheng, JKW, Chew, WL, Widrick, JJ, Yan, WX, Maesner, C, Wu, EY, Xiao, R, Ran, FA, Cong, L, Zhang, F, Vandenberghe, LH, Church, GM, Wagers, AJ (2016). In vivo gene editing in dystrophic mouse muscle and muscle stem cells. *Science (80-.).* **351**: 407–411.

26. Nelson, CE, Hakim, CH, Ousterout, DG, Thakore, PI, Moreb, EA, Rivera, RMC, Madhavan, S, Pan X, Ran FA, Yan WX, Asokan, A, Zhang, F, Duan, D, Gersbach, CA (2016). In vivo genome editing improves muscle function in a mouse model of Duchenne muscular dystrophy. *Science (80-.).* **351**: 403–407.

27. Kotterman, MA, Chalberg, TW, Schaffer, DV (2015). Viral Vectors for Gene Therapy: Translational and Clinical Outlook. *Annu. Rev. Biomed. Eng.* **17**: 63–89.

28. Mingozzi, F, High, KA (2013). Immune responses to AAV vectors: Overcoming barriers to

successful gene therapy. *Blood* **122**: 23–36.

29. Chew, WL, Tabebordbar, M, Cheng, JKW, Mali, P, Wu, EY, Ng, AH, Zhu, K, Wagers, AJ, Church, GM (2016). A multifunctional AAV-CRISPR-Cas9 and its host response. *Nat Meth* **13**: 868–874.

30. Truong, D-JJ, Kuhner, K, Kuhn, R, Werfel, S, Engelhardt, S, Wurst, W, Ortiz, O (2015). Development of an intein-mediated split-Cas9 system for gene therapy. *Nucleic Acids Res.*: 1–9doi:10.1093/nar/gkv601.

31. Wright, A V, Sternberg, SH, Taylor, DW, Staahl, BT, Bardales, JA, Kornfeld, JE, Doudna, JA (2015). Rational design of a split-Cas9 enzyme complex. *Proc. Natl. Acad. Sci. U. S. A.* **112**: 2984–9.

32. Zetsche, B, Volz, SE and Zhang, F (2015). A split-Cas9 architecture for inducible genome editing and transcription modulation. *Nat. Biotechnol.* **33**: 139–142.

33. Hartong, DT, Berson, EL and Dryja, TP (2006). Retinitis pigmentosa. *Lancet* **368**: 1795–1809.

34. Hamel, C (2006). Retinitis pigmentosa. *Orphanet J. Rare Dis.* **1**: 40.

35. Montana, CL, Kolesnikov, A V, Shen, SQ, Myers, C a, Kefalov, VJ and Corbo, JC (2013). Reprogramming of adult rod photoreceptors prevents retinal degeneration. *Proc. Natl. Acad. Sci. U. S. A.* **110**: 1732–7.

36. Cheng, H, Khanna, H, Oh, ECT, Hicks, D, Mitton, KP and Swaroop, A (2004). Photoreceptor-specific nuclear receptor NR2E3 functions as a transcriptional activator in rod photoreceptors. *Hum. Mol. Genet.* **13**: 1563–1575.

37. Yu, W, Mookherjee, S, Chaitankar, V, Hiriyanna, S, Kim, J-W, Brooks, M, Ataeijannati, Y, Sun, X, Dong, L, Li, T, Swaroop, A, Wu, Z (2017). Nrl knockdown by AAV-delivered CRISPR/Cas9 prevents retinal degeneration in mice. *Nat. Commun.* **8**: 14716.

38. Zhu, J, Ming, C, Fu, X, Duan, Y, Hoang, DA, Rutgard, J, Zhang, R, Wang, W, Hou, R, Zhang, D, Zhang, E, Zhang, C, Hao, X, Zhang, K (2017). Gene and mutation independent therapy via CRISPR-Cas9 mediated cellular reprogramming in rod photoreceptors. *Cell Res*. **27**: 830-833.

39. Truong, DJ, Kühner, K, Kühn, R, Werfel, S, Engelhardt, S, Wurst, W, Ortiz, O (2015). Development of an intein-mediated split–Cas9 system for gene therapy. *Nucleic Acids Res.* **43**: 6450–6458.

40. Güell, M, Yang, L and Church, GM (2014). Genome editing assessment using CRISPR Genome Analyzer (CRISPR-GA). *Bioinformatics* **30**: 2968–2970.

41. Davis, KM, Pattanayak, V, Thompson, DB, Zuris, JA, Liu, DR (2015). Small molecule-triggered Cas9 protein with improved genome-editing specificity. *Nat. Chem. Biol.* **11**: 316–

8.

42. Nguyen, DP, Miyaoka, Y, Gilbert, LA, Mayerl, SJ, Lee, BH, Weissman, JS, Conklin, BR, Wells, JA (2016). Ligand-binding domains of nuclear receptors facilitate tight control of split CRISPR activity. *Nat. Commun.* **7**: 12009.

43. Chavez, A, Scheiman, J, Vora, S, Pruitt, BW, Tuttle, M, P R Iyer, E, Lin, S, Kiani, S, Guzman, CD, Wiegand, DJ, Ter-Ovanesyan, D, Braff, JL, Davidsohn, N, Housden, BE, Perrimon, N, Weiss, R, Aach, J, Collins, JJ, Church, GM (2015). Highly efficient Cas9-mediated transcriptional programming. *Nat. Methods*: **4**L326-8.

44. Farzadfard, F, Perli, SD and Lu, TK (2013). Tunable and Multifunctional Eukaryotic Transcription Factors Based on CRISPR/Cas. *ACS Synth. Biol.* **2**: 604–613.

45. Gilbert, LA, Larson, MH, Morsut, L, Liu, Z, Gloria, A, Torres, SE, Stern-Ginossar, N, Brandman, O, Whitehead, EH, Doudna, JA, Lim, WA, Weissman, JS, Qi, LS (2013). CRISPR-Mediated Modular RNA-Guided Regualtion of Transcription in Eukaryotes. *Cell* **154**: 442–451.

46. Kearns, NA, Genga, RMJ, Enuameh, MS, Garber, M, Wolfe, SA and Maehr, R (2014). Cas9 effector-mediated regulation of transcription and differentiation in human pluripotent stem cells. *Development* **141**: 219 LP-223.

47. Thakore, PI, M, DA, Song, L, Safi, A, Shivakumar, NK, Kabadi, AM, Reddy, TE, Crawford, GE, Gersbach, CA (2015). Highly specific epigenome editing by {CRISPR-Cas9} repressors for silencing of distal regulatory elements. *Nat Methods* **12**: 1143–1149.

48. Amabile, A, Migliara, A, Capasso, P, Biffi, M, Cittaro, D, Naldini, L, Lombardo, A (2016). Inheritable Silencing of Endogenous Genes by Hit-and-Run Targeted Epigenetic Editing. *Cell* **167**: 219–232.

49. Liu, XS, Wu, H, Ji, X, Stelzer, Y, Wu, X, Czauderna, S, Jian, Shu, Dadon, D, Young, RA, Jaenish, R (2016). Editing DNA Methylation in the Mammalian Genome. *Cell* **167**: 233–247.

50. O'Geen, H, Ren, C, Nicolet, CM, Perez, AA, Halmai, J, Le, VM, Mackay, JP, Farnham PJ, Segal DJ (2017). DCas9-based epigenome editing suggests acquisition of histone methylation is not sufficient for target gene repression. *Nucleic Acids Res.* **45**: 9901–9916.

51. Shen, JP, Zhao, D, Sasik, R, Luebeck, J, Birmingham, A, Bojorquez-Gomez, A, Licon, K, Klepper, K, Pekin, D, Beckett, A, Sanchez, K, Thomas, A, Kuo, CC, Du, D, Roguev, A, Lewis, NE, Chang, AN, Kreisberg, JF, Krogan, N, Qi, L, Ideker, T, Mali, P (2017). Combinatorial CRISPR-Cas9 screens for de novo mapping of genetic interactions. *Nat Meth*. **14**: 573-576.

52. Petrs-Silva, H, Dinculescu, A, Li, Q, Min, S-H, Chiodo, V, Pang, JJ, Zhong, L, Zolotukhin, S, Srivastava, A, Lewin, AS, Hauswirth, WW (2009). High-efficiency transduction of the mouse retina by tyrosine-mutant AAV serotype vectors. *Mol. Ther.* **17**: 463–471.

53. Chang, B, Hawes, NL, Hurd, RE, Davisson, MT, Nusinowitz, S and Heckenlively, JR (2002). Retinal degeneration mutants in the mouse. *Vision Res.* **42**: 517–525.

54. Calvert, PD, Krasnoperova, N V., Lyubarsky, AL, Isayama, T, Nicolo, M, Kosaras, B (2000). Phototransduction in transgenic mice after targeted deletion of the rod transducin alpha -subunit. *Proc. Natl. Acad. Sci.* **97**: 13913–13918.

55. Miyamoto, M, Aoki, M, Hirai, K, Sugimoto, S, Kawasaki, K and Imai, R (2010). A nonsense mutation in Gnat1, encoding the α subunit of rod transducin, in spontaneous mouse models of retinal dysfunction. *Exp. Eye Res.* **90**: 63–69.

56. Zalatan, JG, Lee, ME, Almeida, R, Gilbert, LA, Whitehead, EH, La Russa, M, Tsai, JC, Weissman, JS, Dueber, JE, Qi, LS, Lim, WA (2015). Engineering Complex Synthetic Transcriptional Programs with CRISPR RNA Scaffolds. *Cell* **160**: 339–350.

57. Horlbeck, MA, Gilbert, LA, Villalta, JE, Adamson, B, Pak, RA, Chen, Y, Fields, AP, Park CY, Corn, JE, Kampmann M, Weissman, JS (2016). Compact and highly active next-generation libraries for CRISPR-mediated gene repression and activation. *Elife* **5**.

58. Grieger, JC, Choi, VW and Samulski, RJ (2006). Production and characterization of adeno-associated viral vectors. *Nat. Protoc.* **1**: 1412–1428.

59. Matsuda, T and Cepko, CL (2004). Electroporation and RNA interference in the rodent retina in vivo and in vitro. *Proc. Natl. Acad. Sci. U. S. A.* **101**: 16–22.

60. Wang, S, Sengel, C, Emerson, MM and Cepko, CL (2014). A gene regulatory network controls the binary fate decision of rod and bipolar cells in the vertebrate retina. *Dev. Cell* **30**: 513–527.

61. Luo, J, Baranov, P, Patel, S, Ouyang, H, Quach, J, Wu, F, Qiu, A, Luo, H, Hicks, C, Zeng, J, Zhu, J, Lu, J, Sfeir, N, Wen, C, Zhang, M, Reade, V, Patel, S, Sinden, J, Sun, X, Shaw, P, Young, M, Zhang, K (2014). Human retinal progenitor cell transplantation preserves vision. *J. Biol. Chem.* **289**: 6362–6371.

Chapter 3 – Exploring protein orthogonality in immune space: a case study with AAV and Cas9 orthologs.

3.1 Abstract

A major hurdle in protein-based therapeutics, including CRISPR-Cas gene targeting approaches, is the interaction with the adaptive immune system which can lead to neutralization by circulating antibodies and clearance of treated cells by cytotoxic T-lymphocytes. To address this issue, we propose here the sequential use of orthologous proteins whose function is constrained by natural selection, but whose structure is subject to diversification via forces such as genetic drift. This would, in principle, allow for repeated treatments by 'immune orthogonal' orthologs without reduced efficacy due to lack of immune cross-reactivity among the proteins. To explore and validate this concept we chose 284 DNA targeting and 84 RNA targeting CRISPR effectors (including Cas9, Cpf1/Cas12a, and Cas13a, b, and c), and 167 Adeno-associated virus (AAV) capsid protein orthologs and developed a pipeline to compare total sequence similarity as well as predicted binding to class I and class II Major Histocompatibility Complex (MHC) proteins. Interestingly, MHC binding predictions revealed wide diversity among the set of DNA-targeting Cas orthologs, with 79% of pairs predicted not to elicit cross-reacting immune responses, while no global immune orthogonality among AAV serotypes was observed. We validated the computationally predicted immune orthogonality among three important Cas9 orthologs, from *S.*

pyogenes, *S. aureus*, and *C. jejuni* observing cross-reacting antibodies against AAV but not Cas9 orthologs in sera from immunized mice. Finally, to demonstrate the efficacy of multiple dosing with immune orthogonal orthologs, we delivered AAV-Cas9 targeting PCSK9 into BALB/c mice previously immunized against the AAV vector and/or the Cas9 payload, demonstrating that editing efficiency is compromised by immune recognition of either the AAV or Cas9, but, importantly, this effect is abrogated when using immune orthogonal orthologs. Moving forward, we anticipate this framework can be applied to prescribe sequential transient regimens of immune orthogonal protein therapeutics to circumvent pre-existing or induced immunity, and eventually, to rationally engineer immune orthogonality among protein orthologs.

3.2 Introduction

Protein therapeutics, including protein-based gene therapy, have several advantages over small-molecule drugs. They generally serve complex, specific functions, and have minimal off-target interference with normal biological processes. However, one of the fundamental challenges to any protein-based therapeutic is the interaction with the adaptive immune system. Neutralization by circulating antibodies through B-cell activation and clearance of treated cells by CD8+ cytotoxic T-lymphocytes (CTLs) create a substantial barrier to effective protein therapies [1-4]. Although for some applications the delay in the adaptive immune response to novel proteins may allow sufficient time for the initial dose to work, subsequent doses face faster and stronger secondary immune responses due to the presence of memory T- and B- cells. In addition, gene transfer studies have shown that host immune responses against the delivery vector and/or therapeutic transgene can eliminate treated cells, thus limiting the efficacy of the treatment [5-11].

A common approach to circumventing these issues has been to utilize human proteins, or to humanize proteins by substitution of non-human components [12,13]. However, this approach is

limited to a small set of therapeutic proteins naturally occurring in humans or closely related species. In addition, although the humanization of proteins can result in a significantly less immunogenic product, they still carry immunological risk [13]. Another way to circumvent an immune response to protein therapeutics is the removal of immunogenic T cell epitopes [14-16]. Once these epitopes are identified, substitution of key amino acids may reduce the protein's immunogenicity since modification of critical anchor residues can abrogate binding to MHC molecules and prevent antigen presentation. However, this can prove difficult due to the massive diversity at HLA loci. As epitope engineering must account for the substrate specificity of each different HLA allele, therapeutics would likely require unique modification for each patient. While epitope deletion/mutation has been successfully applied to several proteins [16,17], this can only preserve protein function when limited to small numbers of HLA alleles unrepresentative of the full diversity. Structural modifications such as PEGylation have also been known to reduce immunogenicity by interfering with antigen-processing mechanisms. However, there is evidence that PEG-specific antibodies are elicited in patients treated with PEGylated therapeutic enzymes [18-21].

Furthermore, protein therapies often require repeated treatments due to degradation of the protein, turnover of treated cells, or, in the case of gene therapy, reduced expression of the transgene [22,23]. This provides an even greater challenge as repeated exposure to the same antigen can elicit a more robust secondary immune response [24], which may completely inhibit subsequent dosage or even sensitize the immune system to antigens remaining from the initial exposure. In order to facilitate efficacious repeat protein therapies, we propose the use of orthologous proteins whose function is constrained by natural selection, but whose structure is subject to diversification by genetic drift. An ortholog, given sufficient sequence divergence, will not cross-react with the

immune response generated by exposure to the others, allowing repeat doses to avoid neutralization by existing antibodies and treated cells to avoid clearance by activated CTLs.

As a case study for exploring this approach we focused on the CRISPR-Cas9 system, perhaps the most anticipated therapeutic for gene editing [25-35]. Comparative genomics has demonstrated that Cas9 proteins are widely distributed across bacterial species and have diversified over an extensive evolutionary history [36-40]. Although there may be pre-existing immunity to Cas9s from pathogenic or commensal species [41-43], we hypothesized this diversity could provide a mechanism to circumvent inducing immunological memory by utilizing orthologous Cas9 proteins for each treatment.

An additional important consideration is the immunogenicity of the delivery vehicle or administration route for the Cas9 and associated guide RNA (gRNA). In this regard, adeno-associated viruses (AAVs) have emerged as a highly preferred vehicle for gene delivery, as they are associated with low immunogenicity and toxicity [8,9], which promotes transgene expression [44,45] and treatment efficacy. Despite the relatively low immunogenicity of AAV vectors, antibodies against both the capsid and transgene may still be elicited [10,46-52]. Additionally, the prevalence of neutralizing antibodies (NAB) against AAVs in the human population [53] and cross-reactivity between serotypes [54] remains a hurdle for efficacious AAV therapy. Although AAVs were initially considered non-immunogenic due to their poor transduction of antigen-presenting cells (APCs) [55], it is now known that they can transduce dendritic cells (DCs) [56] and trigger innate immune responses through Toll-like receptor (TLR) signaling pathways [57]. The ability to transduce DCs is dependent on AAV serotype and genome, and may be predictive of overall immunogenicity [58]. A previous study exploring the utility of the AAV-Cas9 system observed a humoral immune response to both AAV and Cas9, as well as an expansion of myeloid and T-cells

in response to Cas9 [52], highlighting the need to confront this issue when further developing gene therapies.

To evaluate the immune orthogonality of AAV-delivered CRISPR-Cas systems, we analyzed 284 DNA targeting and 84 RNA targeting CRISPR effectors, and 167 AAV VP1 orthologs. By comparing total sequence similarity as well as predicted binding strengths to class I and class II MHC molecules, we constructed graphs of immune cross-reactivity and computed cliques of proteins that are orthogonal in immunogenicity profiles. Although MHC epitopes do not predict antibody epitopes, the induction of the more powerful memory response is primarily dependent on reactivation of memory B-cells with help from memory T-cells through the presentation of antigens on class II MHC molecules [59,60]. Next, we experimentally confirmed our immunological predictions by assaying treated mice for induction of protein-targeting antibodies and of T-cell-mediated cytotoxicity against AAV and Cas9 proteins. Finally, we demonstrated in multiple contexts that consecutive dosing with immune orthogonal orthologs circumvents the inhibition of effective gene editing caused by immune recognition of the AAV vector and Cas9 transgene.

3.3 Methods

3.3.1 K-mer Analyses

For Cas9, we initially chose 91 orthologs cited in exploratory studies cataloging the diversity of the Cas9 protein [36,40,84-87], including several that are experimentally well-characterized. We subsequently expanded our analysis to a total of 240 Cas9 orthologs and 44 Cpf1/Cas12a orthologs for DNA-targeting CRISPR-associated effector proteins, and 84 RNA-targeting CRISPR-associated effectors including Cas13a, b and c. For AAVs, we analyzed 167

sequences, focusing in on all 13 characterized human serotypes, as well as one isolate from rhesus macaque (rh32), one engineered variant (DJ), and one reconstructed ancestral protein (Anc80L65). We then compared total sequence similarity (immunologically uninformed) as well as predicted binding to class I and class II MHC molecules (immunologically informed) between these proteins. Immunologically uninformed sequence comparison was carried out by checking a sliding window of all contiguous k-mers in a protein for their presence in another protein sequence with either zero or one mismatch.

3.3.2 MHC Binding Predictions

Immunologically informed comparison was done in a similar fashion, but using only those k-mers predicted to bind to at least one of 81 HLA-1 alleles using netMHC 4.0 [88] for class I (alleles can be found at http://www.cbs.dtu.dk/services/NetMHC/MHC_allele_names.txt), and at least one of 5,620 possible MHC II molecules based on 936 HLA-2 alleles using netMHCIIpan 3.1[89] for class II (alleles can be found at http://www.cbs.dtu.dk/services/NetMHCIIpan-3.1/alleles_name.list). We compared the use of netMHC to alternative immune epitope prediction platforms such as the Immune Epitope Database (iedb.org) [90] and found very strong agreement across software. Ultimately, we chose netMHC because of the larger number of HLA alleles it supports. Sequences were defined as binding if the predicted affinity ranked in the top 2% of a test library of 400,000 random peptides as suggested in the software guidelines. Generation of immune orthogonal cliques was carried out using the Bron-Kerbosch algorithm. Briefly, a graph was constructed with each ortholog as a vertex, where the edges are defined by the number of shared immunogenic peptides between the connecting vertices. Sets of proteins for which every pair in the set is immune orthogonal constitutes a clique.

3.3.3 Phylogenetics and Species Classification

For phylogenetic analyses, protein sequences were aligned using MUSCLE, and distance was calculated using the BLOSUM 62 matrix excluding indels. Phylogeny of AAV serotypes was created using neighbor-joining on major serotype sequences. Categorization of Cas9 orthologs into commensal, pathogenic, environmental, and extremophile species of origin was done by assessing the source of the sample sequence. Sequences isolated from species which had been observed in human-associated samples were classified as pathogenic if they had been reported to cause disease (this would include species which are normally commensal, but opportunistically pathogenic), and commensal otherwise. Sequences from species which are not known to be associated with the human microbiome were classified as environmental unless the species was uniquely isolated from extreme environments including but not limited to geothermal vents, deep anoxic groundwater, fossil fuel deposits, and polar ice.

3.3.4 Vector design and construction

Split-SpCas9 AAV vectors were constructed by sequential assembly of corresponding gene blocks (IDT) into a custom synthesized rAAV2 vector backbone [91,92]. The first AAV contains a gRNA driven by a human RNA polymerase III promoter, U6, and a N-terminal Cas9 (NCas9) fused to an N-intein driven by a CMV promoter, as well as a polyadenylation (polyA) signal (Truong et al., Moreno et al.) The second AAV cassette contains a CMV driven C-terminal Cas9 (CCas9) fused to a C-intein as well as a polyA signal. gRNA sequences were inserted into NCas9 plasmids by cloning oligonucelotides (IDT) encoding spacers into AgeI cloning sites via Gibson assembly. pX601-AAV-CMV::NLS-SaCas9-NLS-3xHA-bGHpA;U6::BsaI-sgRNA was a gift from Feng Zhang (Addgene plasmid # 61591)

3.3.5 AAV Production

AAV2/8, AAV2/2, AAV2/5, AAV2/DJ virus particles were produced using HEK293T cells via the triple transfection method and purified via an iodixanol gradient [93]. Confluency at transfection was between 80% and 90%. Media was replaced with pre-warmed media 2 hours before transfection. Each virus was produced in 5 x 15 cm plates, where each plate was transfected with 7.5 μg of pXR-capsid (pXR-8, pXR-2, pXR-5, pXR-DJ), 7.5 of μg recombinant transfer vector, and 22.5 μg of pAd5 helper vector using PEI (1μg/μl linear PEI in 1x DPBS pH 4.5, using HCl) at a PEI:DNA mass ratio of 4:1. The mixture was incubated for 10 minutes at RT and then applied dropwise onto the media. The virus was harvested after 72 hours and purified using an iodixanol density gradient ultracentrifugation method. The virus was then dialyzed with 1x PBS (pH 7.2) supplemented with 50 mM NaCl and 0.0001% of Pluronic F68 (Thermo Fisher) using 100kDA filters (Millipore), to a final volume of ~1 ml and quantified by qPCR using primers specific to the ITR region, against a standard (ATCC VR-1616).

AAV-ITR-F: 5'-CGGCCTCAGTGAGCGA-3' and

AAV-ITR-R: 5'-GGAACCCCTAGTGATGGAGTT-3'.

3.3.6 Animal studies

All animal procedures were performed in accordance with protocols approved by the Institutional Animal Care and Use Committee (IACUC) of the University of California, San Diego. All mice were acquired from Jackson labs. AAV injections were done in adult male C57BL/6J or BALB/c mice (10 weeks) through retro-orbital injections using $1x10^{12}$ vg/mouse.

3.3.7 CFA immunizations

CFA immunizations were prepared by mixing CFA (Sigma-Aldrich) with 5 μg Cas9 protein or PBS at a 1:1 ratio using two syringes connected by an elbow joint to create an even emulsion. 200 μL of CFA emulsion was injected subcutaneously into the flanks of adult mice.

3.3.8 ELISA

PCSK9: Levels of serum PCSK9 were measured using the Mouse Proprotein Convertase 9/PCSK9 Quantikine ELISA kit (R&D Systems) according to manufacturer's guidelines. Briefly, serum samples were diluted 1:200 in Calibrator diluent and allowed to bind for 2 h onto microplate wells that were precoated with the capture antibody. Samples were then sequentially incubated with PCSK9 conjugate followed by the PCSK9 substrate solution with extensive intermittent washes between each step. The amount of PCSK9 in serum was estimated colorimetrically using a standard microplate reader (BioRad iMark).

Cas9 and AAV: Recombinant SpCas9 protein (PNA Bio, cat. no. CP01), or SaCas9 protein (ABM good, cat no. K144), was diluted in 1x coating buffer (Bethyl), and 0.5 μg was used to coat each well of 96-well Nunc MaxiSorp Plates (ab210903) overnight at 4 °C. For AAV experiments, 10^9 vg of AAV-2, -5, -8 or -DJ in 1x coating buffer was used to coat each well of 96-well Nuc MaxiSorp Plates. Plates were washed three times for 5 min with 350 μl of 1x Wash Buffer (Bethyl) and blocked with 300 μl of 1x BSA Blocking Solution (Bethyl) for 2 h at RT. The wash procedure was repeated. Serum samples were added at 1:40 dilution, and plates were incubated for 5 h at 4 °C with shaking. Wells were washed three times for 5 min, and 100 μl of HRP-labeled goat anti-mouse IgG1 (Bethyl; diluted 1:100,000 in 1% BSA Blocking Solution) was added to each well. After incubating for 1hr at RT, wells were washed four times for 5 min, and 100 μl of TMB Substrate

(Bethyl) was added to each well. Optical density (OD) at 450 nm was measured using a plate reader (BioRad iMark).

3.3.9 NGS quantification of editing

Genomic DNA was extracted from samples of mouse livers using a DNA extraction kit (Qiagen). A 200 bp region containing the target cut site of the PCSK9 gene was amplified by PCR using 0.5 μg DNA (~100,000 diploid genomes) as the template. Libraries were prepared using NEBNext Illumina library preparation kit and sequenced on an Illumina HiSeq. Each sample was sequenced to a target depth of 100,000 reads. Adaptors were trimmed from resulting fastqs using AdapterRemoval [94] and NHEJ-repaired cleavage events resulting in a mutation were quantified using CRISPResso [95].

3.3.10 Splenocyte Clearance Assay

Splenocyte clearance assays were performed similarly to previous work [96]. Briefly, spleens from adult C57BL/6J mice were harvested and treated to remove erythrocytes and dead cells. These cells were then diluted to 10^7 cells/ml and split into two pools, one of which was pulsed for 40 min with a pool of the 30 most immunogenic T-cell epitopes in SpCas9 (according to our predictions) at 1 μg/ml each and labeled with the CellTrace Violet fluorescent dye (ThermoFisher). The other pool was pulsed with a matching amount of DMSO, and labeled with the green fluorescent dye CFSE (ThermoFisher). A 1:1 mixture of these cells were then injected into naïve or CFA-immunized mice at week 1 or 3.5 retro-orbitally at 3-6 x 10^7 cells per mouse. Spleens from these mice were harvested 16-20 hours later, treated to remove erythrocytes, and analyzed by flow cytometry to assess the degree of specific clearance of the CTV+ cells which were pulsed with Cas9 peptides.

3.3.11 Statistics

PCSK9 ELISA data from immunization experiments (Figures 3, S7), were normalized per mouse to the average of the first 4 weeks of the experiment (during which time no active dose was given), and then analyzed using a two-way repeated measures ANOVA to account for both time and group membership as independent variables. Post hoc Tukey tests were used to compare across groups at each timepoint as shown in Figure 3.3c.

3.3.12 Epitope prediction and peptide synthesis

The MHC-binding peptides for our mouse model were predicted using the netMHC-4.0 and netMHCIIpan-3.1 online software with the alleles H-2-Db and H-2-Kb for class I and H-2-IAb for class II. For MHCII, the top 10 peptides for Sp- and SaCas9 and top 5 peptides for AAV-8 and AAV-DJ by percentile binding were selected for synthesis by Synthetic Biomolecules as crude materials. For MHCI, we selected the top 20 peptides for Sp- and SaCas9 and the top 10 for AAV-8 and AAV-DJ. All peptides were dissolved in DMSO with a concentration of 40 mg ml^{-1} and stored at −20 °C.

3.3.13 IFN-γ ELISPOT assay

CD8+ T cells were isolated from splenocytes using magnetic bead positive selection (Miltenyi Biotec) 6 weeks after virus infection. A total of 2×10^5 CD8+ T cells were stimulated with 1×10^5 LPS-blasts loaded with 10 μg of individual peptide in 96-well flat-bottom plates (Immobilon-P, Millipore) that were coated with anti-IFN-γ mAb (clone AN18, Mabtech) in triplicate. Concanavalin A (ConA) was used as positive control. After 20 h of incubation, biotinylated anti-mouse IFN-γ mAb (R4-6A2; Mabtech), followed by ABC peroxidase (Vector

Laboratories) and then 3-amino-9-ethylcarbazole (Sigma-Aldrich) were added into the wells. Responses are expressed as number of IFN-γ SFCs per 1×10^6 CD8+ T cells.

3.4 Results

3.4.1 Immune response to AAV and Cas9

One of the major obstacles for sequential gene therapy treatments is the presence of neutralizing antibodies against the delivery vehicle and transgene cargo induced by the first administration of the therapy (Figure 3.1a). To determine the humoral immune response kinetics to AAV-CRISPR therapeutics (Figure 3.1b), focusing as an exemplar on the AAV8 capsid and the Cas9 transgene, we first injected C57BL/6J mice retro-orbitally with 10^{12} vg of AAV8-SaCas9 targeting proprotein convertase subtilisin/kexin type 9 (PCSK9), a promising gene target that when disrupted can reduce Low Density Lipoprotein (LDL) levels and protect against cardiovascular disease. Consistent with a previous study [61], mice had reduced PCSK9 serum levels as early as one week post-injection due to successful SaCas9 mediated gene-editing, which was sustained for the entire duration of the experiment (4 weeks) (Figure 3.1c). We noted that a subset of the mice developed IgG1 antibodies against the SaCas9 protein (Figure 3.1d). Additionally, mice developed humoral immunity to the AAV8 capsid within one-week post-injection (Figure 3.1e). Finally, we also confirmed a CD4+ T-cell response against AAV8 and SaCas9 for a subset of predicted MHCII epitopes on these proteins using an ELISPOT (Figure S2.1). To evaluate the feasibility of multiple dosing with AAV-Cas9, we next investigated whether immune orthogonal sets of AAV and Cas9 orthologs exist.

Figure 3.1: Protein based therapeutics elicit an adaptive immune response: experimental and *in silico* analyses. (a) Proteins have substantial therapeutic potential, but a major drawback is the immune response to both the therapeutic protein and its delivery vehicle. **(b)** As a case study, we explored the CRISPR-Cas9 systems and corresponding delivery vehicles based on AAVs. **(c)** Mice were injected retro-orbitally with 10^{12} vg/mouse of AAV8-SaCas9 targeting the PCSK9 gene or a non-targeting control (empty vector). A decrease in PCSK9 serum levels, due to successful gene targeting, can be seen in mice receiving AAV-SaCas9-PCSK9 virus (n=6 mice for each group). Each line represents an individual mouse. **(d)** Immune response to the payload was detected in ELISAs for the SaCas9 protein. (n=12) Each line represents an individual mouse. **(e)** Immune response to the delivery vehicle was detected in ELISAs for the AAV8 virus capsid (n=12 mice). Each line represents an individual mouse. **(f)** *In silico* workflow used to find immune orthogonal protein homolog cliques. **(g)** Immunologically uninformed sequence comparison was carried out by checking all *k*-mers in a protein for their presence in another protein sequence with either zero or one mismatch. The x-axis corresponds to *k*, while MHC I and MHC II show overlap only of peptides predicted to bind to MHC class I and class II molecules. 48% of Cas9 pairs show no 6-mer overlap, and 79% of pairs show no overlapping MHC-binding peptides. **(h)** Same as **(g)** but for AAV VP1 capsid proteins. All AAV pairs contain overlapping MHC-binding peptides.

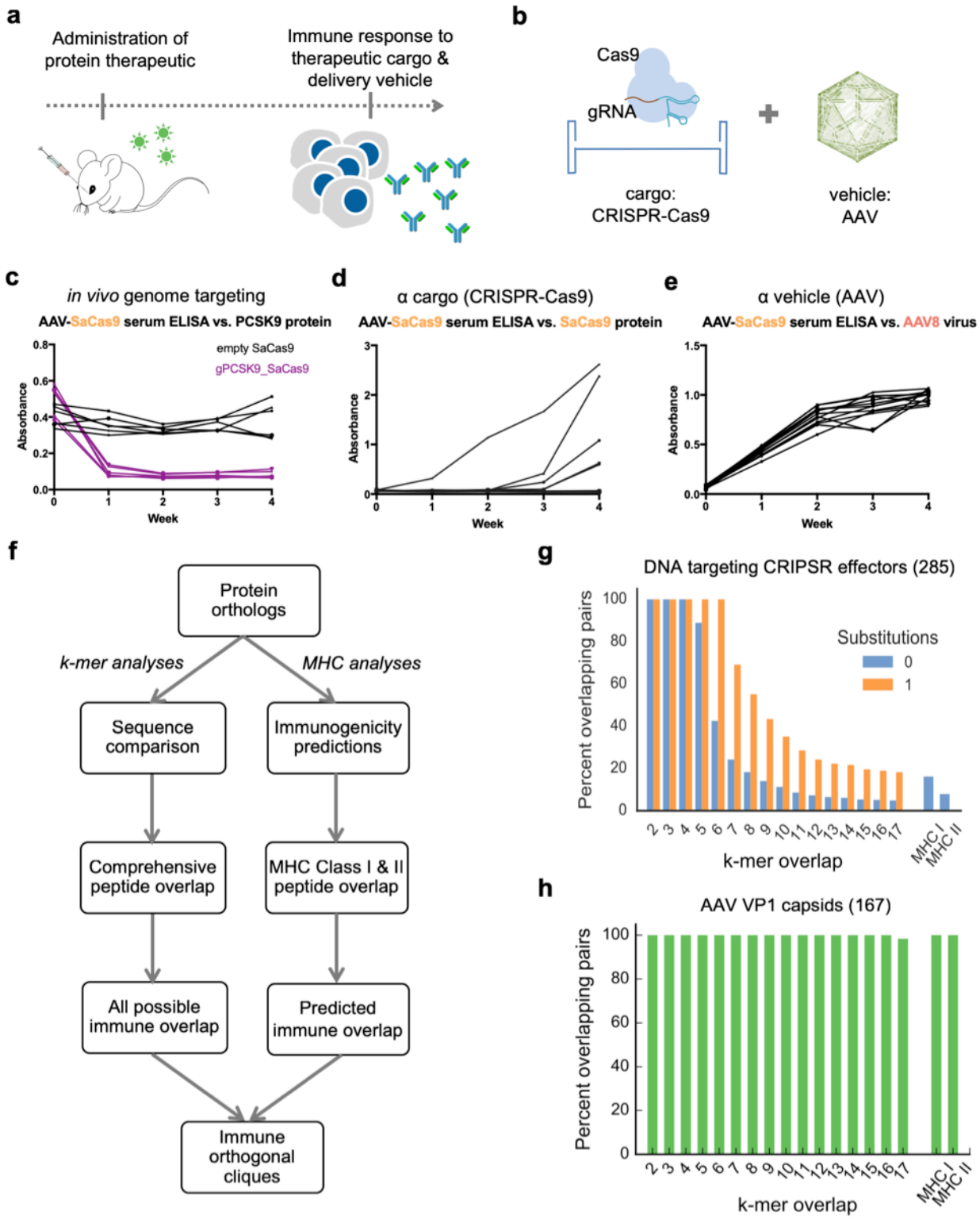
a
Administration of protein therapeutic
Immune response to therapeutic cargo & delivery vehicle
b
Cas9
gRNA
cargo: CRISPR-Cas9
vehicle: AAV
c
in vivo genome targeting
AAV-SaCas9 serum ELISA vs. PCSK9 protein
empty SaCas9
gPCSK9_SaCas9
Absorbance
Week
d
α cargo (CRISPR-Cas9)
AAV-SaCas9 serum ELISA vs. SaCas9 protein
Absorbance
Week
e
α vehicle (AAV)
AAV-SaCas9 serum ELISA vs. AAV8 virus
Absorbance
Week
f
Protein orthologs
k-mer analyses
MHC analyses
Sequence comparison
Immunogenicity predictions
Comprehensive peptide overlap
MHC Class I & II peptide overlap
All possible immune overlap
Predicted immune overlap
Immune orthogonal cliques
g
DNA targeting CRIPSR effectors (285)
Substitutions
0
1
Percent overlapping pairs
k-mer overlap
MHC I
MHC II
h
AAV VP1 capsids (167)
Percent overlapping pairs
k-mer overlap
MHC I
MHC II

3.4.2 Identifying immune-orthogonal proteins

Natural selection produces diverse structural variants with conserved function in the form of orthologous genes. We assayed the relevance of this diversity for immunological cross-reactivity of 284 DNA targeting and 84 RNA targeting CRISPR effectors (Table S2.1) and 167 AAV orthologs (Table S2.2) by first comparing their overall amino acid sequence similarities, and second, using a more specific constraint of how their respective amino acid sequences are predicted to bind MHC Type I and II molecules (Figure 3.1f). From these analyses we obtained first an estimate of the comprehensive immune overlap among Cas and AAV orthologs based purely at the sequence level, and second a more stringent estimate of predicted immune overlap based on predicted MHC binding (Figure 3.1g,h, S2.2). By sequence-level clustering and clique finding methods, we defined many sets of Cas9 orthologs containing up to 9 members with no 6-mer overlap (Figure S2.3). Notably, based on MHC-binding predictions, we find among the set of DNA-targeting Cas proteins (240 Cas9s and 44 Cpf1s) that 79% of pairs are predicted to have non cross-reacting immune responses, i.e. they are predicted to be orthogonal in immune space (Figure 3.1g). On the contrary, among AAV capsid (VP1 protein) orthologs we did not find full orthogonality up to the 14-mer level, even when restricting predictions with MHC-binding strengths (Figure 3.1h), likely reflecting the strong sequence conservation and shorter evolutionary history of AAVs [62]. This analysis suggests, consistent with previous observations [63,64], that exposure to one AAV serotype can induce broad immunity to all AAVs, which presents a significant challenge to AAV delivery platforms, as some serotypes are prevalent in human populations. Despite the most divergent AAV serotype (AAV5) showing the fewest shared immunogenic peptides, there remain tracts of sequences fully conserved within the VP1 orthologs. As expected, predicted immune cross-reaction negatively correlates with phylogenetic distance (Figure S2.4), though there is significant variation

not captured by that regression, suggesting that MHC-binding predictions can refine the choice of sequential orthologs beyond phylogenetic distance alone.

3.4.3 Confirming humoral immune-orthogonality among Cas9 proteins

To test our immunological predictions and to establish the utility of this approach, we narrowed in on a 5-member clique containing the ubiquitously used *S. pyogenes* Cas9 in addition to the well-characterized *S. aureus* Cas9 (Figure S2.3). To determine whether either of these proteins have cross-reacting antibody responses, we injected mice with 10^{12} vg of either AAV8 or AAVDJ capsids containing SaCas9 or SpCas9 transgenes via retro-orbital injections and harvested serum at days 0 (pre-injection), and periodically over 4-6 weeks (Figure 3.2a). SpCas9-specific antibodies were detected in the plasma of all mice injected with SpCas9 (n=6), and notably none of the mice injected with SaCas9 (n=12) (Figure 3.2b). Half of the mice injected with SaCas9 AAVs (n=12) developed detectable antibodies against SaCas9, whereas none of the mice injected with SpCas9 AAVs (n=6) developed an antibody response against SaCas9. These results were confirmed in an independent study in which SpCas9-specific antibodies, but not SaCas9-specific antibodies, were detected in the plasma of mice injected with AAV-SpCas9 (n=12). These mice were injected retro-orbitally with 10^{12} vg of AAV8-SpCas9 or AAVDJ-SpCas9, and also received an additional intramuscular injection with 10^{11} vg at week 4. (Figure 3.2c). Taken together, our data confirms that SpCas9 and SaCas9 have humoral immune-orthogonality. As an additional step, we tested another Cas9 ortholog from *Campylobacter jejuni*, useful for AAV-based delivery due to its small size. Mice injected retro-orbitally with 10^{12} vg AAV8-CjCas9 (n=12) showed no significant humoral response to Sp- or SaCas9 after 4 weeks (Figure S2.5), confirming immune orthogonality for a set of 3 unique Cas9 orthologs.

3.4.4 Confirming broad immune cross-reactivity among AAV serotypes

AAVs are becoming a preferred delivery vehicle due to their ability to avoid induction of a strong CD8+ T-cell response, however, the presence of neutralizing antibodies remains a significant barrier to successful application of AAV therapies. Consistent with previous results [63], we found shared immunogenic peptides among all human AAV serotypes (Figure S2.6). We confirmed the lack of orthogonality for two serotypes, AAV8 and AAVDJ, in which we found that antibodies produced in mice injected with AAV8 or AAVDJ react to both AAV8 and AAVDJ antigens (Figure 3.2d). Our analysis suggests that there are no two known AAVs for which exposure to one would guarantee immune naïveté to another across all MHC genotypes. However, immune cross-reaction could be minimized through the use of AAV5 [64,65], the most phylogenetically divergent serotype. Our predictions identify only a single shared highly immunogenic peptide between AAV5 and the commonly used AAV2 and AAV8 in the mouse model (though several other shared peptides of mild MHC affinity exist). We confirmed this via ELISAs, where mice injected with AAV2 did not elicit antibodies against AAV5 and AAV8, and mice injected with AAV5 did not elicit antibodies against AAVDJ and AAV8 (Figure 3.2d).

Figure 3.2: Experimental validation of Cas9 and AAV immunogenicity predictions. (a) Mice were exposed to antigens via retro-orbital injections at 10^{12} vg/mouse. Serum was harvested prior to injection on day 0, and at multiple points over the course of 4-6 weeks. **(b)** anti-SpCas9 antibodies generated in mice injected with SpCas9 (n=6) and SaCas9 (n=12), and anti-SaCas9 antibodies generated in mice injected with SpCas9 (n=6) and SaCas9 (n=12). Results are shown as mean ± s.e.m. Each data point represents an individual mouse. **(c)** anti-SpCas9 and anti-SaCas9 antibodies generated by mice injected with AAV8 SpCas9 (n=12; left panel), or AAVDJ SpCas9 (n=12; right panel). Results are shown as mean ± s.e.m. Each data point represents an individual mouse. **(d)** anti-AAV8/DJ/2/5 antibodies generated against mice injected with AAV8 or AAVDJ (n=4 for all panels), or with AAV2 or AAV5 (n=5-6 for all panels). Results are shown as mean ± s.e.m. Each data point represents an individual mouse.

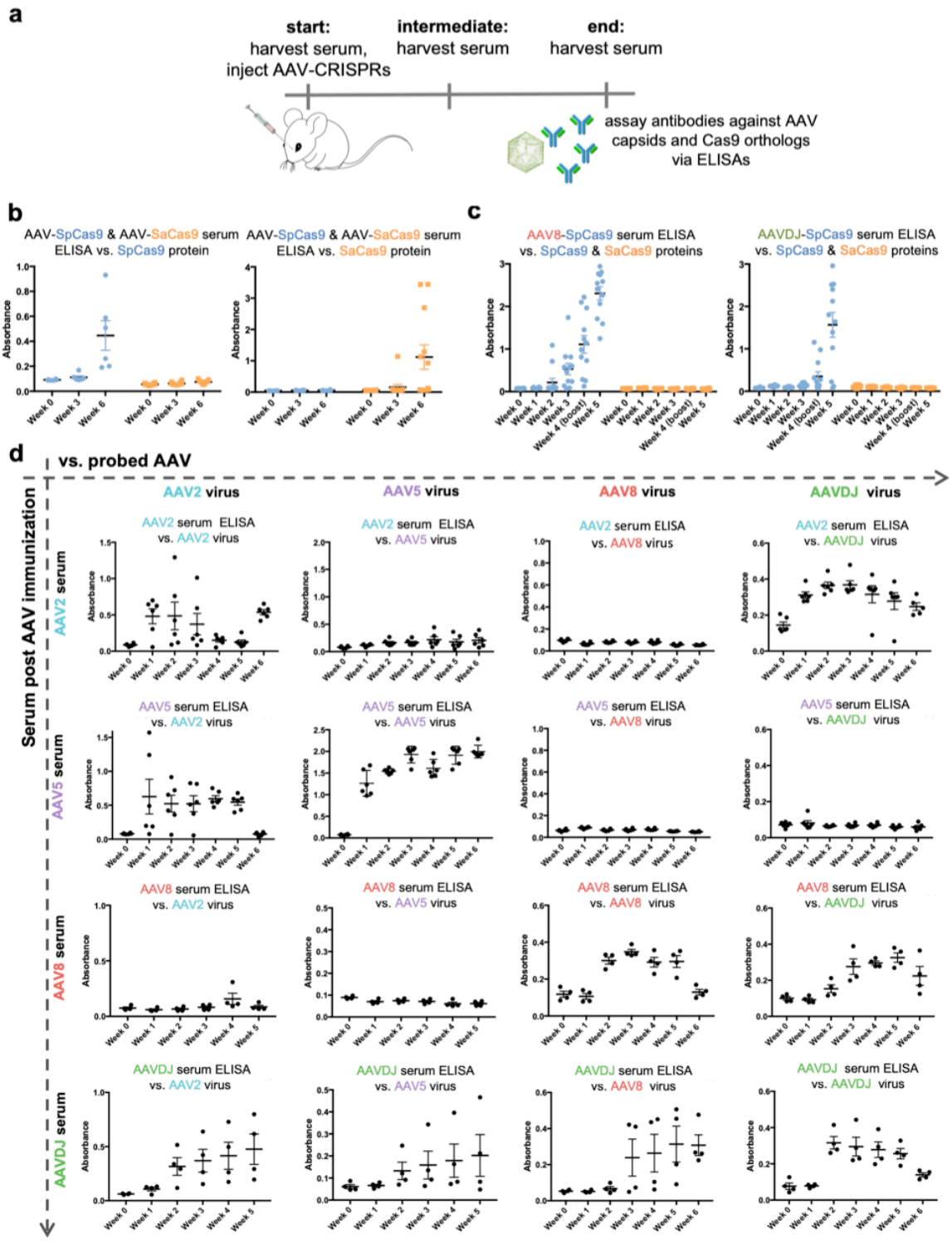
a
start:
harvest serum,
inject AAV-CRISPRs
intermediate:
harvest serum
end:
harvest serum
assay antibodies against AAV
capsids and Cas9 orthologs
via ELISAs
b
AAV-SpCas9 & AAV-SaCas9 serum
ELISA vs. SpCas9 protein
AAV-SpCas9 & AAV-SaCas9 serum
ELISA vs. SaCas9 protein
c
AAV8-SpCas9 serum ELISA
vs. SpCas9 & SaCas9 proteins
AAVDJ-SpCas9 serum ELISA
vs. SpCas9 & SaCas9 proteins
Absorbance
d
vs. probed AAV
Serum post AAV immunization
AAV2 virus
AAV5 virus
AAV8 virus
AAVDJ virus
AAV2 serum
AAV5 serum
AAV8 serum
AAVDJ serum
AAV2 serum ELISA vs. AAV2 virus
AAV2 serum ELISA vs. AAV5 virus
AAV2 serum ELISA vs. AAV8 virus
AAV2 serum ELISA vs. AAVDJ virus
AAV5 serum ELISA vs. AAV2 virus
AAV5 serum ELISA vs. AAV5 virus
AAV5 serum ELISA vs. AAV8 virus
AAV5 serum ELISA vs. AAVDJ virus
AAV8 serum ELISA vs. AAV2 virus
AAV8 serum ELISA vs. AAV5 virus
AAV8 serum ELISA vs. AAV8 virus
AAV8 serum ELISA vs. AAVDJ virus
AAVDJ serum ELISA vs. AAV2 virus
AAVDJ serum ELISA vs. AAV5 virus
AAVDJ serum ELISA vs. AAV8 virus
AAVDJ serum ELISA vs. AAVDJ virus

3.4.5 Overcoming immune barriers to effective gene editing

Having demonstrated that AAV-Cas9s elicit an immune response in the mouse model, and that the humoral responses to SpCas9 and SaCas9 do not cross-react, we next performed a two-step dosing experiment to test whether these immune responses inhibit the efficacy of multi-dose gene editing, and whether using immune-orthogonal orthologs in sequence can avoid immune-mediated inhibition of gene editing (Figures 3.3A, S2.7). For this experiment, we used another mouse strain, BALB/c, in order to verify and characterize the immune response in two independent strains. The first round of dosing contained no gRNA and served to immunize the mice against the second dose, which contained an active AAV8-SaCas9 with gRNA targeting PCSK9, allowing us to directly measure genome editing efficiency by sequencing, as well as serum PCSK9 levels as a phenotypic readout for therapeutic efficacy. Additionally, we measured IgG responses to all AAV and Cas9 used in the experiment. As expected from previous preclinical work on AAV therapies, prior exposure and humoral immunity to AAV8 (AAV8-mCherry) abolished the effectiveness of subsequent gene editing when using AAV8 as the delivery vector (AAV8-SaCas9). Importantly, this effect was not seen with previous exposure to AAV5 (AAV5-mCherry), and subsequent dosing with AAV8-SaCas9 resulted in strong genome editing and PCSK9 knockdown similar to the effects of AAV8-SaCas9 dosing in naïve mice (Figure 3.3B, 3.3C).

Although we do not necessarily expect this observed orthogonality between AAV8 and AAV5 to carry over into the human setting, here it allowed us to specifically test the effects of the immune response to the Cas9 payload with minimal interference from the AAV delivery vector. Mice first immunized against SaCas9 using AAV5 showed a 35% reduced level of editing, a 38% reduction in PCSK9 decrease, and a wider variation between mice. This may reflect a weak immune response to SaCas9 in our mouse model, and/or a domination of private (individual) T-cell responses to SaCas9. IgG ELISAs revealed that only a subset of mice immunized with AAV5-

SaCas9 developed an antibody response. We correlated the level of serum antibodies induced upon SaCas9 immunization with the efficiency of PCSK9 editing after the second dose, finding that mice with a stronger antibody response showed lower editing efficiency (Figure 3.3D). In contrast, we found that mice first dosed with AAV5-SpCas9 showed robust editing similar to that in naïve mice, suggesting that the predicted and measured immune orthogonality of Sp- and SaCas9 can be harnessed to circumvent immune barriers to gene editing.

To replicate these results in a different context, and to verify that immunity to Cas9 specifically can create a barrier to effective gene therapy, we conducted a slightly modified immunization experiment. Here we used a Cas9 protein vaccine combined in emulsion with Complete Freund's Adjuvant (CFA) as the initial dose, thereby immunizing a Cas9-specific primary response independently of AAV (Figure 3.3E). Subsequent dosing with AAV8-SaCas9 targeting PCSK9 recapitulated the results of AAV-based immunization, showing that prior exposure to the SaCas9 protein, but not SpCas9, significantly reduced the effectiveness of SaCas9-based gene editing by 42% and PCSK9 reduction by 51% (Figure 3.3F, 3.3G). Additionally, we also tested the ability of CFA-Cas9 immunized mice to clear injected splenocytes pulsed with immunogenic Cas9 epitopes. We observed 39% specific clearance of Cas9-pulsed cells 3.5 weeks after immunization, but no clearance 1 week after immunization, demonstrating that anti-Cas9 T-cells can specifically recognize and kill cells presenting Cas9 epitopes (Figure S2.8).

Taken together, anti-AAV and anti-Cas9 immunity represents a significant obstacle to therapeutic efficacy, and the use of immune orthogonal AAVs and Cas proteins, by bypassing immune recall, enables effective gene-editing from repeated administrations of these therapeutic modalities.

Figure 3.3: Multiple dosing with immune orthogonal orthologs circumvents immune inhibition of gene editing. **(a)** Mice were initially immunized with saline, AAV8-mCherry, AAV5-mCherry, AAV5-SaCas9, or AAV5-SpCas9 with no gRNA. After 4 weeks, the mice were given a second dose of saline or AAV8-SaCas9 with a gRNA targeting PCSK9. Serum was harvested prior to the first injection, and again at each subsequent week for 8 weeks. Mice were exposed to antigens via retro-orbital injections at 10^{12} vg/mouse. **(b)** Final PCSK9 serum levels (week 8), the phenotypic result of gene editing, decrease sharply after an active second dose of AAV8-SaCas9 with gRNA. This effect is abolished when mice are first immunized against AAV8, but not when mice are first immunized against AAV5. Previous immunization with AAV5-SaCas9 reduces, but does not eliminate editing, whereas previous dosing with AAV5-SpCas9 has no effect on editing. Show are the full time-course data for each week. **(c)** Genome editing rates, quantified by sequencing, are entirely abolished when mice are immunized against AAV8, and moderately inhibited when immunized against SaCas9. No effect is seen when mice are immunized against AAV5 or SpCas9. **(d)** Per mouse SaCas9 and SpCas9 antibody levels (refer Figure S7) were correlated with PCSK9 levels at weeks 7 and 8 to determine if mice mounting stronger immune responses had reduced editing. PCSK9 knockdown significantly correlates with SaCas9, but not SpCas9 antibody levels (F-test for non-zero slope; SaCas9 week 8: $p=0.032$, SaCas9 week 7: $p=0.023$; SpCas9 week 8: $p=0.329$, SpCas9 week 7: $p=0.354$). **(e)** Mice were immunized with CFA + 5 μg Cas9 1 week prior to active AAV-SaCas9 injections. **(f)** At week 3, mice immunized with SaCas9 show a significantly reduced editing rate compared to mice injected with CFA+PBS. No change in editing rate is seen when immunized with SpCas9. **(g)** Serum PCSK9 reduction is partially inhibited when mice are immunized with CFA+SaCas9, but not CFA+PBS or CFA+SpCas9.

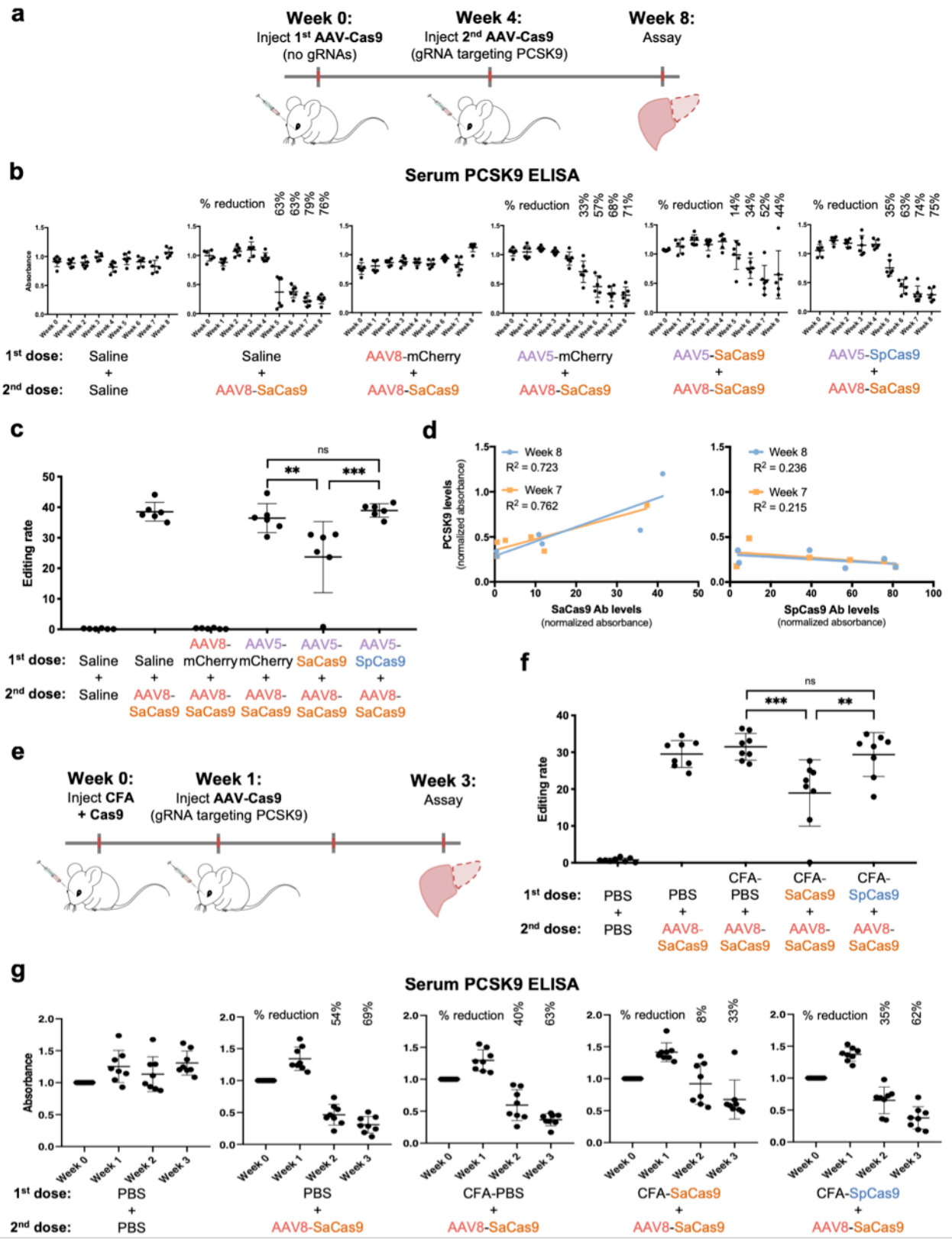
a
Week 0:
Inject 1st AAV-Cas9
(no gRNAs)
Week 4:
Inject 2nd AAV-Cas9
(gRNA targeting PCSK9)
Week 8:
Assay
b
Serum PCSK9 ELISA
% reduction 63% 63% 79% 76%
% reduction 33% 57% 68% 71%
% reduction 14% 34% 52% 44%
% reduction 35% 63% 74% 75%
Absorbance
1st dose: Saline + 2nd dose: Saline
Saline + AAV8-SaCas9
AAV8-mCherry + AAV8-SaCas9
AAV5-mCherry + AAV8-SaCas9
AAV5-SaCas9 + AAV8-SaCas9
AAV5-SpCas9 + AAV8-SaCas9
c
Editing rate
ns
**
***
1st dose: Saline + 2nd dose: Saline
Saline + AAV8-SaCas9
AAV8-mCherry + AAV8-SaCas9
AAV5-mCherry + AAV8-SaCas9
AAV5-SaCas9 + AAV8-SaCas9
AAV5-SpCas9 + AAV8-SaCas9
d
PCSK9 levels (normalized absorbance)
Week 8 R2 = 0.723
Week 7 R2 = 0.762
SaCas9 Ab levels (normalized absorbance)
Week 8 R2 = 0.236
Week 7 R2 = 0.215
SpCas9 Ab levels (normalized absorbance)
e
Week 0:
Inject CFA + Cas9
Week 1:
Inject AAV-Cas9
(gRNA targeting PCSK9)
Week 3:
Assay
f
Editing rate
ns
***
**
1st dose: PBS + 2nd dose: PBS
PBS + AAV8-SaCas9
CFA-PBS + AAV8-SaCas9
CFA-SaCas9 + AAV8-SaCas9
CFA-SpCas9 + AAV8-SaCas9
g
Serum PCSK9 ELISA
% reduction 54% 69%
% reduction 40% 63%
% reduction 8% 33%
% reduction 35% 62%
Absorbance
1st dose: PBS + 2nd dose: PBS
PBS + AAV8-SaCas9
CFA-PBS + AAV8-SaCas9
CFA-SaCas9 + AAV8-SaCas9
CFA-SpCas9 + AAV8-SaCas9

3.5 Discussion

The use of protein therapeutics requires ways to evade the host's immune response. Cas9, as an example, has prokaryotic origins and can evoke a long-lived T-cell response [42,53], which may lead to clearance of transduced cells. In addition, circulating antibodies can neutralize the AAV vector and prevent efficient transduction upon repeated doses. Immunosuppressive drugs could mitigate some of these aspects, but not without significant side-effects, and are not applicable to patients in poor health [66-69]. Similar to what has been done in cancer antibody therapeutics [70], the SpCas9 protein could be de-immunized by swapping high-immunogenicity domains. This is a promising approach; however, it will be complex and laborious as we anticipate tens of mutations to achieve stealth, which might often result in a reduction in activity and an overall less effective therapy.

Another consideration is that various applications of the CRISPR system will have significantly different immune consequences. For example, contrast genome editing applications, in which only transient expression of Cas9 is needed, to cases of gene regulation (CRISPRi or CRISPRa), in which continuous Cas9 expression is required. While ongoing expression applications will have to continuously contend with T-cell surveillance, genome editing with transient expression may not be compromised by a primary T-cell response if Cas9 expression is lost before CTL activation and clonal expansion. Building on this advantage, we note that promising new techniques may achieve stable gene regulation via transient i.e. hit-and-run approaches using epigenome editing [71]. Despite this, efficacious single-dose therapies may require high titers, especially in cases such as Duchenne muscular dystrophy where systemic delivery is needed. Such high doses may lead to toxicity issues, as demonstrated in a recent study of high-dose AAV9 delivery in rhesus macaques [72]. Multiple lower, non-toxic doses delivered

sequentially have the potential to achieve high transduction efficiency but must contend with the stronger and faster secondary adaptive immune response mediated by memory T- and B-cells.

To circumvent this issue, we developed here a framework to compare protein orthologs and their predicted binding to MHC I and MHC II by checking a sliding window of all k-mers in a protein for their presence in another, focusing on peptides predicted to bind to at least one MHC allele. Through this analysis, we identified cliques of Cas9 proteins that are immune orthogonal. Based on these predictions, specific T-cell responses from one ortholog would not cross-react with another ortholog of the same clique, preventing the re-activation of CD8+ cytotoxic T-cells, as well as the CD4+ T-cell help necessary to re-activate memory B-cells. We confirmed these results through ELISAs and verified three well-characterized Cas9 proteins (SpCas9, SaCas9, and CjCas9) to be immune orthogonal. Finally, we demonstrated in multiple contexts that consecutive dosing with the same AAV or Cas9 ortholog can face diminished editing efficacy which can be overcome with the use of immune orthogonal orthologs. Therefore, we expect that proteins belonging to the same clique can be used sequentially without eliciting memory T- and B- cell responses.

An important caveat is that each sequential ortholog should also be immune orthogonal to the pre-existing immune repertoire. Very recent work has begun to explore pre-existing immunity to Sp- and SaCas9 [41-43] in human donors. One potential repository of Cas9 to which humans may not have any pre-existing immunity is in the genomes of extremophiles. However, although humans are not likely to be exposed to these organisms previously, their Cas9s may nevertheless be closely related to commensal or pathogenic species, and therefore immune orthogonality to pre-existing immunity must be rigorously evaluated. To explore this issue, we categorized 240 Cas9s orthologs based on their species of origin as commensal, pathogenic, environmental, or extremophile, and compared the immune orthogonality between these groups (Figure S2.9). Preliminary analysis suggests that there may be extremophile Cas9s divergent enough as to be

orthogonal to pre-existing immunity, even when taking into account both pathogens and commensals. Many more candidates are likely to be discovered as we continue cataloging microbial diversity in a variety of environments using metagenomic approaches. Alongside this process, more diverse Cas9s must be tested and studied to determine if and under what conditions they will be usable in a mammalian setting.

Due to the importance of AAVs as a delivery agent in gene therapy, we also analyzed AAV serotypes through our MHC I and II comparison framework and have demonstrated that no two AAVs are predicted to be entirely immune orthogonal. However, with a known HLA genotype, it may be possible to define a personalized regimen of immune orthogonal AAVs using currently defined serotypes. For instance, use of AAV5 minimizes immune cross-reactivity in mice and non-human primates, as demonstrated by a recent study in which chimeric-AAV5 immunized mice and non-human primates successfully received a second dose of treatment with AAV1 [65]. However, in the human setting we predict that there may be substantially more immune overlap between AAV5 and other AAVs. Additionally, it has been shown that memory B-cells heavily contribute to the antibody response to similar but not identical antigens [73], indicating that partial orthogonality may not be sufficient. Our analysis suggests that creating a pair of globally orthogonal AAV capsids for human application would require >10 mutations in one of the two proteins. This hypothetical orthogonal AAV capsid presents a substantial engineering challenge, as it requires mutating many of the most conserved regions to achieve immune orthogonality.

Although we characterize the adaptive immune response to both the AAV VP1 and Cas9 proteins, it is not expected that these will induce the same type nor kinetics of response due to the differing nature of the antigens. The mice receive VP1 protein in the form of a viral capsid, as contrasted with Cas9 in the form of DNA. The delivery of AAV capsids is expected to produce a strong antibody response through the canonical MHC class II pathway. It may also induce a CTL

response through MHC class I presentation via transduction of APCs or cross-presentation of endocytosed viral proteins.

Alternatively, the Cas9 transgene is expressed as protein only once inside a transduced cell, and therefore could be expected to induce both an antibody and CTL response through two separate but non-mutually exclusive mechanisms. One potential avenue is that a subset of AAVs transduce APCs, an event that has been previously observed to occur [56]. After expression, Cas9 may be presented on class I MHC molecules through the canonical pathway, or presented on class II MHC molecules after being encapsulated in autophagosomes (a substantial fraction of MHCII-bound peptides is derived from internal proteins through autophagy) [74]. Another potential mechanism involves transduced non-APCs expressing Cas9 and subsequently undergoing apoptosis or necrosis. APCs then scavenge these dying cells, presenting the Cas9 proteins found within on class II MHC molecules through the canonical pathway, or on class I MHC molecules through cross-presentation, a process important for anti-viral immune responses.

Previous work has identified that MHC affinity is highly dependent on anchor residues at either end of the binding pocket [75]. Residue diversity is more tolerated in the center of the binding pocket, though it may be these residues that most impact antigen specificity, as it is thought that they are central to interaction with the T-cell receptor (TCR). Comparing the number of orthologous pairs in 9-mer space with the number of predicted orthologous pairs based on class II binding predictions suggests that only approximately 65% of 9-mer peptides serve as appropriate MHC class II binding cores, even across the thousands of HLA-2 combinations we explore here. This under-sampling of peptide space by MHC molecules likely reflects the requirement for hydrophobic anchor residues and leaves some space for protein de-immunization by mutation of immunogenic peptides to ones which never serve as MHC binding cores. Achieving this while preserving protein function however, has proven difficult even for few HLA alleles, and remains a

major protein engineering challenge. New technologies for directly measuring TCR affinity with MHC-presented antigens [76] will also further clarify the key antigenic peptides contributing to the immune response, and will be useful to inform approaches here.

We also note some limitations to our work. Mainly, we have used two inbred mice strains, C57BL/6J and BALB/c, as our model, which have limited MHC diversity [77], and might not recapitulate other human immunological features, such as differences in antigen processing and presentation. Our use of highly conservative models of potential human immunity suggests that any immune barriers to gene editing we observe here could be significantly magnified in the human setting. In this regard, we attempted to measure the human T-cell response with the IFN-γ ELISPOT assay for a subset of predicted MHCI and MHC II peptides (refer Tables S2.3, S2.4), corroborating recent studies of pre-existing immunity to Sp- and SaCas9 in humans [16,41,42] that showed measurable effector and regulatory T-cell responses. In our C57BL/6J model, we observed a low CD4+ T-cell response against specific MHCII peptides with mice injected with SaCas9 (Figure S2.1). One promising approach is to harness the ability of Treg cells to promote a more tolerogenic immune response to therapeutic proteins [42]. Additionally, B-cell epitopes can also be predicted and incorporated into immune orthogonality analysis. However, since B-cell epitopes may be both linear and conformational, these are more difficult to predict. Advances and further validation of these *in silico* models will allow for better predictions in the future [78-82]. In our study, initial immunization doses were not delivered with a gRNA, therefore Cas9 produced inside the cell or delivered as a protein will be in the apo-Cas9 conformation. This could result in different B-cell epitopes compared to the gRNA-bound Cas9 complex, as the 3D conformations are substantially different. Note that this should not affect MHC-presented peptides however, and thus not affect T-cell responses. Finally, recent work has indicated that MHC class I peptides may have significant contribution from spliced host and pathogen-derived peptides created by proteasomal

processing [83]. It is unclear how this may affect cross-recognition of proteins we predict to be immune orthogonal. On the one hand, it provides a mechanism whereby very short antigenic sequences spliced to the same host protein may result in cross-recognition of substantially different foreign antigens, however, we expect this to be unlikely due to the massive number of possible spliced peptides between the antigen and entire host proteome.

Overall, we believe our framework provides a potential solution for efficacious gene therapy, not solely for Cas9-mediated genome engineering, but also for other protein therapeutics that might necessitate repetitive treatments. Although using this approach still requires mitigating the primary immune response, particularly antibody neutralization and CTL clearance, we expect that epitope deletion and low-immunogenicity delivery vectors such as AAVs will mitigate this problem, and the potential for repeated dosage will reduce the need for very high first-dose titers and efficiency.

3.6 Acknowledgements

We thank members of the Mali lab for advice and help with experiments, and the Salk GT3 viral core for help with AAV production. This work was supported by UCSD Institutional Funds, the Burroughs Wellcome Fund (1013926), the March of Dimes Foundation (5-FY15-450), the Kimmel Foundation (SKF-16-150), and NIH grants (R01HG009285, RO1CA222826, RO1GM123313, R01AI079031 and R01AI106005). A.M. acknowledges a graduate fellowship from CONACYT and UCMEXUS.

Chapter 3 in part is from a reprint of the material *Moreno AM*, Palmer N*, Aleman F, Chen G, Pla A, Jiang N, Chew WL, Law M, Mali P. Exploring protein orthogonality in immune space: a*

case study with AAV and Cas9 orthologs. Nature Biomedical Engineering (2019). in press. The dissertation author was one of the two primary authors.

3.7 References

1. Mingozzi, F, High, KA (2013). Immune responses to AAV vectors: overcoming barriers to successful gene therapy. *Blood* **122**: 23–36.

2. Zaldumbide, A, Hoeben, RC (2008). How not to be seen: Immune-evasion strategies in gene therapy. *Gene Ther.* **15**: 239–246.

3. Yang, Y, Li, Q, Ertl, HC, Wilson, JM (1995). Cellular and humoral immune responses to viral antigens create barriers to lung-directed gene therapy with recombinant adenoviruses. *J. Virol.* **69**: 2004–15.

4. Jawa, V, Cousens, LP, Awwad, M, Wakshull, E, Kropshofer, H and De Groot, AS (2013). T-cell dependent immunogenicity of protein therapeutics: Preclinical assessment and mitigation. *Clin. Immunol.* **149**: 534–555.

5. Mays, LE and Wilson, JM (2011). The Complex and Evolving Story of T cell Activation to AAV Vector-encoded Transgene Products. *Mol. Ther.* **19**: 16–27.

6. Basner-Tschakarjan, E, Bijjiga, E, Martino, AT (2014). Pre-clinical assessment of immune responses to adeno-associated virus (AAV) vectors. *Front. Immunol.* **5**: 28.

7. Ertl, HCJ, High, KA (2017). Impact of AAV Capsid-Specific T-Cell Responses on Design and Outcome of Clinical Gene Transfer Trials with Recombinant Adeno-Associated Viral Vectors: An Evolving Controversy. *Hum. Gene Ther.* **28**: 328–337.

8. Kotterman, MA, Chalberg, TW, Schaffer, DV (2015). Viral Vectors for Gene Therapy: Translational and Clinical Outlook. *Annu. Rev. Biomed. Eng.* **17**: 63–89.

9. Mingozzi, F and High, KA (2011). Therapeutic in vivo gene transfer for genetic disease using AAV: progress and challenges. *Nat. Rev. Genet.* **12**: 341–355.

10. Manno, CS, Arruda, VR, Pierce, GF, Glader, B, Ragni, M, Rasko, JJ, Ozelo, MC, Hoots, K, Blatt, P, Konkle, B, Dake, M, Kaye, R, Rasavi, M, Zajko, A, Zehnder, J, Rustagi, PK, Nakai, H, Chew, A, Leonard, D, Wright, JF, Lessard, RR, Sommer, JM, Tigges, M, Sabatino, D, Luk, A, Jiang, H, Mingozzi, F, Couto, L, Erti HC, High, KA, Kay, MA (2006). Successful transduction of liver in hemophilia by AAV-Factor IX and limitations imposed by the host immune response. *Nat. Med.* **12**: 342–347.

11. Chew, WL (2018). Immunity to CRISPR Cas9 and Cas12a therapeutics. *Wiley Interdiscip.*

Rev. Syst. Biol. Med. **10**: e1408.

12. Sathish, JG, Sethu, S, Bielsky, MC, de Haan, L, French, NS, Govindappa, K, Green, J, Griffiths, CE, Holgate, S, Jones, D, Kimber, J, Moggs, J, Naisbitt, DJ, Pirmohamed, M, Reichmann, G, Sims, J, Subramanyam, M, Todd, MD, Van Der Laan, JW, Weaver, RJ, Park, BK (2013). Challenges and approaches for the development of safer immunomodulatory biologics. *Nat Rev Drug Discov* **12**: 306–324.

13. Harding, FA, Stickler, MM, Razo, J and DuBridge, RB (2010). The immunogenicity of humanized and fully human antibodies: Residual immunogenicity resides in the CDR regions. *MAbs* **2**: 256–265.

14. De Groot, a S, Knopp, PM and Martin, W (2005). De-immunization of therapeutic proteins by T-cell epitope modification. *Dev. Biol. (Basel).* **122**: 171–194.

15. Tangri, S, Mothé, BR, Eisenbraun, J, Sidney, J, Southwood, S, Briggs, K, Zinckgraf, J, Bilsel, P, Newman, M, Chesnut, R, Licalsi, C, Sette, A (2005). Rationally Engineered Therapeutic Proteins with Reduced Immunogenicity. *J. Immunol.* **174**: 3187-3196.

16. Ferdosi, SR, Ewaisha, R, Moghadam, F, Krishna, S, Park, JG, Ebrahimkhani, MR, Kiani, SS, Anderson, KS (2018). Multifunctional CRISPR/Cas9 with engineered immunosilenced human T cell epitopes. *bioRxiv* at <https://www.biorxiv.org/content/biorxiv/early/2018/07/02/360198.full.pdf?%3Fcollection=>.

17. Salvat, RS, Choi, Y, Bishop, A, Bailey-Kellogg, C, Griswold, KE (2015). Protein deimmunization via structure-based design enables efficient epitope deletion at high mutational loads. *Biotechnol. Bioeng.* **112**: 1306–1318.

18. Armstrong, JK, Hempel, G, Koling, S, Chan, LS, Fisher, T, Meiselman, HJ (2007). Antibody against poly(ethylene glycol) adversely affects PEG-asparaginase therapy in acute lymphoblastic leukemia patients. *Cancer* **110**: 103–111.

19. Ganson, NJ, Kelly, SJ, Scarlett, E, Sundy, JS, Hershfield, MS (2006). Control of hyperuricemia in subjects with refractory gout, and induction of antibody against poly(ethylene glycol) (PEG), in a phase I trial of subcutaneous PEGylated urate oxidase. *Arthritis Res. Ther.* **8**: R12.

20. Veronese, FM, Mero, A (2008). The impact of PEGylation on biological therapies. *BioDrugs* **22**: 315–329.

21. Jevševar, S, Kunstelj, M, Porekar, VG (2010). PEGylation of therapeutic proteins. *Biotechnol. J.* **5**: 113–128.

22. Jacobs, F, Gordts, SC, Muthuramu, I, De Geest, B (2012). The liver as a target organ for gene therapy: state of the art, challenges, and future perspectives. *Pharmaceuticals (Basel).* **5**: 1372–92.

23. Kok, CY, Cunningham, SC, Carpenter, KH, Dane, AP, Siew, SM, Logan, GJ, Kuchel, PW, Alexander, IE (2013). Adeno-associated Virus-mediated Rescue of Neonatal Lethality in Argininosuccinate Synthetase-deficient Mice. *Mol. Ther.* **21**: 1823–1831.

24. Courtenay-Luck, NS, Epenetos, AA, Moore, R (1986). Development of primary and secondary immune responses to mouse monoclonal antibodies used in the diagnosis and therapy of malignant neoplasms. *Cancer Res.* **46**: 6489–6493.

25. Jinek, M, Chylinski, K, Fonfara, I, Hauer, M, Doudna, JA, Charpentier, E (2012). A Programmable Dual-RNA – Guided DNA Endonuclease in Adaptice Bacterial Immunity. *Science* **337**: 816–822.

26. Mali, P, Yang, L, Esvelt, KM, Aach, J, Guell, M, DiCarlo, JE, Norville, JE, Church, GM (2013). RNA-guided human genome engineering via Cas9. *Science* **339**: 823–6.

27. Gasiunas, G, Barrangou, R, Horvath, P and Siksnys, V (2012). Cas9-crRNA ribonucleoprotein complex mediates specific DNA cleavage for adaptive immunity in bacteria. *Proc. Natl. Acad. Sci.* **109**: E2579–E2586.

28. Cong, L, Ran, FA, Cox, D, Lin, S, Barretto, R, Habib, N, Hsu, PD, Wu, X, Jiang, W, Marraffini, LA, Zhang, F (2013). Multiplex genome engineering using CRISPR/Cas systems. *Science* **339**: 819–23.

29. Ran, FA, Cong, L, Yan, WX, Scott, DA., Gootenberg, JS, Kriz, AJ, Zetsche, B, Shalem, O, Wu, X, Makarova, KS, Koonin, EV, Sharp, PA, Zhang, F (2015). In vivo genome editing using Staphylococcus aureus Cas9. *Nature* **520**: 186–190.

30. Jinek, M, East, A, Cheng, A, Lin, S, Ma, E, Doudna, J (2013). RNA-programmed genome editing in human cells. *Elife* **2**:e00471.

31. Mali, P, Esvelt, KM, Church, GM (2013). Cas9 as a versatile tool for engineering biology. *Nat. Methods* **10**: 957–963.

32. Hsu, PD, Lander, ES, Zhang, F (2014). Development and applications of CRISPR-Cas9 for genome engineering. *Cell* **157**: 1262–1278.

33. Kelton, WJ, Pesch, T, Matile, S, Reddy, ST (2016). Surveying the Delivery Methods of CRISPR/Cas9 for ex vivo Mammalian Cell Engineering. *Chim. Int. J. Chem.* **70**: 439–442.

34. Cho, SW, Kim, S, Kim, SJM, Kim, SJM (2013). Targeted genome engineering in human cells with the Cas9 RNA-guided endonuclease. *Nat. Biotechnol.* **31**: 230–2.

35. Moreno, AM, Mali, P (2017). Therapeutic genome engineering via CRISPR-Cas systems. *Wiley Interdiscip. Rev. Syst. Biol. Med.* **9**: e1380.

36. Koonin, E V., Makarova, KS , Zhang, F (2017). Diversity, classification and evolution of

CRISPR-Cas systems. *Curr. Opin. Microbiol.* **37**: 67–78.

37. Makarova, KS, Wolf, YI, Alkhnbashi, OS, Costa, F, Shah, SA, Saunders, SJ, Barrangou, R, Bround, SJ, Charpentier, E, Haft, DH, Horvath, P, Moineau, S, Mojica, FJ, Terms, RM, Terns, MP, White, MF, Yakunin, AF, Garrett, RA, van der Oost, J, Backofen, R, Koonin, EV (2015). An updated evolutionary classification of CRISPR–Cas systems. *Nat. Rev. Microbiol.* **13**: 722–736.

38. Chylinski, K, Makarova, KS, Charpentier, E, Koonin, EV. (2014). Classification and evolution of type II CRISPR-Cas systems. *Nucleic Acids Res.* **42**: 6091–6105.

39. Shmakov, S, Smargon, A, Scott, D, Cox, D, Pyzocha, N, Yan, W, Abudayyeh, OO, Gootenberg, JS, Makarova, KS, Wolf, YI, Severinov, K, Zhang, F, Koonin, EV (2017). Diversity and evolution of class 2 CRISPR–Cas systems. *Nat. Rev. Microbiol.* **15**: 169–182.

40. Crawley, AB, Henriksen, JR, Barrangou, R (2018). CRISPRdisco: An Automated Pipeline for the Discovery and Analysis of CRISPR-Cas Systems. *Cris. J.* **1**: 171–181.

41. Charlesworth, CT, Deshpande, PS, Dever, DP, Dejene, B, Gomez-Ospina, N, Mantri, S, Pavel-Dinu, M, Camarena, J, Weinberg, KI, Porteus, MH (2019). Identification of Pre-Existing Adaptive Immunity to Cas9 Proteins in Humans. *Nat. Med*. **25**: 249-254.

42. Wagner, DL, Amini, L, Wendering, DJ, Burkhardt, L-M, Akyüz, L, Reinke, P, Volk, HD, Schmueck-Henneresse, M (2018). High prevalence of Streptococcus pyogenes Cas9-reactive T cells within the adult human population. *Nat. Med.* **25**: 242-248.

43. Simhadri, VL, Mcgill, J, Mcmahon, S, Wang, J, Jiang, H and Sauna, ZE (2018). Prevalence of Pre-existing Antibodies to CRISPR-associated Nuclease Cas9 in the US Population. *Mol. Ther. Methods Clin. Dev.* **10**: 105-112.

44. Wagner, J a, Messner, a H, Moran, ML, Daifuku, R, Kouyama, K, Desch, JK, Manley, S, Norbash, AM, Conrad, CK, Friborg, S, Reynolds, T, Guggino, WB, Moss, RB, Carter, BJ, Wine, JJ, Flotte, TR, Gardner, P (1999). Safety and biological efficacy of an adeno-associated virus vector-cystic fibrosis transmembrane regulator (AAV-CFTR) in the cystic fibrosis maxillary sinus. *Laryngoscope* **109**: 266–74.

45. Song, S, Morgan, M, Ellis, T, Poirier, A, Chesnut, K, Wang, J, Brantly, M, Muzcyzka, N, Byrne, BJ, Atkinson, M, Flotte, TR (1998). Sustained secretion of human alpha-1-antitrypsin from murine muscle transduced with adeno-associated virus vectors. *Proc. Natl. Acad. Sci. U. S. A.* **95**: 14384–8.

46. Chirmule, N, Xiao, W, Truneh, A, Schnell, MA, Hughes, J V, Zoltick, P, Wilson, JM (2000). Humoral Immunity to Adeno-Associated Virus Type 2 Vectors following Administration to Murine and Nonhuman Primate Muscle. *J. Virol.* **74**: 2420–2425.

47. Fields, P a, Arruda, VR, Armstrong, E, Chu, K, Mingozzi, F, Hagstrom, JN, Herzog, RW, High, KA (2001). Risk and prevention of anti-factor IX formation in AAV-mediated gene

transfer in the context of a large deletion of F9. *Mol. Ther.* **4**: 201–210.

48. Herzog, RW, Fields, PA, Arruda, VR, Brubaker, JO, Armstrong, E, McClintock, D, Bellinger, DA, Couto, LB, Nichols, TC, High, KA (2002). Influence of vector dose on factor IX-specific T and B cell responses in muscle-directed gene therapy. *Hum. Gene Ther.* **13**: 1281–91.

49. Lozier, JN, Tayebi, N, Zhang, P (2005). Mapping of genes that control the antibody response to human factor IX in mice. *Blood* **105**: 1029–1035.

50. Zhang, HG, High, KA, Wu, Q, Yang, P, Schlachterman, A, Yu, S, Yi, N, Hsu, HC, Mountz, JD (2005). Genetic analysis of the antibody response to AAV2 and factor IX. *Mol.Ther.* **11**: 866–874.

51. Tam, HH, Melo, MB, Kang, M, Pelet, JM, Ruda, VM, Foley, MH, Hu, JK, Kumari, S, Crampton, J, Baldeon, AD, Sanders, RW, Moore, JP, Crooty, S, Langer, R, Anderson, DG, Chakraborty, AK, Irvine, DJ (2016). Sustained antigen availability during germinal center initiation enhances antibody responses to vaccination. *Proc. Natl. Acad. Sci. U. S. A.* **113**: E6639–E6648.

52. Chew, WL, Tabebordbar, M, Cheng, JKW, Mali, P, Wu, EY, Ng, AH, Zhu, K, Wagers, AJ, Church, GM (2016). A multifunctional AAV–CRISPR–Cas9 and its host response. *Nat. Methods* **13**: 868–874.

53. Boutin, S, Monteilhet, V, Veron, P, Leborgne, C, Montus, MF, Masurier, C (2010). Prevalence of Serum IgG and Neutralizing Factors Against Adeno-Associated Virus (AAV) Types 1,2,5,6,8, and 9 in the Healthy Population: Implications for Gene Therapy Using AAV Vectors. *Hum. Gene Ther.* **21**: 704–712.

54. Gao, G-P, Alvira, MR, Wang, L, Calcedo, R, Johnston, J and Wilson, JM (2002). Novel adeno-associated viruses from rhesus monkeys as vectors for human gene therapy. *Proc. Natl. Acad. Sci.* **99**: 11854–11859.

55. Jooss, K, Yang, Y, Fisher, KJ and Wilson, JM (1998). Transduction of Dendritic Cells by DNA Viral Vectors Directs the Immune Response to Transgene Products in Muscle Fibers. *J. Virol.* **72**: 4212–4223.

56. Gernoux, G, Guilbaud, M, Dubreil, L, Larcher, T, Babarit, C, Ledevin, M, Jaulin, N, Planel, P, Moullier, P, Adjali, O (2015). Early Interaction of Adeno-Associated Virus Serotype 8 Vector with the Host Immune System Following Intramuscular Delivery Results in Weak but Detectable Lymphocyte and Dendritic Cell Transduction. *Hum. Gene Ther.* **26**: 1–13.

57. Zhu, J, Huang, X, Yang, Y (2009). The TLR9-MyD88 pathway is critical for adaptive immune responses to adeno-associated virus gene therapy vectors in mice. *J. Clin. Invest.* **119**: 2388–2398.

58. Gernoux, G, Wilson, JM, Mueller, C (2017). Regulatory and Exhausted T Cell Responses to

AAV Capsid. *Hum. Gene Ther.* **28**: 338–349.

59. Kurosaki, T, Kometani, K, Ise, W (2015). Memory B cells. *Nat. Rev. Immunol.* **15**: 149–159.

60. Zabel, F, Fettelschoss, A, Vogel, M, Johansen, P, Kündig, TM, Bachmann, MF (2017). Distinct T helper cell dependence of memory B-cell proliferation versus plasma cell differentiation. *Immunology* **150**: 329–342.

61. Ding, Q, Strong, A, Patel, KM, Ng, S-L, Gosis, BS, Regan, SN, Cowan, CA, Rader, DJ, Musunuru, K (2014). Permanent Alteration of PCSK9 With In Vivo CRISPR-Cas9 Genome Editing. *Circ. Res.* **115**: 488–492.

62. Zinn, E, Pacouret, S, Khaychuk, V, Turunen, HT, Carvalho, LS, Andres-Mateos, E, Shah, S, Shelke, R, Maurer AC, Plovie, E, Xiao, R, Vandenberghe, LH (2017). In Silico Reconstruction of the Viral Evolutionary Lineage Yields a Potent Gene Therapy Vector. *Cell Rep.* **12**: 1056–1068.

63. Calcedo, R, Wilson, JM (2016). AAV Natural Infection Induces Broad Cross-Neutralizing Antibody Responses to Multiple AAV Serotypes in Chimpanzees. *Hum. Gene Ther. Clin. Dev.* **27**: 79–82.

64. Harbison, CE, Weichert, WS, Gurda, BL, Chiorini, JA, Agbandje-McKenna, M, Parrish, CR (2012). Examining the cross-reactivity and neutralization mechanisms of a panel of mabs against adeno-associated virus serotypes 1 and 5. *J. Gen. Virol.* **93**: 347-355

65. Majowicz, A, Salas, D, Zabaleta, N, Rodríguez-Garcia, E, González-Aseguinolaza, G, Petry, H, Ferreira, V (2017). Successful Repeated Hepatic Gene Delivery in Mice and Non-human Primates Achieved by Sequential Administration of AAV5^{ch} and AAV1. *Mol. Ther.* **25**: 1831–1842.

66. McIntosh, JH, Cochrane, M, Cobbold, S, Waldmann, H, Nathwani, SA, Davidoff, AM, *et al.* (2012). Successful attenuation of humoral immunity to viral capsid and transgenic protein following AAV-mediated gene transfer with a non-depleting CD4 antibody and cyclosporine. *Gene Ther* **19**: 78–85.

67. Mingozzi, F, Chen, Y, Edmonson, SC, Zhou, S, Thurlings, RM, Tak, PP (2013). Prevalence and pharmacological modulation of humoral immunity to AAV vectors in gene transfer to synovial tissue. *Gene Ther* **20**: 417–424.

68. Mingozzi, F, Chen, Y, Murphy, SL, Edmonson, SC, Tai, A, Price, SD (2017). Pharmacological Modulation of Humoral Immunity in a Nonhuman Primate Model of AAV Gene Transfer for Hemophilia B. *Mol. Ther.* **20**: 1410–1416.

69. Unzu, C, Hervás-Stubbs, S, Sampedro, A, Mauleón, I, Mancheño, U, Alfaro, C (2012). Transient and intensive pharmacological immunosuppression fails to improve AAV-based liver gene transfer in non-human primates. *J. Transl. Med.* **10**: 122.

70. Riechmann, L, Clark, M, Waldmann, H, Winter, G (1988). Reshaping human antibodies for therapy. *Nature* **332**: 323–7.

71. Amabile, A, Migliara, A, Capasso, P, Biffi, M, Cittaro, D, Naldini, L (2016). Inheritable Silencing of Endogenous Genes by Hit-and-Run Targeted Epigenetic Editing. *Cell* **167**: 219–232.

72. Hinderer, C, Katz, N, Buza, EL, Dyer, C, Goode, T, Bell, P (2018). Severe toxicity in nonhuman primates and piglets following high-dose intravenous administration of an AAV vector expressing human SMN. *Hum. Gene Ther.* **29**.

73. Vollmers, C, Sit, R V., Weinstein, JA, Dekker, CL, Quake, SR (2013). Genetic measurement of memory B-cell recall using antibody repertoire sequencing. *Proc. Natl. Acad. Sci.* **110**: 13463–13468.

74. Adamopoulou, E, Tenzer, S, Hillen, N, Klug, P, Rota, IA, Tietz, S (2013). Exploring the MHC-peptide matrix of central tolerance in the human thymus. *Nat. Commun.* **4**: 2039.

75. Ruppert, J, Sidney, J, Celis, E, Kubo, RT, Grey, HM, Sette, A (2017). Prominent role of secondary anchor residues in peptide binding to HLA-A2.1 molecules. *Cell* **74**: 929–937.

76. Zhang, S-Q, Parker, P, Ma, K-Y, He, C, Shi, Q, Cui, Z (2016). Direct measurement of T cell receptor affinity and sequence from naïve antiviral T cells. *Sci. Transl. Med.* **8**: 341ra77.

77. Baker, MP, Reynolds, HM, Lumicisi, B and Bryson, CJ (2010). Immunogenicity of protein therapeutics: The key causes, consequences and challenges. *Self Nonself* **1**: 314–322.

78. EL-Manzalawy, Y, Dobbs, D, Honavar, V (2008). Predicting linear B-cell epitopes using string kernels. *J. Mol. Recognit.* **21**: 243–255.

79. Larsen, JEP, Lund, O, Nielsen, M (2006). Improved method for predicting linear B-cell epitopes. *Immunome Res.* **2**: 2.

80. Sollner, J, Grohmann, R, Rapberger, R, Perco, P, Lukas, A and Mayer, B (2008). Analysis and prediction of protective continuous B-cell epitopes on pathogen proteins. *Immunome Res.* **4**: 1.

81. Dalkas, GA and Rooman, M (2017). SEPIa, a knowledge-driven algorithm for predicting conformational B-cell epitopes from the amino acid sequence. *BMC Bioinformatics* **18**: 95.

82. Sun, P, Ju, H, Liu, Z, Ning, Q, Zhang, J, Zhao, X (2013). Bioinformatics resources and tools for conformational B-cell epitope prediction. *Comput. Math. Methods Med.* **2013**.

83. Liepe, J, Marino, F, Sidney, J, Jeko, A, Bunting, DE, Sette, A (2016). A large fraction of HLA class I ligands are proteasome-generated spliced peptides. *Science.* **354**: 354-358.

84. Fonfara, I, Le Rhun, A, Chylinski, K, Makarova, KS, Lécrivain, A-L, Bzdrenga, J (2014).

Phylogeny of Cas9 determines functional exchangeability of dual-RNA and Cas9 among orthologous type II CRISPR-Cas systems. *Nucleic Acids Res.* **42**: 2577–2590.

85. Shmakov, S, Smargon, A, Scott, D, Cox, D, Pyzocha, N, Yan, W (2017). Diversity and evolution of class 2 CRISPR–Cas systems. *Nat. Rev. Microbiol.* **15**: 169–182.

86. Burstein, D, Harrington, LB, Strutt, SC, Probst, AJ, Anantharaman, K, Thomas, BC (2016). New CRISPR–Cas systems from uncultivated microbes. *Nature* **542**: 237–241.

87. Shmakov, S, Abudayyeh, OO, Makarova, KS, Wolf, YI, Gootenberg, JS, Semenova, E (2015). Discovery and Functional Characterization of Diverse Class 2 CRISPR-Cas Systems. *Mol. Cell* **60**: 385–397.

88. Andreatta, M, Nielsen, M (2015). Gapped sequence alignment using artificial neural networks: application to the MHC class I system. *Bioinformatics* **32**: 511–517.

89. Andreatta, M, Karosiene, E, Rasmussen, M, Stryhn, A, Buus, S, Nielsen, M (2015). Accurate pan-specific prediction of peptide-MHC class II binding affinity with improved binding core identification. *Immunogenetics* **67**: 641–650.

90. Vita, R, Overton, JA, Greenbaum, JA, Ponomarenko, J, Clark, JD, Cantrell, JR (2015). The immune epitope database (IEDB) 3.0. *Nucleic Acids Res.* **43**: D405-12.

91. Truong, D-JJ, Kühner, K, Kühn, R, Werfel, S, Engelhardt, S, Wurst, W (2015). Development of an intein-mediated split–Cas9 system for gene therapy. *Nucleic Acids Res.* **43**: 6450–6458.

92. Moreno, AM, Fu, X, Zhu, J, Katrekar, D, Shih, Y-R V, Marlett, J (2018). In Situ Gene Therapy via AAV-CRISPR-Cas9-Mediated Targeted Gene Regulation. *Mol. Ther.* **0**.

93. Grieger, JC, Choi, VW, Samulski, RJ (2006). Production and characterization of adeno-associated viral vectors. *Nat. Protoc.* **1**: 1412–1428.

94. Schubert, M, Lindgreen, S, Orlando, L (2016). AdapterRemoval v2: rapid adapter trimming, identification, and read merging. *BMC Res. Notes* **9**: 88.

95. Pinello, L, Canver, MC, Hoban, MD, Orkin, SH, Kohn, DB, Bauer, DE (2016). Analyzing CRISPR genome-editing experiments with CRISPResso. *Nat. Biotechnol.* **34**: 695–697.

96. Clemente, T, Dominguez, MR, Vieira, NJ, Rodrigues, MM, Amarante-Mendes, GP (2013). In vivo assessment of specific cytotoxic T lymphocyte killing. *Methods* **61**: 105–109.

Chapter 4 - *In situ* repression of a sodium channel leads to long-term amelioration of pain

4.1 Abstract

Chronic pain affects more than 100 million Americans and 1.5 billion people worldwide. Current therapeutic regimens for chronic pain rely largely on opioids despite their limited efficacy, unwanted side effects, and risk of addiction. Interestingly, the human genome encodes genes that have been linked to contributing to the pathobiology of chronic pain. Specifically, genetic studies have correlated a hereditary loss-of-function mutation in a human-voltage gated sodium channel isoform – $Na_V1.7$ – with a rare genetic disorder, Congenital Insensitivity to Pain (CIP), which leads to insensitivity to pain without other neurodevelopmental alterations. However, the high sequence identity between Na_V subtypes has frustrated most efforts to develop selective inhibitors. Here, we investigated the epigenetic repression of $Na_V1.7$ as a potential treatment for chronic pain. To achieve this, we first transfected Neuro2a cells with two genetic engineering tools, KRAB-CRISPR-dCas9 and KRAB-Zinc-Fingers, for targeted *in vitro* $Na_V1.7$ repression. We observed 71% and 88% repression of $Na_V1.7$ using KRAB-CRISPR-dCas9 and KRAB-Zinc-Fingers, respectively. Next, we tested these genome engineering tools in a mouse model of Carrageenan-induced inflammatory pain. Our results demonstrate robust *in vivo* repression of $Na_V1.7$ and a phenotypic improvement in thermal pain tolerance in the inflammatory state. We foresee that these tools have tremendous potential, such as for preemptive administration in anticipation of a pain

stimulus (pre-operatively), or during an established chronic pain state. The use of *in situ* epigenome engineering may therefore represent a viable non-opioid alternative for the treatment of chronic pain and other chronic diseases.

4.2 Introduction

Chronic pain affects between 19% to 50% of the world population [1-4], with more than 100 million people affected in the U.S. alone [5]. Moreover, the number of chronic pain patients is expected to increase by 2035 due to the aging global population and prevalence of chronic diseases [6,7]. While chronic pain is more prevalent than cancer, diabetes and cardiovascular disease combined [8], drug development has not undergone the remarkable progress seen in these other therapeutic areas. Current treatments of preference for chronic pain rely on opioids, which can have adverse side effects and high addiction risk. Despite decades of research, broad-acting, long-lasting, non-addictive, and effective therapeutics for chronic pain have remained elusive.

Notably, the human genome encodes multiple genes that play a critical role in pain regulation, such as conferring protection from excessive pain. There are nine voltage gated sodium channel subtypes, of which $Na_V1.7$ [9,10], $Na_V1.8$ [11-13], and $Na_V1.9$ [14,15] have been implicated in nociceptive transmission and contribution to the hyperexcitability in primary afferent nociceptive and sympathetic neurons. Previous studies have demonstrated that decreased $Na_V1.7$, $Na_V1.8$ and $Na_V1.9$ activity leads to a reduction in inflammatory or neuropathic pain [9-16]. In addition, characterization of mutations in these channels has confirmed a causative link to human pain disorders [17-23]. Since the discovery of the relationship between individuals with loss-of-function $Na_V1.7$ (SCN9A) mutations and Congenital Insensitivity to Pain (CIP), this sodium channel has been an attractive target for developing chronic pain therapies [24]. However, efforts to

develop selective small molecule inhibitors have been hampered due to the high sequence similarity between Na_V subtypes, and many small-molecule drugs targeting $Na_V1.7$ have failed due to side effects caused by lack of targeting specificity. Additionally, antibody-based therapies lack potency due to their ability to bind only a specific (open or closed) conformation of the channel [25], with binding not always translating into successful channel inhibition [26,27]. Consequently, no drug targeting this gene has reached the final phase of clinical trials [28]. We therefore took an alternative approach by epigenetically modulating the expression of $Na_V1.7$, such that one could engineer highly specific, long-lasting, and reversible treatments for pain.

The CRISPR-Cas9 system has emerged as a potent tool for genome manipulation, and has shown therapeutic efficacy in multiple animal models of human diseases [29-35] through its ability to target and precisely edit disease-causing DNA mutations. However, certain diseases would not benefit from editing, leading to permanent alteration of the underlying gene's function. For example, although pain can often be a discomforting sensory and emotional experience, it plays a critical role in alerting of tissue damage initiation or of alteration in a biological process, and hence, permanent ablation of pain could have detrimental consequences. For these reasons, we have employed a catalytically inactivated "dead" Cas9 (dCas9) fused to a repressor domain (Krüppel-associated box -KRAB-) to enable non-permanent gene repression of $Na_V1.7$. Previously, we and others have shown that through addition of a KRAB epigenetic repressor motif to dCas9, gene repression can be enhanced with a high level of specificity both *in vitro* [36-40] and *in vivo* [41, 42]. This transcriptional modulation system takes advantage of the high specificity of CRISPR-Cas9 while simultaneously increasing the safety profile, as no permanent modification of the genome is performed. As a second approach for *in situ* epigenome repression of $Na_V1.7$, we utilized Zinc-Fingers containing a KRAB repressor (KRAB-ZFs). KRAB-ZFs constitute the largest individual family of transcriptional repressors encoded by the genomes of higher organisms, and

obtain gene-specific transcriptional repression by interacting with chromatin-remodeling factors [43].

Pain that we perceive is felt through a process called nociception. Nociception occurs when pain signals are transmitted from the point of sensation to the central nervous system by the activation of pain-sensing primary afferent nociceptive neurons. Pain signals from these peripheral sites are conducted from the point of sensation into the spinal cord in a somatotopic fashion at levels from the most caudal (sacral) to the most rostral (cervical). In the spinal cord, at the level of the first order synapse, this input is encoded and transmitted to the brain, where it is processed into the pain experience. Just before entering the spinal cord, sensory signals pass through the cell bodies of the primary afferent, and are collectively called the dorsal root ganglion (DRG). It is now appreciated that these cell bodies, synthesizing the receptors and channels (including $Na_V1.7$) robustly contribute to the excitability of the nociceptive primary afferent following tissue and nerve injury. Therefore, because nociceptive signals all pass through the DRG, localized treatments targeting the DRG specifically can optimally block pain signals [44], while also having the advantage of requiring a lower drug dosage, therefore increasing the therapeutic index. Consequently, we chose to administer our therapy via an intrathecal route of administration, which more efficiently targets DRG neurons compared to systemic administration [45]. Here, we first tested various KRAB-dCas9 and KRAB-ZFs constructs in a mouse neuroblastoma cell line that highly expresses $Na_V1.7$ (Neuro2a) and confirmed robust repression. We next packaged the two KRAB-Zinc-Finger constructs with the strongest *in vitro* repression into AAV9, which has been shown to transduce DRGs [46], and injected these intrathecally into C57BL/6J mice. Three weeks later, we induced inflammation via injection of Carrageenan into the ipsilateral hind paw, and tested for thermal hyperalgesia. Remarkably, our results demonstrated robust *in vivo* repression of $Na_V1.7$ concomitant with a decrease in thermal hyperalgesia. As many pain states occurring after chronic

inflammation and nerve injury represent an enduring condition, typically requiring constant re-medication, these genetic approaches provide ongoing and controllable regulation of this aberrant processing. Harnessing these *in situ* engineering approaches could therefore represent a viable replacement for opioids and serve as a potential therapeutic approach chronic pain and for other chronic disorders.

4.3 Methods

4.3.1 Vector Design and Construction

Cas9 and Zinc-Finger AAV vectors were constructed by sequential assembly of corresponding gene blocks (Integrated DNA Technologies) into a custom synthesized rAAV2 vector backbone. gRNA sequences were inserted into dNCas9 plasmids by cloning oligonucleotides (IDT) encoding spacers into AgeI cloning sites via Gibson assembly. gRNAs were designed utilizing an *in silico* tool to predict gRNAs [47].

4.3.2 Mammalian Cell Culture

Neuro2a cells were grown in EMEM supplemented with 10% fetal bovine serum (FBS) and 1% Antibiotic-Antimycotic (Thermo Fisher Scientific) in an incubator at 37°C and 5% CO2 atmosphere.

4.3.3 Lipid-Mediated Cell Transfections

One day prior to transfection, Neuro2a cells were seeded in a 24-well plate at a cell density of 1 or 2E+5 cells per well. 0.5 μg of each plasmid was added to 25 μL of Opti-MEM medium, followed by addition of 25 μL of Opti-MEM containing 2 μL of Lipofectamine 2000. The mixture

was incubated at room temperature for 15 min. The entire solution was then added to the cells in a 24-well plate and mixed by gently swirling the plate. Media was changed after 24 h, and the plate was incubated at 37°C for 72 h in a 5% CO2 incubator. Cells were harvested, spun down, and frozen at 80°C.

4.3.4 Production of AAVs

Virus was prepared by the Gene Transfer, Targeting and Therapeutics (GT3) core at the Salk Institute of Biological Studies (La Jolla, CA) or in-house utilizing the GT3 core protocol. Briefly, AAV2/1, AAV2/5, and AAV2/9 virus particles were produced using HEK293T cells via the triple transfection method and purified via an iodixanol gradient. Confluency at transfection was between 80% and 90%. Media was replaced with pre-warmed media 2 h before transfection. Each virus was produced in five 15 cm plates, where each plate was transfected with 10 μg of pXR-capsid (pXR-1, pXR-5, and pXR-9), 10 of μg recombinant transfer vector, and 10 μg of pHelper vector using polyethylenimine (PEI; 1 mg/mL linear PEI in DPBS [pH 4.5], using HCl) at a PEI:DNA mass ratio of 4:1. The mixture was incubated for 10 min at room temperature and then applied dropwise onto the media. The virus was harvested after 72 h and purified using an iodixanol density gradient ultracentrifugation method. The virus was then dialyzed with 1x PBS (pH 7.2) supplemented with 50 mM NaCl and 0.0001% of Pluronic F68 (Thermo Fisher Scientific) using 50-kDa filters (Millipore) to a final volume of ~100 μL and quantified by qPCR using primers specific to the ITR region, against a standard (ATCC VR-1616): AAV-ITR-F: 5’ -CGGCCTCAGTGAGCGA-3’ and

AAV-ITR-R: 5’ -GGAACCCCTAGTGATGGAGTT-3’

4.3.5 Animals Experiments

All animal procedures were performed in accordance with protocols approved by the Institutional Animal Care and Use Committee (IACUC) of the University of California, San Diego. All mice were acquired from Jackson Laboratory. Two month old adult male C57BL/6 mice (25-30g) were housed with food and water provided ad libitum, under a 12 h light/dark cycle with up to 5 mice per cage.

4.3.6 Intrathecal AAV Injections

Anesthesia was induced with 2.5 % isoflurane delivered in equal parts O2 and room air in a closed chamber until a loss of the righting reflex was observed. The lower back of mice were shaven and swabbed with 70% ethanol. Mice were then intrathecally (i.t.) injected using a Hamilton syringe and 30G needle as previously described [48] between vertebrae L4 and L5 with 5 μL of AAV for a total of ~1E+12 vg/mouse. A tail flick was considered indicative of appropriate needle placement. Following injection, all mice resumed motor activity consistent with that observed prior to i.t. injection.

4.3.7 Intraplantar Carrageenan Injection

Carrageenan-induced inflammation is a classic model of edema formation and hyperalgesia [49-51]. Three weeks after AAV pre-treatment, anesthesia was induced as described above. Lambda Carrageenan (Sigma Aldrich; 2% (W/V) 0.9% NaCl, 20 μL) was subcutaneously injected with a 30G needle into the plantar (ventral) surface of the ipsilateral paw. An equal amount of isotonic saline was injected into the contralateral paw. Paw thickness was measured with a caliper before and 4h after Carrageenan/saline injections as an index of edema/inflammation. Hargreaves testing

was performed before injection (t=0) and (t= 30, 60, 120, 240 minutes and 24 hours post-injection). The experimenter was blinded to the composition of treatment groups. Mice were euthanized after the 24-hour time point.

4.3.8 Thermal Withdrawal Latency (Hargreaves Test)

To determine the acute nociceptive thermal threshold, the Hargreaves' test was conducted using a plantar test device (Ugo Basile, Italy) [52]. Animals were allowed to freely move within a transparent plastic enclosement (6 cm diameter × 16 cm height) on a glass floor 40 min before the test. A mobile radiant heat source was then placed under the glass floor and focused onto the hind paw. Paw withdrawal latencies were measured with a cutoff time of 30 seconds. An IR intensity of 40 was employed. The heat stimulation was repeated three times on each hind paw with a 10 min interval to obtain the mean latency of paw withdrawal. The experimenter was blinded to composition of treatment groups.

4.3.9 Tissue collection

After the 24-hour time Carrageenan time point, spinal cords were collected via hydroextrusion (injection of 2 mL of iced saline though a short blunt 20 gauge needle placed into the spinal canal following decapitation). After spinal cord tissue harvest, the L4-L6 DRGs on each side were combined and frozen as for the spinal cord. Samples were placed in DNase/RNase-free 1.5 mL centrifuge tubes, quickly frozen on dry ice, and then stored at 80°C for future analysis.

4.3.10 Gene Expression Analysis and RT-qPCR

RNA from cells was extracted using RNeasy Kit (QIAGEN; 74104) and from DRGs using RNeasy Micro Kit (QIAGEN; 74004). cDNA was synthesized from RNA using Protoscript II

Reverse Transcriptase Kit (NEB; E6560L). Real-time PCR (qPCR) reactions were performed using the KAPA SYBR Fast qPCR Kit (Kapa Biosystems; KK4601), with gene-specific primers (Table S3.3) in technical triplicates and in biological triplicates (Neuro2a cells). Relative mRNA expression was normalized to GAPDH levels and fold change was calculated using the comparative CT (ΔΔCT) method and normalized to GAPDH. Mean fold change and SD were calculated using Microsoft Excel.

4.3.11 Statistical analysis

Results are expressed as mean +/- standard error (SE). Statistical analysis was performed using GraphPad Prism (version 8.0, GraphPad Software, San Diego, CA, USA). Results were analyzed using one-way ANOVA (for multiple groups), or two-way ANOVA with the Bonferroni *post hoc* test (for multiple groups time-course experiments). Differences in area under the curves (AUCs) were analyzed by one-way ANOVA followed by Bonferroni *post hoc* test. Differences between groups with $p < 0.05$ were considered statistically significant.

4.4 Results

4.4.1 *In vitro* optimization of KRAB-CRISPR-dCas9 gRNAs and KRAB-Zinc-Finger constructs.

We first compared *in vitro* repression of $Na_V1.7$ using KRAB-CRISPR-dCas9 and KRAB-Zinc-Finger constructs. To that end, we cloned ten guide-RNAS (gRNAs)—designed by an *in silico* model [47] that accurately predicts highly effective gRNAs based on chromatin, position, and sequence features—into our previously developed split-dCas9 platform [41]. We also cloned the

two gRNAs that were predicted to have the highest efficiency (SCN9A-1 and SCN9A-2) into a single construct, since we have shown that higher efficacy can be achieved by using multiple gRNAs [41]. We then designed KRAB-Zinc-Finger constructs targeting a single (pD4, pD18, gD9, and gD25) or dual $Na_V1.7$ DNA sequence (pD4+PD18 and gD9+gD25). Next, we transfected our constructs into a mouse neuroblastoma cell line that expresses $Na_V1.7$ (Neuro2a) and confirmed robust repression of $Na_V1.7$ with RT-qPCR. Six of ten gRNAs repressed the $Na_V1.7$ transcript by >50% compared to the non-targeting control (empty control), with gRNA-2 having the highest repression level (56%; $p < 0.0001$) and with the dual-gRNA having repression levels of 71% ($p < 0.0001$) (Figure 4.1). Interestingly, unlike with dual-gRNA systems that are known to have stronger efficacy than single-gRNA systems, we found the dual-ZF constructs to have lower efficacy than the single-ZF constructs. Two single-ZF constructs in particular, ZF-pD18 and ZF-gD25, had strong repression levels, with 68% and 88% respectively ($p < 0.0001$) compared to the negative control (mCherry), which we chose for future *in vivo* studies (Figure 4.1).

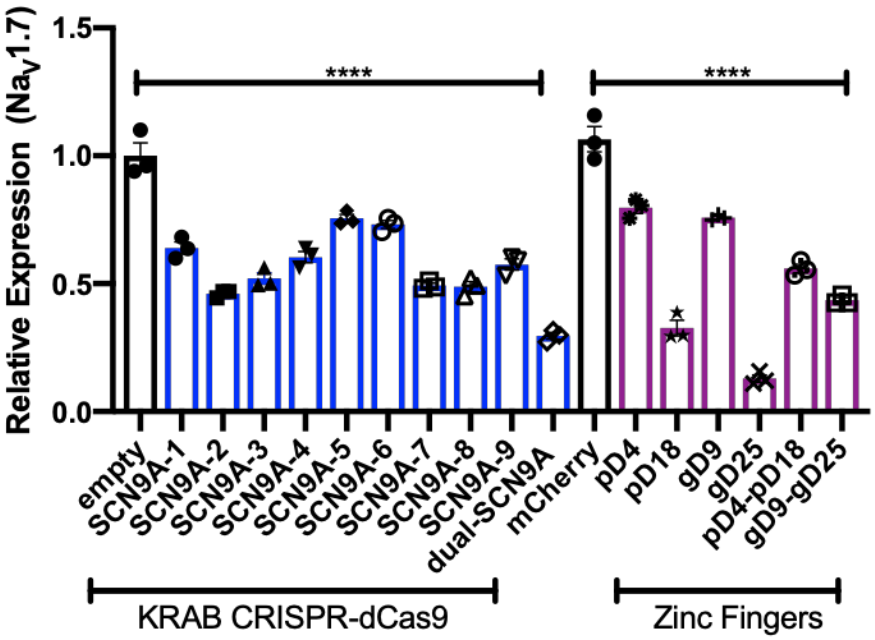

Figure 4.1: *In vitro* optimization of KRAB-CRISPR-dCas9 gRNAs and KRAB-Zinc-Fingers for Na$_V$1.7 repression. *In vitro* Na$_V$1.7 repression in a mouse neuroblastoma cell line (Neuro2a) using KRAB-CRISPR-dCas9 or KRAB-Zinc-Fingers targeting Na$_V$1.7 as determined by RT-qPCR. A non-targeting gRNA (empty) was used as a control for KRAB-CRISPR-dCas9 constructs targeting Na$_V$1.7, while mCherry was used as a control for KRAB-Zinc-Fingers constructs targeting Na$_V$1.7 (n=3; error bars are SEM; one-way ANOVA; ****$p < 0.0001$).

4.4.2 *In vivo* validation of KRAB-ZF and KRAB-CRISPR-dCas9 treatment efficacy in a Carrageenan Model of Pain

Having established robust *in vitro* Na$_V$1.7 repression, we next focused on testing the effectiveness of the best KRAB-ZF constructs from the *in vitro* optimization, (pD18 and gD25), in a Carrageenan-induced model of inflammatory pain. Thermal pain sensitivity was first measured in all mice with the Hargreaves assay in order to establish a baseline level of sensitivity. We then intrathecally (i.t.) injected mice with AAV9-mCherry (negative control; n=5), AAV9-KRAB-ZF-pD18 (n=6), AAV9-KRAB-ZF-gD25 (n=6), or saline (n=5). Three weeks later, and one hour before Carrageenan administration, the mice that received saline were injected with intraperitoneal Gabapentin, a synthetic analogue of gamma aminobutyric acid, (positive control; 100 mg/kg),

which is known to reduce Carrageenan-induced thermal hyperalgesia in rodents [53,54]. One hour after, inflammation was induced in all four groups of mice by injecting the ipsilateral hind paw with Carrageenan, while the contralateral hind paw was injected with saline to serve as an in-mouse control. We then tested mice for thermal pain sensitivity at 30 minutes, and 1, 2, 4, and 24 hours after Carrageenan injection. As expected, compared to saline-injected paws, Carrageenan-injected paws had an increase in thermal hyperalgesia, measured by a decrease in paw withdrawal latency (PWL) after application of a thermal stimulus (Figure 4.2b-d).

We then calculated the paw withdrawal latencies for all groups at each time point and compared these to the AAV9-mCherry Carrageenan injected control using a two-way ANOVA calculation to determine whether there was any significant reduction in thermal hyperalgesia (Table 4.1). We observed all groups to have significantly higher PWL in the saline-injected hind paws as compared to the Carrageenan-injected AAV9-mCherry hind paws. However, when comparing Carrageenan-injected hind paws, only AAV9-KRAB-ZF-gD25 had significantly higher PWL at all the time points following Carrageenan injection when compared to the AAV9-mCherry control. We did see significance in PWL for the Gabapentin positive control group at the 30 minutes and 1 hour time points. However, the PWL for the Gabapentin group were not significant for the remainder of the experiment. We then calculated the area under the curve (AUC) to add the mean withdrawal latencies for all the groups at all time points. Both KRAB-ZF groups had a significant increase in PWL in Carrageenan-injected paws (133% improvement $p=0.0222$ for ZF-gD25; 124% improvement with $p=0.0430$ for ZF-pD18), while the Carrageenan-injected Gabapentin group was not significant when compared to the Carrageenan-injected AAV9-mCherry control (Figure 4.2b-d). Although the half-life of Gabapentin is between 5-7 hours, no effect was seen beyond the 1-hour time point as noted above. In fact, the AAV9-KRAB-ZF-gD25 group had 62% higher PWL than the Gabapentin positive control group.

Twenty-four hours after Carrageenan administration, mice were euthanized and DRGs (L4-L6) were extracted. The expression levels of $Na_V1.7$ were determined by RT-qPCR, and a significant repression of $Na_V1.7$ was observed in AAV9-KRAB-ZF-gD25 and Gabapentin groups (Figure 4.2e). Our results are consistent with previous studies that demonstrated the inhibitory effect of Gabapentin on $Na_V1.7$ expression levels, ultimately leading to a reduction of neuronal excitability [55]. As an index of edema/inflammation, we measured the ipsilateral and contralateral paws with a caliper before and 4 hours after Carrageenan injection, which is the time point with the highest thermal hyperalgesia. We observed significant edema formation in both experimental and control groups, indicating that $Na_V1.7$ repression has no effect on inflammation (Supplementary Figure S3.1). Although it has been previously reported that Gabapentin can lower inflammation on rat paw edema induced by Carrageenan [56], we did not find any reduction in inflammation in the Gabapentin group. This could be due to a difference in animal model, gabapentin dosage, or the concentration of carrageenan injected (they inject 1% carrageenan whereas we inject 2% carrageenan).

Figure 4.2: *In vivo* efficacy of KRAB-Zinc-Fingers in a Carrageenan inflammatory pain model. (a) Schematic of AAV-KRAB-Zinc-Finger gene repression vector. **(b,c,d)** Time course of thermal hyperalgesia after the injection of Carrageenan (solid lines) or saline (dotted lines) into the hind paw of mice injected with Gabapentin (100mg/kg, n=5), AAV9-KRAB-ZFgD25-SCN9A (n=6), AAV9-KRAB-ZFpD18-SCN9A (n=6), or AAV9-mCherry (n=5) are plotted. Mean withdrawal latencies (PWL) are shown. The areas under the curve (AUC) of the thermal-hyperalgesia time-course are plotted to the right. A significant increase in PWL is seen in the Carrageenan-injected paws of mice injected with AAV9-KRAB-ZFgD25 (p=0.222) and AAV9-KRAB-ZFpD18 (p=0.0430), but not in the Gabapentin group. **(e)** $Na_V1.7$ repression from mice DRG (L4-L6) as determined by RT-qPCR is shown (error bars are SEM).

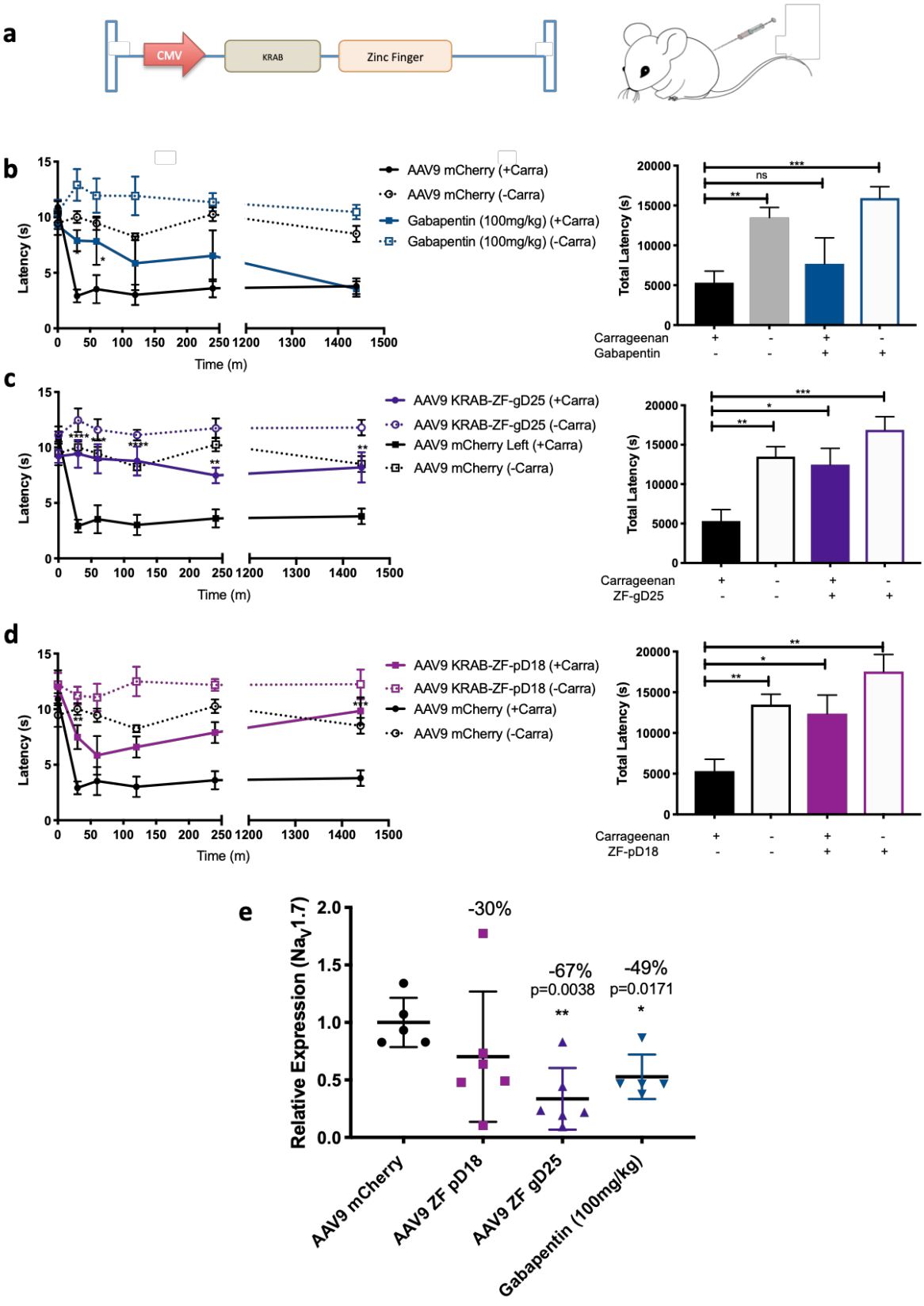
a
CMV
KRAB
Zinc Finger
b
Latency (s)
Time (m)
AAV9 mCherry (+Carra)
AAV9 mCherry (-Carra)
Gabapentin (100mg/kg) (+Carra)
Gabapentin (100mg/kg) (-Carra)
Total Latency (s)
ns
Carrageenan
Gabapentin
c
AAV9 KRAB-ZF-gD25 (+Carra)
AAV9 KRAB-ZF-gD25 (-Carra)
AAV9 mCherry Left (+Carra)
AAV9 mCherry (-Carra)
ZF-gD25
d
AAV9 KRAB-ZF-pD18 (+Carra)
AAV9 KRAB-ZF-pD18 (-Carra)
AAV9 mCherry (+Carra)
AAV9 mCherry (-Carra)
ZF-pD18
e
Relative Expression (Nav1.7)
-30%
-67%
p=0.0038
-49%
p=0.0171
AAV9 mCherry
AAV9 ZF pD18
AAV9 ZF gD25
Gabapentin (100mg/kg)

After having established robust *in vivo* efficacy via KRAB-ZF, we went on to replicate these results with KRAB-ZF and also tested KRAB-CRISPR-dCas9. To increase robustness of our results, we increased the group size to ten mice per group. Similarly, thermal pain sensitivity was first measured in all mice with the Hargreaves assay in order to establish a baseline level of sensitivity. We then intrathecally (i.t.) injected mice with AAV9-mCherry (negative control; n=10), AAV9-KRAB-ZF-gD25 (n=10), AAV9-KRAB-CRISPR-dCas9-dual-SCN9A (n=10), and AAV9-KRAB-CRISPR-dCas9-empty (negative control; n=10). Three weeks later, inflammation was induced in all four groups of mice by injecting the ipsilateral hind paw with Carrageenan, while the contralateral hind paw was injected with saline to serve as an in-mouse control. We then tested mice for thermal pain sensitivity at 30 minutes, and 1, 2, 4, and 24 hours after Carrageenan injection. We calculated the paw withdrawal latencies for all groups at each time point and compared KRAB-ZF-gD25 to the AAV9-mCherry Carrageenan injected control and AAV9-KRAB-CRISPR-dCas9-dual-SCN9A to the AAV9-KRAB-CRISPR-dCas9-empty group using a two-way ANOVA calculation to determine whether there was any significant reduction in thermal hyperalgesia. We observed that both AAV9-KRAB-ZF-gD25 and AAV9-KRAB-CRISPR-dCas9-dual-SCN9A had significantly higher PWL as compared to the Carrageenan-injected AAV9-mCherry and AAV9-KRAB-CRISPR-dCas9-empty hind paws, with 221% and 112% improvement, respectively (Figure 4.3a,b). The expression levels of $Na_V1.7$ were determined by RT-qPCR, and a significant repression of $Na_V1.7$ was observed in KRAB-ZF-gD25 and KRAB-CRISPR-dCas9-dual-SCN9A groups (Figure 4.3c).

Figure 4.3: *In vivo* efficacy of KRAB-Zinc-Fingers and KRAB-CRISPR-dCas9 in a Carrageenan inflammatory pain model. (a) Time course of thermal hyperalgesia after the injection of Carrageenan (solid lines) or saline (dotted lines) into the hind paw of mice injected AAV9-mCherry (n=10), AAV9-KRAB-ZFgD25-SCN9A (n=10) are plotted. Mean paw withdrawal latencies are shown. The areas under the curve (AUC) of the thermal-hyperalgesia time-course are plotted to the right. A significant increase in PWL is seen in the Carrageenan-injected paws of mice injected with AAV9-KRAB-ZFgD25 (p=0.02). **(b)** Time course of thermal hyperalgesia after the injection of Carrageenan (solid lines) or saline (dotted lines) into the hindpaw of mice injected with AAV9-KRAB-CRISPR-dCas9-dual-SCN9A (n=10), or AAV9-KRAB-CRISPR-dCas9-empty (n=10) are plotted. Mean withdrawal latencies (PWL) are shown. The areas under the curve (AUC) of the thermal-hyperalgesia time-course are plotted to the right. A significant increase in PWL is seen in the Carrageenan-injected paws of mice injected with AAV9-KRAB-CRISPR-dCas9-dual-SCN9A (p=0.0325) **(c)** $Na_V1.7$ repression from mice DRG (L4-L6) as determined by RT-qPCR is shown.

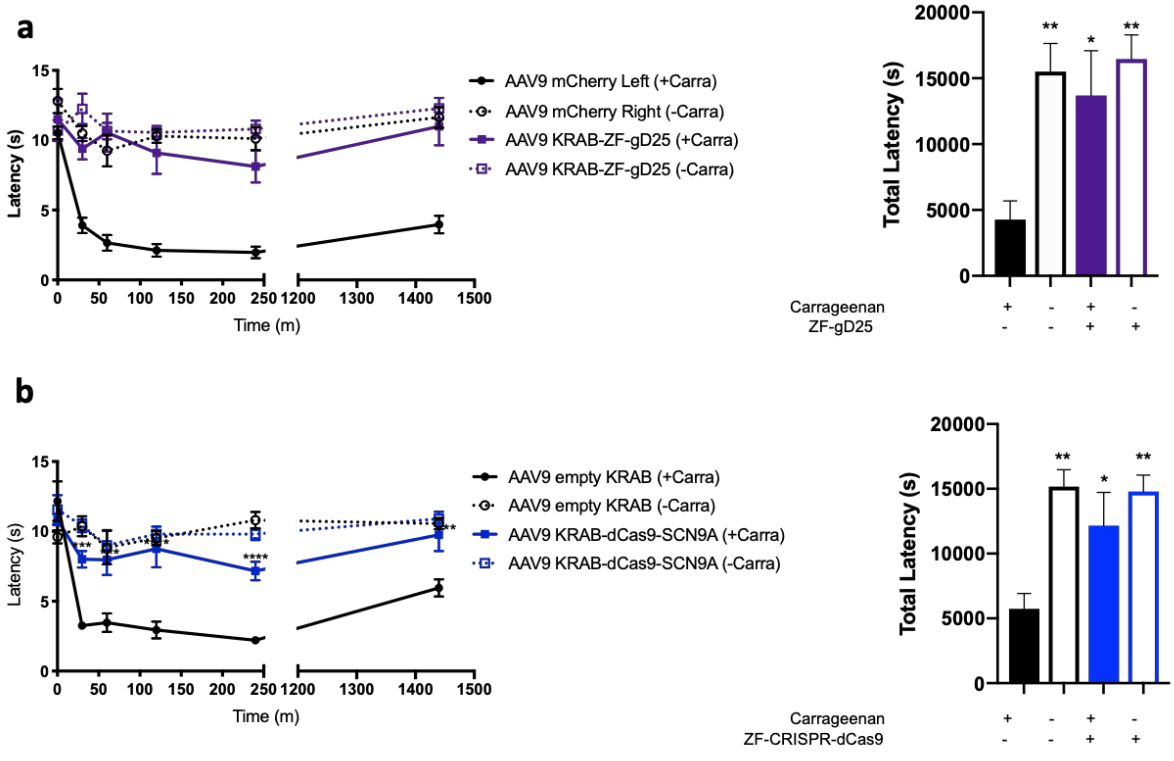
a
Latency (s)
Time (m)
AAV9 mCherry Left (+Carra)
AAV9 mCherry Right (-Carra)
AAV9 KRAB-ZF-gD25 (+Carra)
AAV9 KRAB-ZF-gD25 (-Carra)
Total Latency (s)
Carrageenan
ZF-gD25
b
Latency (s)
Time (m)
AAV9 empty KRAB (+Carra)
AAV9 empty KRAB (-Carra)
AAV9 KRAB-dCas9-SCN9A (+Carra)
AAV9 KRAB-dCas9-SCN9A (-Carra)
Total Latency (s)
Carrageenan
ZF-CRISPR-dCas9

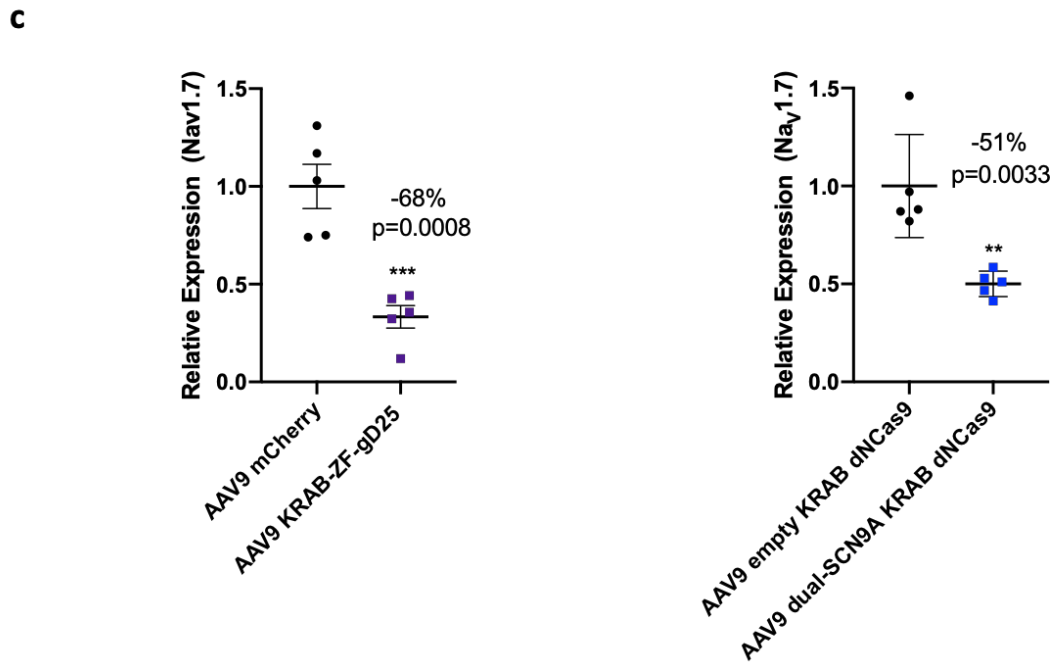
c
Relative Expression (Nav1.7)
-68%
p=0.0008
AAV9 mCherry
AAV9 KRAB-ZF-gD25
Relative Expression (Nav1.7)
-51%
p=0.0033
AAV9 empty KRAB dNCas9
AAV9 dual-SCN9A KRAB dNCas9

Table 4.1: Significance of paw withdrawal latencies in mice receiving AAV9-KRAB-ZFs and Gabapentin (100 mg/kg) as compared to AAV9-mCherry Carrageenan-injected paw (negative control).

Group	Pre-Carrageenan (Baseline)	Post-Carrageenan				
	0 minutes	30 minutes	1 hour	2 hours	4 hours	24 hours
AAV9-KRAB-ZF-pD18 (+Carrageenan)	n.s.	**	n.s.	n.s.	*	***
AAV9-KRAB-ZF-pD18 (-Carrageenan)	n.s.	****	****	****	****	****
AAV9-KRAB-ZF-gD25 (+Carrageenan)	n.s.	****	***	****	*	**
AAV9-KRAB-ZF-gD25 (-Carrageenan)	n.s.	****	****	****	****	****
Gabapentin (100 mg/kg) (+Carrageenan)	n.s.	*	*	n.s.	n.s	n.s.
Gabapentin (100 mg/kg) (-Carrageenan)	n.s.	****	****	****	****	***

Two-way ANOVA with Bonferroni *post hoc* test; ****p<0.0001, ***p < 0.001, **p < 0.01, *p < 0.05; n.s.=not significant).

4.5 Discussion

In this study, the efficacy of *in vitro* repression of $Na_V1.7$ using two genome engineering platforms—KRAB-dCas9 and KRAB-Zinc-Fingers—was investigated. We observed robust *in vitro* repression of $Na_V1.7$. In addition, we tested KRAB-Zinc-Fingers and KRAB-CRISPR-dCas9 targeting $Na_V1.7$ *in vivo*, and found that mice that were injected with KRAB-ZF-gD25 had suppressed inflammatory hyperalgesia, with a ~67% repression of $Na_V1.7$ being sufficient for pain amelioration and ~51% repression of $Na_V1.7$ using KRAB-CRISPR-dCas9 being sufficient for pain amelioration. Previous studies have shown clear evidence in the correlation between an increased $Na_V1.7$ expression in nociceptive neurons and the development of inflammatory hyperalgesia in a Carrageenan-induced model. Thus, our study demonstrates that *in situ* repression of Nav1.7 blocks consequent inflammatory hyperalgesia.

While this study has established evidence for the efficacy of repressing $Na_V1.7$ transcription in treating inflammatory hyperalgesia, there are other aspects that may be investigated and optimized. Within experimental groups, mice often exhibited large phenotypic variations. In order

to account for this in the future, larger sample sizes should be utilized for stronger statistical power. In addition, we performed Carrageenan inflammatory hyperalgesia studies three weeks after AAV injections due to known high expression of AAV vectors at this time point. However, long-term studies need to be performed to evaluate the actual duration of treatment and whether any compensatory mechanisms take place due to $Na_V1.7$ repression. In addition, because in theory KRAB-dCas9 and KRAB-ZFs provide transient pain relief, further studies to determine the efficacy of repeat-dosing also need to be explored. In addition, another avenue to pursue in the future is to target other sodium channels, such as $Na_V1.3$ [57], $Na_V1.8$ [11-13], $Na_V1.9$ [14,15], which have also been associated with neuropathic and inflammatory pain. As such, single or combinatorial repression of these channels could be performed for improved analgesia.

We also note some drawbacks of our study. We chose Gabapentin due to evidence that it decreases Carrageenan-induced thermal hyperalgesia in rodents and because it is known to repress $Na_V1.7$. However, in our study, Gabapentin only significantly increased paw withdrawal latency at two time-points after Carrageenan administration, and therefore, did not result in a very robust positive control. Because only one dosage of Gabapentin was utilized for these experiments, an additional group of mice receiving a different Gabapentin dosage can be utilized as a secondary positive control. Another reason that Gabapentin might not be the best positive control is that although Gabapentin has been shown to work in ameliorating thermal hyperalgesia in rodents, it does not work in humans with inflammatory pain [58]. For future experiments, other positive controls that may be utilized include morphine or a well-documented $Na_V1.7$ inhibitor, such as Tetrodotoxin (TTX) [59,60]. Furthermore, additional models of inflammatory pain should be tested to further validate our results. Carrageenan produces a model of persistent pain and hyperalgesia that best represents an acute phase from 1-24 hours and that converts to chronic inflammation by two weeks [61]. Therefore, the above experiments can be repeated two-weeks after administering

Carrageenan to determine efficacy in a chronic inflammatory pain state. Another pain model that could be tested, for example, is the Complete Freund's adjuvant (CFA) model, which when injected into the tail, paw, muscle, and joint, can result in higher chronic inflammation than Carrageenan. Mice injected with CFA develop thermal and mechanical hyperalgesia, reduced weight bearing, a decreased physical activity. For these reasons, CFA is used to model chronic inflammatory pain conditions that might occur with rheumatoid arthritis or tendonitis. Other inflammatory pain models that could be tested are rheumatoid arthritis models, in which mice are injected with collagen type II antibodies (CAIA) or serum from K/BxN transgenic mice, which mimic the pathology of rheumatoid arthritis such as: widespread inflammation with the greatest effect distally, cartilage degradation, and elevated inflammatory cytokines in the joint fluid [62].

As a potential clinical treatment, KRAB-dCas9 and KRAB-ZFs show promise for treating chronic inflammatory pain. These systems allow for transient gene therapy, which is advantageous in the framework of chronic pain, as permanent pain insensitivity is not desired. While the treatment is transient, the weeks-long duration still presents a significant advantage compared to existing drugs which must be taken daily or hourly, and which may have undesirable addictive qualities. Taken together, the results of these studies show a promising new avenue for treatment of chronic pain, a significant and increasingly urgent issue in our society.

4.6 Acknowledgements

Chapter 4 in part is from a manuscript that is being prepared for publication *Moreno AM, Mali P. In situ repression of a sodium channel via CRISPR-dCas9 and Zinc-Fingers leads to pain-amelioration.* The dissertation author is the primary author.

4.7 References

1. Johannes, CB, Le, TK, Zhou, X, Johnston, JA, Dworkin, RH (2010). The Prevalence of Chronic Pain in United States Adults: Results of an Internet-Based Survey. *J. Pain* **11,** 1230–1239.

2. Souza, JB, Grossmann, E, Perissinotti, DM, Oliveira, JO, Posso, I (2017). Prevalence of Chronic Pain, Treatments, Perception, and Interference on Life Activities: Brazilian Population-Based Survey. *Pain Res. Manag.* **2017**.

3. Fayaz, A, Croft, P, Langford, RM, Donaldson, LJ, Jones, GT (2016). Prevalence of chronic pain in the UK: A systematic review and meta-analysis of population studies. *BMJ Open* **6**.

4. Breivik, H, Collett, B, Ventafridda, V, Cohen, R, Gallacher, D (2006). Survey of chronic pain in Europe: Prevalence, impact on daily life, and treatment. *Eur. J. Pain* **10**: 287–333.

5. Institute of Medicine (US) Committee on Advancing Pain Research, Care, and E. *Relieving Pain in America: A Blueprint for Transforming Prevention, Care, Education, and Research.* (2011). doi:10.17226/13172

6. Hudson, TJ, Painter, JT, Martin, BC, Austen, MA, William, JS, Fortney, JC, Sullivan, MD, Edlund, MJ (2017). Pharmacoepidemiologic analyses of opioid use among OEF/OIF/OND veterans. *Pain* **158**: 1039–1045.

7. Reid, MC, Eccleston, C, Pillemer, K (2015). Management of chronic pain in older adults. *BMJ* **350**: h532.

8. Baumbauer, KM, Young, EE, Starkweather AR, Guite, JW, Russell, BS, Manworren RC (2016). Managing Chronic Pain in Special Populations with Emphasis on Pediatric, Geriatric, and Drug Abuser Populations. *Med. Clin. North Am.* **100**: 183–197.

9. Reimann, F, Cox, JJ, Belfer, I, Diatchenko, L, Zaykin, DV, McHale, DP, Drenth, JP, Dai, F, Wheeler, J, Sanders, F, Wood, L, Wu, TX, Karppinen, J, Nikolajsen, L, Mannikko M, Max, MB, Kiselyczynyk, C, Poddar, M, Te Morsche, RH, Smith, S, Gibson, D, Kelempisioti, A, Maixner, W, Gribble, FM, Woods, CG (2010). Pain perception is altered by a nucleotide polymorphism in SCN9A. *Proc. Natl. Acad. Sci. U. S. A.* **107**: 5148–5153.

10. Cox, JJ, Reimann, F, Nicholas, AK, Thornton, G, Roberts, E, Springell, K, Karbani, G, Jafri, H, Mannan, J, Raashid, Y, Al-Gazali, L, Hamamy, H, Valente, EM, Gorman, S, Williams, R, McHale, DP, Wood, JN, Gribble, FM, Woods, CG (2006). An SCN9A channelopathy causes congenital inability to experience pain. *Nature* **444**: 894–898.

11. Waxman, SG (2013). Painful Na-channelopathies: an expanding universe. *Trends Mol. Med.* **19**: 406–409.

12. Starobova, H, Vetter I (2017). Pathophysiology of Chemotherapy-Induced Peripheral Neuropathy. *Front. Mol. Neurosci.* **10**: 174.

13. Han, C, Huang, J, Waxman, SG (2016). Sodium channel Nav1.8: Emerging links to human disease. *Neurology* **86**: 473–483.

14. Sun, J, Guangyou, D, Li, N, Guo, S, Zhang, Y, Ying, Y, Zhang, M, Wang, Q, Liu, JY, Zhang, W (2017). SCN11A variants may influence postoperative pain sensitivity after gynecological surgery in Chinese Han female patients. *Medicine (Baltimore)*. **96**: e8149.

15. Castoro, R, Simmons, M, Ravi, V, Huang, D, Lee, C, Sergent, J, Zhou, L, Li, J (2018). SCN11A Arg225Cys mutation causes nociceptive pain without detectable peripheral nerve pathology. *Neurol. Genet.* **4**: e255.

16. Cregg, R, Momin, A, Rugiero, F, Wood, JN, Zhao, J (2010). Pain channelopathies. *J. Physiol.* **588**: 1897–1904.

17. Bennett, DLH, Woods, CG (2014). Painful and painless channelopathies. *Lancet. Neurol.* **13**: 587–599.

18. Faber, CG, Hoejimakers, JG, Ahn, HS, Cheng, X, Han, X, Choi, JS, Estacion, M, Lauria, G, Vanhoutte, EK, Gerrits, MM, Dib-Haji, S, Drenth, JP, Waxman, SG, Merkles, IS (2012). Gain of function Nav1.7 mutations in idiopathic small fiber neuropathy. *Ann. Neurol.* **71**: 26–39.

19. Faber, CG, Lauria, G, Merkles, IS, Cheng, X, Han, C, Ahn, HS, Persson, AK, Hoejimakers, JG, Gerrits, MM, Pierro, T, Lombardi, R, Kapetis, D, Dib-Hajj, SD, Waxman, SG (2012). Gain-of-function Nav1.8 mutations in painful neuropathy. *Proc. Natl. Acad. Sci. U. S. A.* 109: 19444–19449.

20. Huang, J, Han, C, Estacion, M, Vasylayev, D, Hoeijmakers, JG, Gerrits, MM, Tyrrell, L, Lauria, G, Faber, CG, Dib-Hajj SD, Merkies, IS, Waxman, SG (2014). Gain-of-function mutations in sodium channel Na(v)1.9 in painful neuropathy. *Brain* **137**: 1627–1642.

21. Huang, J, Vanoye, CG, Cutts, A, Goldberg, YP, Dib-Hajj, SF, Cohen, CJ, Waxman, SG, George AL Jr. (2017). Sodium channel NaV1.9 mutations associated with insensitivity to pain dampen neuronal excitability. *J. Clin. Invest.* **127**: 2805–2814.

22. Dib-Hajj, SD, Black, JA, Waxman, SG (2015). NaV1.9: a sodium channel linked to human pain. *Nat. Rev. Neurosci.* **16**: 511–519.

23. Dib-Hajj, SD, Yang, Y, Black, JA, Waxman, SG (2013). The Na(V)1.7 sodium channel: from molecule to man. *Nat. Rev. Neurosci.* **14**: 49–62.

24. Yang, Y, Mis, MA, Estacion, M, Dib-Hajj, SD, Waxman, SG (2018). NaV1.7 as a Pharmacogenomic Target for Pain: Moving Toward Precision Medicine. *Trends Pharmacol. Sci.* **39**: 258–275.

25. Hutchings, CJ, Colussi, P, Clark, TG (2019). Ion channels as therapeutic antibody targets. *MAbs* **11**: 265–296.

26. Sun, H, Li, M (2013). Antibody therapeutics targeting ion channels: are we there yet? *Acta Pharmacol. Sin.* **34**: 199.

27. Bang, S, Yoo, J, Gong, X, Liu, D, Han, Q, Luo, X, Chang, W, Chen, G, Im, ST, Kim, YH, Strong, JA, Zhang, MZ, Zhang, JM, Lee, SY, Ji, RR (2018). Differential Inhibition of Nav1.7 and Neuropathic Pain by Hybridoma-Produced and Recombinant Monoclonal Antibodies that Target Nav1.7. *Neurosci. Bull.* **34**: 22–41.

28. Lee, JH, Park, CK, Chen, G, Han, Q, Xie, RG, Liu, T, Ji, RR, Lee, SY (2014). A Monoclonal Antibody that Targets a $Na_V1.7$ Channel Voltage Sensor for Pain and Itch Relief. *Cell* **157**: 1393–1404.

29. Tabebordbar, M, Zhu, K, Cheng, JKW, Chew, WL, Widrick, JJ, Yan, WX, Maesner, C, Wu, EY, Xiao, R, Ran, FA, Cong, L, Zhang, F, Vanderberghe, LH, Church, GM, Wagers, AJ (2016). In vivo gene editing in dystrophic mouse muscle and muscle stem cells. *Science* **351**: 407–411.

30. Nelson, CE, Hakim, CH, Ousterout, DG, Thakore, PI, Moreb, EA, Rivera, RMC, Madhavan, S, Pan, X, Ran, FA, Yan, WX, Asokan, A, Zhang, F, Duan, D, Gersbach, CA (2016). In vivo genome editing improves muscle function in a mouse model of Duchenne muscular dystrophy. *Science* **351**: 403–407.

31. Long, C, Amoasii, L, Mireault, AA, McAnally, JR, Li, H, Sanchez-Ortiz, E, *et al.* (2015). Postnatal genome editing partially restores dystrophin expression in a mouse model of muscular dystrophy. *Science* **351**: aad5725.

32. Amoasii, L, Hildyard, JCW, Li, H, Sanchez-Ortiz, E, Mireault, A, Caballero, D, Harron, R, Stathopoulou, TR, Massey, C, Shelton, JM, Bassel-Duby, R, Piery, RJ, Olson, EN (2018). Gene editing restores dystrophin expression in a canine model of Duchenne muscular dystrophy. *Science* **362**: 86-91.

33. Yang, Y, Wang, L, Bell, P, McMenamin, D, He, Z, White, J, Yu, H, Xu, C, Mirizono, H, Musunuru, K, Batshaw, ML, Wilson, JM (2016). A dual AAV system enables the Cas9-mediated correction of a metabolic liver disease in newborn mice. *Nat Biotech* **34**: 334–338.

34. Yin, H, Song, CQ, Dorkin, JR, Zhu, LJ, Li, Y, Wu, Q, Park, A, Yang, J, Suresh, S, Bizhanova, A, Gupta, A, Bolukbasi, MF, Walsh, S, Bogorad, RL, Gao, G, Weng, Z, Dong, Y, Koteliasnky, V, Wolfe, SA, Langer, R, Xue, W, Anderson, DG (2016). Therapeutic genome editing by combined viral and non-viral delivery of CRISPR system components in vivo. *Nat. Biotechnol.* **34**: 328–333.

35. Monteys, AM, Ebanks, SA, Keiser, MS, Davidson, BL (2017). CRISPR/Cas9 Editing of the Mutant Huntingtin Allele In Vitro and In Vivo. *Mol. Ther.* **25**: 12–23.

36. Gilbert, L a, Larson, MH, Morsut, L, Liu, Z, Gloria, A, Torres, SE, Stern-Ginossar, N, Brandman, O, Whitehead, EH, Doudna, JA, Lim, WA, Weissman, JS, Qi, LS (2013). CRISPR-Mediated Modular RNA-Guided Regulation of Transcription in Eukaryotes. *Cell* **154**: 442–451.

37. Gilbert, LA, Horlbeck, MA, Adamson, B, Villalta, JE, Chen, Y, Whitehead, EH, Guimaraes, C, Panning, B, Ploegh, HL, Bassik, MC, Qi, LS, Kampmann, M, Weissman, JS (2014). Genome-Scale CRISPR-Mediated Control of Gene Repression and Activation. *Cell* **159**: 647–661.

38. Kearns, NA, Pham, H, Tabak, B, Genga, RM, Silverstein, NJ, Garber, M, Maehr, R (2015). Functional annotation of native enhancers with a Cas9–histone demethylase fusion. *Nat. Methods* **12**: 401.

39. Gaba, F, Tsang, JCH, Gao, X, Lu, L, Liu, P, Wu, D (2014). Comparison of TALE designer transcription factors and the CRISPR/dCas9 in regulation of gene expression by targeting enhancers. *Nucleic Acids Res.* **42**: e155–e155.

40. Thakore, PI, M, DA, Song, L, Safi, A, Shivakumar, NK, Kabadi, AM, Reddy, TE, Crawford, GE, Gersbach, CA (2015). Highly specific epigenome editing by {CRISPR-Cas9} repressors for silencing of distal regulatory elements. *Nat Methods* **12**: 1143–1149.

41. Moreno, AM, Fu, X, Zhu, J, Katrekar, D, Shih, YR V, Marlett, J, Cabotaje, J, Tat, J, Naughton, J, Lisowsky, L, Varghese, S, Zhang, K, Mali, P (2018). *In situ* gene therapy via AAV-CRISPR-Cas9 mediated targeted gene regulation. *Mol. Ther.* **26**: 1818-1827.

42. Thakore, PI, Kwon, JB, Nelson, CE, Rouse, DC, Gemberling, MP, Oliver, ML, Gersbach, CA (2018). RNA-guided transcriptional silencing in vivo with S. aureus CRISPR-Cas9 repressors. *Nat. Commun.* **9**: 1674.

43. Lupo, A, Cesaro, E, Montano, G, Zurlo, D, Izzo, P, Costanzo, P (2013). KRAB-Zinc Finger Proteins: A Repressor Family Displaying Multiple Biological Functions. *Curr. Genomics* **14**: 268–278.

44. Sapunar, D, Kostic, S, Banozic, A, Puljak, L (2012). Dorsal root ganglion - a potential new therapeutic target for neuropathic pain. *J. Pain Res.* **5**: 31–38.

45. Schuster, DJ, Dykstra, JA, Riedl, MS, Kitto, KF, Belur, LR, McIvor, RS, Elde, RP, Fairbanks, CA, Vulchanova, L (2014). Biodistribution of adeno-associated virus serotype 9 (AAV9) vector after intrathecal and intravenous delivery in mouse. *Front. Neuroanat.* **8**: 42.

46. Hirai, T, Enomoto, M, Kaburagi, H, Sotome, S, Yoshida-Tanaka, K, Ukegawa, M, Kuwahara, H, Yamamoto, M, Taijiri, M, Miyata, H, Hirai, Y, Tominaga, M, Shinomiya, K, Mizusawa, H, Okawa, A, Yokota, T (2014). Intrathecal AAV serotype 9-mediated delivery of shRNA against TRPV1 attenuates thermal hyperalgesia in a mouse model of peripheral nerve injury. *Mol. Ther.* **22**: 409–419.

47. Horlbeck, MA, Witkowsky, LB, Guglielmi, B, Replogle, JM, Gilbert, LA, Villalta, JE, Torigoe, SE, Tijuan, R (2016). Nucleosomes impede Cas9 access to DNA in vivo and in vitro. In: Adelman, K (ed.). *Elife* **5**: e12677.

48. Ichikizazi, K, Toysa, S, Hoshino, T (1979). A new procedure for lumbar puncture in the mouse (intrathecal injection) preliminary report. Keio J. Med. 28: 165-171.

49. Lucas, KK, Svensson, CI, Hua, X-Y, Yaksh, TL, Dennis, EA (2005). Spinal phospholipase A2 in inflammatory hyperalgesia: role of group IVA cPLA2. *Br. J. Pharmacol.* **144**: 940–952.

50. Svensson, CI, Lucas, KK, Hua, X-Y, Powell, HC, Dennis, EA, Yaksh, TL (2005). Spinal phospholipase A2 in inflammatory hyperalgesia: Role of the small, secretory phospholipase A2. *Neuroscience* **133**: 543–553.

51. Chaplan, SR, Bach, FW, Pogrel, JW, Chung, JM, Yaksh, TL (1994). Quantitative assessment of tactile allodynia in the rat paw. *J. Neurosci. Methods* **53**: 55–63.

52. Hargreaves, K, Dubner, R, Brown, F, Flores, C, Joris, J (1988). A new and sensitive method for measuring thermal nociception in cutaneous hyperalgesia. *Pain* **32**: 77–88.

53. Lu, Y, Westlund, KN (1999). Gabapentin Attenuates Nociceptive Behaviors in an Acute Arthritis Model in Rats. *J. Pharmacol. Exp. Ther.* **290**: 214-219.

54. Jones, CK, Peters, SC, Shannon, HE (2005). Efficacy of Duloxetine, a Potent and Balanced Serotonergic and Noradrenergic Reuptake Inhibitor, in Inflammatory and Acute Pain Models in Rodents. *J. Pharmacol. Exp. Ther.* **312**: 726-732.

55. Zhang, JL, Yang, JP, Zhang, JR, Li, RQ, Wang, J, Jan, JJ, Zhuang, Q (2013). Gabapentin reduces allodynia and hyperalgesia in painful diabetic neuropathy rats by decreasing expression level of Nav1.7 and p-ERK1/2 in DRG neurons. *Brain Res.* **1493**: 13–18.

56. Abdel-Salam, OM, Amany, AS (2009). Study of the analgesic, anti-inflammatory, and gastric effects of gabapentin. *Drug discoveries & therapeutics* **31** :18-26.

57. Su, S, Shao, J, Zhao, Q, Ren, X, Cai, W, Li, L, Bai, Q, Chen, X, Xu, B, Wang, J, Cao, J, Zang, W (2017). MiR-30b Attenuates Neuropathic Pain by Regulating Voltage-Gated Sodium Channel Nav1.3 in Rats. *Front. Mol. Neurosci.* **10**: 126.

58. Werner, MU, Perkins, FM, Holte, K, Pedersen, JL, Kehlet, H (2001). Effects of Gabapentin in Acute Inflammatory Pain in Humans. *Reg. Anesth. Pain Med.* **26**: 322-328.

59. Sangameswaran, L, Fish, LM, Koch, BD, Rabert, DK, Delgado, SG, Ilnicka, M, Jakeman, LB, Novakovic, S, Wong, K, Sze, P, Tzoumaka, E, Stewart, GR, Herman, RC, Chan, H, Eglen, RM, Hunter, JC (1997). A novel tetrodotoxin-sensitive, voltage-gated sodium channel expressed in rat and human dorsal root ganglia. *J. Biol. Chem.* **272**: 14805–14809.

60. Klugbauer, N, Lacinova, L, Flockerzi, V, Hofmann, F (1995). Structure and functional expression of a new member of the tetrodotoxin-sensitive voltage-activated sodium channel family from human neuroendocrine cells. *EMBO J.* **14**:1084–1090.

61. Radhakrishnan, R, Moore, SA, Sluka, KA (2003). Unilateral carrageenan injection into muscle or joint induces chronic bilateral hyperalgesia in rats. *Pain* **104**: 567–577.

62. Gregory, NS, Harris, AL, Robinson, CR, Dougherty, PM, Fuchs, PN, Sluka, KA (2013). An overview of animal models of pain: disease models and outcome measures. *J. Pain* **14**: 1255–1269.

Chapter 5 - Conclusions

5.1 Recapitulation

In the past decades, advances in genomics have transformed our understanding of genome mutations leading to disease. In addition, changes in gene regulation have also been attributed to disease states, such as in cancer and neurodegenerative diseases. Therefore, tools with the ability to perturb the genome are needed to enable therapeutic amelioration of these disease states. The work presented in this thesis focuses on developing a CRISPR-Cas9 platform via AAVs for *in situ* genome engineering applications for potential translatability to human use.

We first developed an integrated AAV-based CRISPR-Cas9 platform that provides a facile and robust method to edit and regulate the expression of endogenous genes via Cas9 and dCas9 based effectors. This system has several advantages, including the utilization of a split-Cas9 system, which due to the limited cargo capacity of AAVs (~4.7kb), is an optimal approach to enable desired genome engineering applications. In addition, the modular vector architecture of this platform couples dCas9 and several transcriptional regulators with ease, thereby engineering the full spectrum of genome editing and regulation (both activation and repression functionalities). Using this platform, we demonstrated for the first time the utility of AAV-KRAB-dCas9 mediated *in situ* gene repression in the context of gene therapy, specifically, to prevent vision loss in a mouse model of retinitis pigmentosa. We note some potential limitations of the our system: mainly, utilizing a split-Cas9 system will have reduced targeting efficiency as both components, C-Cas9 and N-Cas9, have to be co-delivered to the target cell of interest to restore Cas9 activity. Additionally, because dCas9 does not enable a permanent change to the genome, multiple treatments for efficacious treatment of retinitis pigmentosa might be necessary. We, however, expect that, with steady

improvements in techniques for localized tissue-specific delivery and optimization of AAV production, these aspects will be progressively addressed. Taken together, we believe that our CRISPR-dCas9 mediated *in situ* cellular reprogramming approach represents a promising strategy towards the treatment of human diseases in a gene and mutation independent context.

Next, we focused on tackling an important issue that CRISPR-Cas9 and AAVs will face when trying to reach the clinic, which is the interaction with the adaptive immune system. We proposed the sequential use of immune orthologous proteins whose structure is subject to diversification via genetic drift to address the pre-existing immunity and re-dosing issues. This would, in principle, allow for repeated treatments by 'immune orthogonal' orthologs without reduced efficacy due to the lack of immune cross-reactivity among the proteins. To explore and validate this concept we chose 284 DNA targeting and 84 RNA targeting CRISPR effectors and 167 Adeno-associated virus (AAV) capsid protein orthologs and developed a pipeline to compare total sequence similarity as well as predicted binding to class I and class II Major Histocompatibility Complex (MHC) proteins. Our predictions revealed that 79% of DNA-targeting Cas orthologs do not elicit cross-reacting immune responses, while no global immune orthogonality among AAV serotypes was observed. We then validated three Cas9 orthologs that were predicted to be immune orthogonal: *S. pyogenes*, *S. aureus*, and *C. jejuni* in which we did not observe cross-reacting antibodies against Cas9 orthologs in sera from immunized mice. Finally, to demonstrate the efficacy of multiple dosing with immune orthogonal orthologs, we delivered AAV-Cas9 targeting PCSK9 into BALB/c mice previously immunized against the AAV vector and/or the Cas9 payload, demonstrating that editing efficiency is compromised by immune recognition of either the AAV or Cas9, but, importantly, this effect is abrogated when using immune orthogonal orthologs. We note some limitations to this work. First, we utilized two inbred mice strains as our models, C57BL/6J and BALB/c, which have limited MHC diversity and might not recapitulate other human

immunological features, such as differences in antigen processing and presentation. Another limitation to our work is the lack of implementation of B-cell epitopes into our immune orthogonality analysis. However, since B-cell epitopes may be both linear and conformational, these are more difficult to predict. Advances and further validation of *in silico* models will allow for better predictions in the future. Overall, we believe our framework provides a potential solution for efficacious gene therapy, not solely for Cas9-mediated genome engineering, but also for other protein therapeutics that might necessitate repetitive treatments.

Lastly, we focused on implementing our previously developed platforms to target a mutant-independent disease—chronic pain. Chronic pain affects over 100 million Americans, which is more than cancer, diabetes, and heart disease combined. Chronic pain patients rely on opioid narcotics, which have high addiction risk and adverse side effects, including increased sensitivity to pain. Since the discovery of the relationship between humans with $Na_V1.7$ (SCN9A) mutations and congenital insensitivity to pain, this sodium channel has been an attractive target for developing chronic pain therapies. However, efforts to develop selective small molecule inhibitors have been hampered due to the high sequence identity between Na_V subtypes, including $Na_V1.5$, which is expressed in the heart. We therefore used our KRAB-CRISPR-dCas9 platform, as well as a platform based on human transcription factors, KRAB-Zinc-Fingers, to epigenetically repress $Na_V1.7$. We first optimized these constructs *in vitro* and demonstrated robust repression of $Na_V1.7$ in Neuro2A cells. We then chose the two constructs with the highest *in vitro* efficacy, (KRAB-ZF-gD25 and KRAB-ZF-pD18), packaged these into AAV9 and delivered these intrathecally into mice. After inducing inflammation by injecting Carrageenan into the ipsilateral paws, we tested for thermal withdrawal latency using the Hargreaves model. We observed a 133% increase in paw-withdrawal latency in Carrageenan-injected hind paws of mice that were injected with AAV9-KRAB-ZF-gD25 as compared to the negative control ($p=0.0222$), with a corresponding 67%

repression of Nav1.7 (p=0.0038). We observe some caveats to our study. First, the Gabapentin positive control was only significantly better than the negative control at two time points, and as such, a more robust positive control should be utilized in future studies. In addition, Carrageenan produces a model of persistent pain and hyperalgesia that best represents an acute phase from 1-24 hours and that converts to chronic inflammation by two weeks. Because we terminated our study after 24 hours, additional studies in inflammatory pain models that better recapitulate chronic pain need to be performed. Taken together, we believe that CRISPR-dCas9 and Zinc-Finger mediated *in situ* gene repression represents a promising strategy in the treatment of chronic pain.

5.2 Perspectives for the future

Although the advances in this thesis represent a step forward to the eventual application of CRISPR-Cas9 to the clinic, there are still many hurdles to overcome. A hurdle faced by the gene therapy field in general are efficient, specific, and safe *in vivo* delivery methods. In this thesis, we utilized AAVs due to their mild immune response, low toxicity, long-term transgene expression and favorable safety profile. In fact, AAVs are the only viral vectors approved for clinical use in Europe (Glybera), and are being utilized in multiple U.S. clinical trials for treatment of Hemophilia B and spinal muscular atrophy [1,2]. However, an important issue with therapeutic AAV delivery, as discussed in Chapter 3, is the presence of neutralizing antibodies and CD8+ T-cell mediated cytotoxic immune response towards transduced cells presenting AAV capisd antigens, which remains a significant barrier to successful application of AAV therapies. Some advances are being made to reduce capsid immunogenicity such as modifying AAV capsids by proteasomal de-targeting of AAV vectors, which has shown to decrease both antigen presentation on MHC class I of capsid-derived peptides [3] and the generation of NAbs that are cross-reactive to the parental

serotype. [4,5] In addition, modifications to the nature and the sequence of the vector genome have been reported to impact the AAV immunogenicity in mouse models [6]. In order to help patients with neutralizing antibodies against AAVs, capsid serotype switching may be a solution [7,8], or the use of immunosuppressive drugs might be required [9,10]. The latter, however, will be less useful for long-term genome regulatory modifications. In addition to AAVs, other delivery methods for CRISPR-Cas9 have been developed for mouse models, which could eventually be used in the clinic, including cationic liposomes [11] and gold nanoparticles [12]. Further studies and development of safe and efficacious delivery methods with low immunogenicity need to be explored before translation of CRISPR-Cas9 therapeutics into the clinic.

Another challenge for CRISPR-Cas9 translation into the clinic are potential off-target effects. To minimize the incidence of off-target effects, variants of Cas9 enzymes are being engineered with higher fidelity [13,14]. In addition, the transient expression of Cas9 as a ribonucleoprotein, instead of as a vector, has shown to lower the possibility of off-target effects [15], since reducing the temporal pulse of Cas9 expression can greatly reduce off-target effects. In addition, the nuclease-null Cas9 version (dCas9) fused to a FokI nuclease or a nickase Cas9, which have also been shown to have higher specificity [16,17,18], could also be utilized. For diseases that do not require permanent genome changes, the use of dCas9 for non-permanent genome regulation could also be utilized.

Finally, immunogenicity of therapeutic CRISPR-Cas9 components could also be a hurdle that needs to be overcome. Cas9 is a foreign prokaryotic protein, which has been shown to elicit cellular and humoral responses, with Cas9-specific antibodies elicited post exposure [8, 19]. In addition, anti-Cas9 responses have been found to be present in healthy human adults [20]. Choosing the appropriate delivery system might help dampen immune response to Cas9. For instance, studies have shown strong immune responses when transgenes have been delivered by adenoviruses but not

by adeno-associated viruses [21-24]. One could also shield the Cas9 protein with chemical conjugates to evade humoral responses [25]. Additionally, Cas9 could be 'humanized' whereby the nonhuman regions of the Cas9 protein are replaced by the human equivalent. Finally, as suggested in chapter 3, one could in theory prescribe the use of sequential immune-orthogonal Cas9 proteins for efficacious repeat dosing. Taken together, the rapid progress in genome engineering toolsets based on CRISPR-Cas systems, coupled with the development of new generation of viral and nonviral delivery approaches will lead the way for efficacious gene therapy applications.

5.3 References

1. Nathwani, AC, Rosales, C, McIntosh, J, Rastegarlari, G, Nathwani, D, Raj, D, Nawathe, S, Waddington, SN, Bronson, R, Jackson, S (2011). Long-term safety and efficacy following systemic administration of a self-complementary AAV vector encoding human FIX pseudotyped with serotype 5 and 8 capsid proteins. *Mol. Ther*. **19**: 876–885.

2. Mendell, JR, Al-Zaidy, S, Shell, R, Arnold, WD, Rodino-Klapac, LR, Prior, TW, Lowes L, Alfano L, Berry K, Church K (2017). Single-dose gene-replacement therapy for spinal muscular atrophy. *N. Engl. J. Med*. **377**: 1713–1722.

3. Martino, AT, Basner-Tschakarjan, E, Markusic, DM, Finn, JD, Hinderer, C, Zhou, S, Ostrov, DA, Srivastava, A, Ertl, HC, Terhorst, C (2013). Engineered AAV vector minimizes in vivo targeting of transduced hepatocytes by capsid-specific CD8+ T cells. *Blood*. **121**:2224–2233.

4. Gabriel, N, Hareendran, S, Sen, D, Gadkari, RA, Sudha, G, Selot, R, Hussain, M, Dhaksnamoorthy, R, Samuel, R, Srinivasan, N (2013). Bioengineering of AAV2 capsid at specific serine, threonine, or lysine residues improves its transduction efficiency in vitro and in vivo. *Hum. Gene Ther. Methods*. **24**:80–93.

5. Sen, D, Gadkari, RA, Sudha, G, Gabriel, N, Kumar, YS, Selot, R, Samuel, R, Rajalingam, S, Ramya, V, Nair, SC (2013). Targeted modifications in adeno-associated virus serotype 8 capsid improves its hepatic gene transfer efficiency in vivo. *Hum. Gene Ther. Methods*. **24**: 104–116.

6. Colella, P, Ronzitti, G, Mingozzi, F (2017). Emerging Issues in AAV-Mediated In Vivo Gene Therapy. *Mol. Ther. Methods Clin. Dev.* **8**: 87–104.

7. Majowicz, A, Salas, D, Zabaleta, N, Rodríguez-Garcia, E, González-Aseguinolaza, G, Petry, H, Ferreira, V (2017). Successful repeated hepatic gene delivery in mice and non-human primates achieved by sequential administration of AAV5ch and AAV1. *Mol. Ther.* **25**: 1831–1842.

8. Moreno, AM, Palmer, N, Aleman, F, Chen, G, Pla, A, Jiang, N, Chew, WL, Law, M, Mali, P (2019) Exploring protein orthogonality in immune space: a case study with AAV and Cas9 orthologs. Nature Biomedical Engineering *(2019) in press.*

9. Nathwani, AC, Tuddenham, EG, Rangarajan, S, Rosales, C, McIntosh, J, Linch, DC, Chowdary, P, Riddell, A, Pie, AJ, Harrington, C (2011). Adenovirus-associated virus vector-mediated gene transfer in hemophilia B. N. *Engl. J. Med.* **365**: 2357–2365.

10. Nathwani, AC, Reiss, UM, Tuddenham, EG, Rosales, C, Chowdary, P, McIntosh, J, Della Peruta, M, Lheriteau, E, Patel, N, Raj, D (2014). Long-term safety and efficacy of factor IX gene therapy in hemophilia B. *N. Engl. J. Med.* **371**: 1994–2004.

11. Zhang, L, Wang, P, Feng, Q, Wang, N, Chen, Z, Huang, Y, Cheng, W (2017). Lipid nanoparticle-mediated efficient delivery of CRISPR/Cas9 for tumor therapy. *Npg Asia Mater.* **9**: e441.

12. Lee, B, Lee, K, Panda, S, Gonzales-Rojas, R, Chong, A, Bugay, V, Park, HM, Brenner, R, Murthy, N, Lee, HY (2018). Nanoparticle delivery of CRISPR into the brain rescues a mouse model of fragile X syndrome from exaggerated repetitive behaviours. *Nat. Biomed. Eng.* **2**: 497–507.

13. Kleinstiver, BP, Pattanayak, V, Prew, MS, Tsai, SQ, Nguyen, NT, Zheng, Z, Joung, JK (2016) High-fidelity CRISPR–Cas9 nucleases with no detectable genome-wide off- target effects. *Nature* **529**: 490-5.

14. Vakulskas, CA, Dever, DP, Rettig, GR, Turk, R, Jacobi, AM, Collingwood, MA, Bode, NM, McNeill, MS, Yan, S, Camarena, J, Lee, CM, Park, SH, Wiebking, V, Bak, RO, Gomez-Ospina, N, Pavel-Dinu, M, Sun, W, Bao, G, Porteus, MH, Behlke, MA (2018). A high-fidelity Cas9 mutant delivered as a ribonucleoprotein complex enables efficient gene editing in human hematopoietic stem and progenitor cells. *Nat Med*. **24**: 1216-24.

15. Kim, S, Kim, D, Cho, SW, Kim, J, Kim, JS (2014). Highly efficient RNA-guided genome editing in human cells via delivery of purified Cas9 ribonucleoproteins. *Genome Res* **24**:1012-9.

16. Tsai, SQ, Wyvekens, N, Khayter, C, Foden, JA, Thapar, V, Reyon, D, Goodwin, MJ, Aryee, MJ, Joung, JK (2014). Dimeric CRISPR RNA-guided FokI nucleases for highly specific genome editing. *Nat Biotechnol.* **32**: 569–576.

17. Guilinger, JP, Thompson, DB, Liu, DR (2014). Fusion of catalytically inactive Cas9 to FokI nuclease improves the specificity of genome modification. *Nat Biotechnol*. **32**:577–582.

18. Zhang, XH, Tee, LY, Wang, XG, Yang, SH (2015). Off-target effects in CRISPR/Cas9-mediated genome engineering. *Mol Ther Nucl Acids.* **4**: e264.

19. Chew, WL, Tabebordbar, M, Cheng, JKW, Mali, P, Wu, EY, Ng, AHM, Zhu, K, Wagers, AJ, Church, GM (2016). A multifuncitonal AAV-CRISPR-Cas9 and its host reponse. *Nat Methods.* **13**: 868-874.

20. Charlesworth, CT, Deshpande, PS, Dever, DP, Dejene, B, Gomez-Ospina, N, Mantri, S, Pavel-Dinu, M, Camarena, J, Weinberg, KI, Porteus, MH (2019). Identification of Pre-Existing Adaptive Immunity to Cas9 Proteins in Humans. *Nat. Med*. **25**: 249-254.

21. Jooss, K, Yang, Y, Fisher, KJ, Wilson, JM (1998). Transduction of dendritic cells by DNA viral vectors directs the immune response to transgene products in muscle fibers. *J Virol*. **72**: 4212–4223.

22. Fisher, KJ, Jooss, K, Alston, J, Yang, Y, Haecker, SE, High, K, Pathak, R, Raper, SE, Wilson, JM (1997). Recombinant adeno-associated virus for muscle directed gene therapy. *Nat Med* **3**: 306–312.

23. Xiao, X, Li, J, Samulski, RJ (1996). Efficient long-term gene transfer into muscle tissue of immunocompetent mice by adeno-associated virus vector. *J Virol*. **70**: 8098–8108.

24. Kessler, PD, Podsakoff, GM, Chen, X, McQuiston, SA, Colosi, PC, Matelis, LA, Kurtzman, GJ, Byrne, BJ (1996). Gene delivery to skeletal muscle results in sustained expres- sion and systemic delivery of a therapeutic protein. *Proc Natl Acad Sci USA*. **93**:14082–14087.

25. Zelikin, AN, Ehrhardt, C, Healy, AM (2016). Materials and methods for delivery of biological drugs. *Nat Chem* **8**:997–1007.

Chapter S1: Supplement to Chapter 2

S1.1 Supplementary Figures and Tables

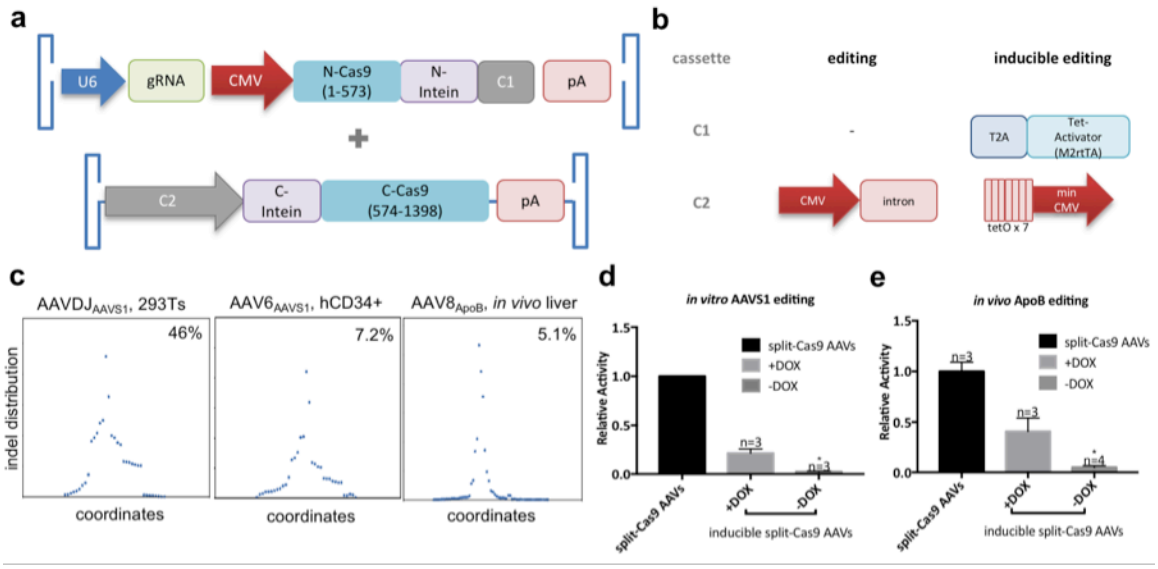

Figure S1.1: Genome editing via a modular dual-AAV split-Cas9 system. (a) Schematic of intein-mediated split-Cas9 pAAVs for genome editing. **(b)** Approach for modular usage of effector and regulatory cassettes to enable genome editing and inducible genome editing applications. **(c)** From left to right, indel frequency and distribution at the *AAVS1* locus *in vitro* in HEK293T cells and in CD34+ hematopoietic stem cells, and *in vivo* at the *ApoB* locus. For all panels shown, the x-axis is centered on the predicted SpCas9 cut site (3bp upstream of the PAM) and the data shown is next generation sequencing (NGS) analysis of sequences 30 bp upstream to 30 bp downstream of the PAM sequence. **(d)** Relative activity of *in vitro AAVS1* locus editing with split-Cas9 AAVs as compared to inducible split-Cas9 (iCas9) AAVs, media supplied with doxycycline. (n=3; dox: 200µg/ml; error bars are s.e.m.; Student's *t*-test; p=0.0106). **(e)** Relative activity of *in vivo ApoB* editing between split-Cas9 AAVs and inducible split-Cas9 (iCas9) AAVs. Mice were transduced with 5E+11 vg/split-Cas9/mouse. Mice transduced with iCas9 AAVs were administered saline with or without doxycycline. (n=3; dox: 200 mg; total of 12 IP injections; error bars are s.e.m.; Student's *t*-test; p=0.0248).

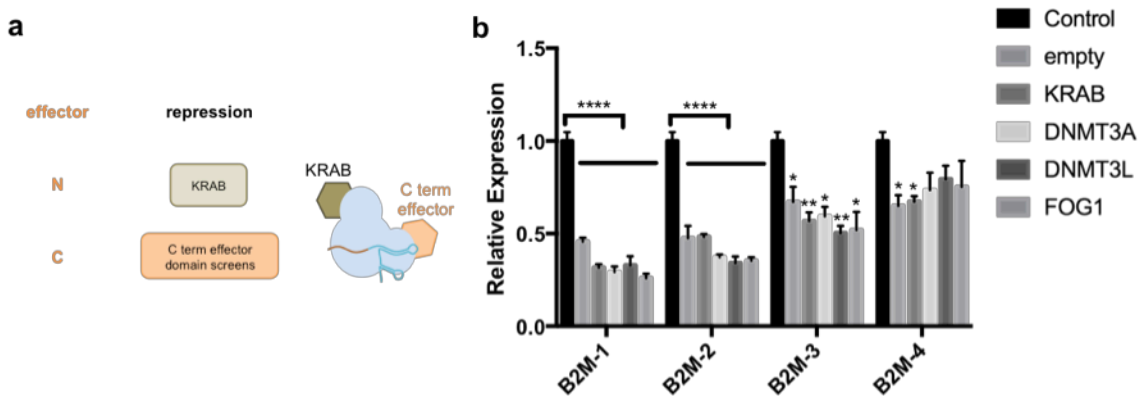

Figure S1.2: Domain optimization for AAV-CRISPR repression. (a) Additional repression domains were fused onto the C-terminal. **(b)** Four additional domains were separately fused onto the C-terminal (KRAB, DNMT3A, DNMT3L, or FOG1) and were delivered to HEK293T cells targeting the B2M locus using four different gRNAs. (n=3; error bars are s.e.m.; one-way ANOVA; ****p<0.0001).

Figure S1.3: Nrl genome editing and repression in Nrl-EGFP mice. (a) T7E1 assay of *Nrl* gRNAs in mouse embryonic fibroblasts (MEFs). MEFs were co-transfected with split-Cas9-Nrl vectors or non-targeting split-Cas9 vectors as a control. T7E1 assay was carried out using genomic DNA. The arrows indicate cleaved DNA produced by T7E1 enzyme that is specific to heteroduplex DNA caused by genome editing. The mutation frequency was calculated from the proportion of cut bands intensity to total bands intensity. A 25% editing rate was seen for split-Cas9-Nrl. **(b)** RT-qPCR analysis of rod and cone specific markers in wild-type mouse retina treated with AAV-split-Cas9-Nrl or AAV-split-dCas9-KRAB-Nrl vectors. RNA from each group were extracted form whole retina tissue. Results are shown as mean ± s.e.m. (*p<0.05. Student's *t*-test, n=3). **(c)** Immunofluorescence analysis of mCAR+ cells in Nrl-EGFP mouse retina treated with AAV-split-Cas9-Nrl or AAV-split-KRAB-dCas9-Nrl. Mice were treated at P7 and harvested at P30. GFP, green; mCAR, Red; DAPI, blue. **(d)** Quantification of mCAR+ cells in Nrl-EGFP mouse retina treated with AAV-split-Cas9-Nrl or AAV-split-KRAB-dCas9-Nrl. Results are shown as mean ± s.e.m. (*p<0.05. Student's *t*-test, n=3). **(e)** Quantification of mCAR+ cells in wt mouse retina treated with AAV-split-Cas9-Nrl or AAV-split-KRAB-dCas9-Nrl. Results are shown as mean ± s.e.m. (*p<0.05. Student's t-test). **(f)** Quantification of M-Opsin+ cells in wt mouse retina treated with AAV-split-Cas9-Nrl or AAV-split-KRAB-dCas9-Nrl. Results are shown as mean ± s.e.m. (*p<0.05. Student's *t*-test)

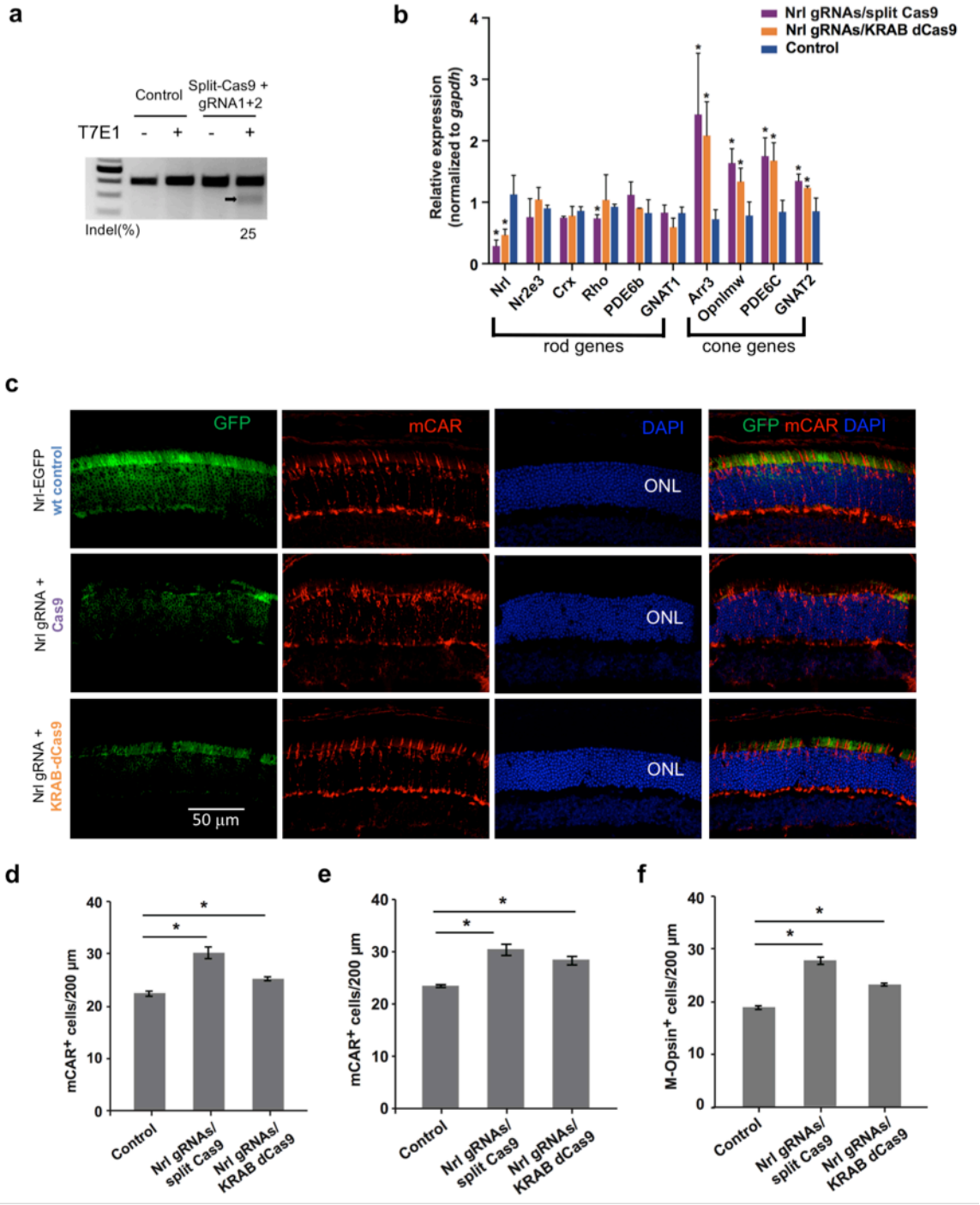
a
Control
Split-Cas9 + gRNA1+2
T7E1
- + - +
Indel(%)
25
b
Nrl gRNAs/split Cas9
Nrl gRNAs/KRAB dCas9
Control
Relative expression (normalized to gapdh)
Nrl
Nr2e3
Crx
Rho
PDE6b
GNAT1
Arr3
Opnlmw
PDE6C
GNAT2
rod genes
cone genes
c
GFP
mCAR
DAPI
GFP mCAR DAPI
Nrl-EGFP wt control
Nrl gRNA + Cas9
Nrl gRNA + KRAB-dCas9
ONL
50 µm
d
mCAR+ cells/200 µm
Control
Nrl gRNAs/ split Cas9
Nrl gRNAs/ KRAB dCas9
e
mCAR+ cells/200 µm
f
M-Opsin+ cells/200 µm

Table S1.1: Chapter 2 Guide RNA spacer sequences.

Function	Organism	Gene	Sequence
Editing	*Homo sapiens*	AAVS1	GGGGCCACTAGGGACAGGAT
Editing	*Mus musculus*	ApoB	ACCCCACCATCCATCCGCCA
Editing	*Mus musculus*	Nrl-1	GTATGGTGTGGAGCCCAACG
Editing	*Mus musculus*	Nrl-2	GAGCCTTCTGAGGGCCGATC
Regulation	*Homo sapiens*	CXCR4-1	CGGGTGGTCGGTAGTGAGTC
Regulation	*Homo sapiens*	CXCR4-2	CAGACGCGAGGAAGGAGGGCGC
Regulation	*Homo sapiens*	RHOX1-1	GACGCGTGCTCTCCCTCATC
Regulation	*Homo sapiens*	RHOX1-2	GCTGTGGGTTGGGCCTGCTG
Regulation	*Homo sapiens*	B2M-1	AGGGTAGGAGAGACTCACGC
Regulation	*Homo sapiens*	B2M-2	CTCCCGCTCTGCACCCTCTG
Regulation	*Homo sapiens*	B2M-3	GCGGGCCACCAAGGAGAACT
Regulation	*Homo sapiens*	B2M-4	TTTGGCCTACGGCGACGGGA
Regulation	*Homo sapiens*	ASCL1-1	CGGGAGAAAGGAACGGGAGG
Regulation	*Homo sapiens*	ASCL1-2	AAGAACTTGAAGCAAAGCGC
Regulation	*Mus musculus*	Cd81-1	GATAGTGACTCTCGCGCCTC
Regulation	*Mus musculus*	Cd81-2	CGTTGCGGAGAATGAGACGT
Regulation	*Mus musculus*	Afp-1	GGACAAAGACCACTTCAGAG
Regulation	*Mus musculus*	Afp-2	GCCAATAATTAACAGAGCAG
Regulation	*Mus musculus*	Nrl-1	TCCCTGTATTCAGAACAAGG
Regulation	*Mus musculus*	Nrl-2	AGTCACTGTCAGAACCAGAA

Table S1.2: List of oligonucleotide sequences: qPCR primers.

Organism	Gene	Forward	Reverse
H. sapiens	CXCR4	GAAGCTGTTGGCTGAAAAGG	CTCACTGACGTTGGCAAAGA
H. sapiens	RHOX1	GGAGATTTAGGAAGTATGGGGTTAGTG	AAAACCTCCTCTCTTACTTTTCTACTTC
H. sapiens	ASCL1	CGCGGCCAACAAGAAGATG	CGACGAGTAGGATGAGACCG
H. sapiens	B2M	TATGCCTGCCGTGTGAACCATGT	GGCATCTTCAAACCTCCATGATGCT
H. sapiens	GAPDH	ACAGTCAGCCGCATCTTCTT	ACGACCAAATCCGTTGACTC
H. sapiens	B-ACTIN	CATGTACGTTGCTATCCAGGC	CTCCTTAATGTCACGCACGAT
Mus musculus	ApoB	GCTCAACTCAGGTTACCGTGA	AGGGTGTACTGGCAAGTTTGG
Mus musculus	Afp	CTTCCCTCATCCTCCTGCTAC	ACAAACTGGGTAAAGGTGATGG
Mus musculus	Cd81	GCTCTTCGTCTTCAATTTCGTCT	TGTTGGGTGCCGGTTTGTT
Mus musculus	Gapdh	TGGCCTTCCGTGTTCCTAC	GAGTTGCTGTTGAAGTCGCA
Mus musculus	B-actin	GTGACGTTGACATCCGTAAAGA	GCCGGACTCATCGTACTCC
Mus musculus	Nrl	CCTTCTGAGGGCCGATCTG	GACATGCTGGGCTCCTGTC
Mus musculus	Nr2e3	ACCAGTCCCAGGTGATGCTA	CTCAAAGATGGGAGCAGGAG
Mus musculus	Crx	AAACTGAGCTGGGATGCTGT	TTGTGCCCCCTCAATCTAAC
Mus musculus	Rho	TCAGTCTGCATCCCTCCTCT	CCCAGTTTCCATCCATTTTG
Mus musculus	PDE6b	GCCGTGTTTCATGGCTTT	TCCAAAGTTACATTCGATCTTTTT
Mus musculus	GNAT1	CCCCTCAAATACCGTCCTTT	GCTGCTGTAGGTCCAAGAGG
Mus musculus	Opn1mw	TCTCTTTGGAAAGAAGGTTGATG	TGAGAAGGGAGGTAAAACATGG
Mus musculus	Opn1sw	CAGAATGGCCTCACCTCATT	AGGAGCAGCAGGTGTAAGGA
Mus musculus	PDE6c	ATCCAAAAGAGCCTCCTTGA	TTTCCAGGTCAGCAATGGAT

Table S1.2: List of oligonucleotide sequences: qPCR primers (continued).

Mus musculus	GNAT2	AAACCACCCCAAAGCCTAAC	GAAATAAGCAGGCTCGCATC

Table S1.3: List of oligonucleotide sequences: NGS primers

Function	Organism	Gene	Primers	Sequences
Editing	*Homo sapiens*	AAVS1	Forward	ACACTCTTTCCCTACACGACGCTCTTCCGATCT CGGTTAATGTGGCTCTGGTTCTGG
			Reverse	GACTGGAGTTCAGACGTGTGCTCTTCCGATCTGGGGTTAGACCCAATATCAGGAGACTAG
Editing	*Mus musculus*	ApoB	Forward	ACACTCTTTCCCTACACGACGCTCTTCCGATCT TGTAGAGCAAGCAGCAGGGGC
			Reverse	GACTGGAGTTCAGACGTGTGCTCTTCCGATCT GGTGTCCAAGAACAGTAGCAGGAAC

S1.2 Supplementary Notes: Description of effectors.

I. Split-dCas9 modules

Cintein+dCCas9 (H480A)

MIKIATRKYLGKQNVYDIGVERDHNFALKNGFIASCFDSVEISGVEDRFN
ASLGTYHDLLKIIKDKDFLDNEENEDILEDIVLTLTLFEDREMIEERLKT
YAHLFDDKVMKQLKRRRYTGWGRLSRKLINGIRDKQSGKTILDFLKSDGF
ANRNFMQLIHDDSLTFKEDIQKAQVSGQGDSLHEHIANLAGSPAIKKGIL
QTVKVVDELVKVMGRHKPENIVIEMARENQTTQKGQKNSRERMKRIEEGI
KELGSQILKEHPVENTQLQNEKLYLYYLQNGRDMYVDQELDINRLSDYDV
DAIVPQSFLKDDSIDNKVLTRSDKNRGKSDNVPSEEVVKKMKNYWRQLLN
AKLITQRKFDNLTKAERGGLSELDKAGFIKRQLVETRQITKHVAQILDSR
MNTKYDENDKLIREVKVITLKSKLVSDFRKDFQFYKVREINNYHHAHDAY
LNAVVGTALIKKYPKLESEFVYGDYKVYDVRKMIAKSEQEIGKATAKYFF
YSNIMNFFKTEITLANGEIRKRPLIETNGETGEIVWDKGRDFATVRKVLS
MPQVNIVKKTEVQTGGFSKESILPKRNSDKLIARKKDWDPKKYGGFDSPT
VAYSVLVVAKVEKGKSKKLKSVKELLGITIMERSSFEKNPIDFLEAKGYK
EVKKDLIIKLPKYSLFELENGRKRMLASAGELQKGNELALPSKYVNFLYL
ASHYEKLKGSPEDNEQKQLFVEQHKHYLDEIIEQISEFSKRVILADANLD

KVLSAYNKHRDKPIREQAENIIHLFTLTNLGAPAAFKYFDTTIDRKRYTS
TKEVLDATLIHQSITGLYETRIDLSQLGGDAYPYDVPDYASLGSGSPKKK
RKVEDPKKKRKVD

dNCas9+N-intein (D10A)

MGPKKKRKVAAADYKDDDDKGIHGVPAADKKYSIGLAIGTNSVGWAVITD
EYKVPSKKFKVLGNTDRHSIKKNLIGALLFDSGETAEATRLKRTARRRYT
RRKNRICYLQEIFSNEMAKVDDSFFHRLEESFLVEEDKKHERHPIFGNIV
DEVAYHEKYPTIYHLRKKLVDSTDKADLRLIYLALAHMIKFRGHFLIEGD
LNPDNSDVDKLFIQLVQTYNQLFEENPINASGVDAKAILSARLSKSRRLE
NLIAQLPGEKKNGLFGNLIALSLGLTPNFKSNFDLAEDAKLQLSKDTYDD
DLDNLLAQIGDQYADLFLAAKNLSDAILLSDILRVNTEITKAPLSASMIK
RYDEHHQDLTLLKALVRQQLPEKYKEIFFDQSKNGYAGYIDGGASQEEFY
KFIKPILEKMDGTEELLVKLNREDLLRKQRTFDNGSIPHQIHLGELHAIL
RRQEDFYPFLKDNREKIEKILTFRIPYYVGPLARGNSRFAWMTRKSEETI
TPWNFEEVVDKGASAQSFIERMTNFDKNLPNEKVLPKHSLLYEYFTVYNE
LTKVKYVTEGMRKPAFLSGEQKKAIVDLLFKTNRKVTVKQLKEDYFKKIE
CLSYETEILTVEYGLLPIGKIVEKRIECTVYSVDNNGNIYTQPVAQWHDR
GEQEVFEYCLEDGSLIRATKDHKFMTVDGQMLPIDEIFERELDLMRVDNL
PN

II. Transcriptional regulation modules

VP64

EAGSGRADALDDFDLDMLGSDALDDFDLDMLGSDALDDFDLDMLGSDALD
DFDLDMLINSR

RTA

RDSREGMFLPKPEAGSAISDVFEGREVCQPKRIRPFHPPGSPWANRPLPA
SLAPTPTGPVHEPVGSLTPAPVPQPLDPAPAVTPEASHLLEDPDEETSQA
VKALREMADTVIPQKEEAAICGQMDLSHPPPRGHLDELTTTLESMTEDLN
LDSPLTPELNEILDTFLNDECLLHAMHISTGLSIFDTSLF

P65

SQYLPDTDDRHRIEEKRKRTYETFKSIMKKSPFSGPTDPRPPPRRIAVPS

RSSASVPKPAPQPYPFTSSLSTINYDEFPTMVFPSGQISQASALAPAPPQ

VLPQAPAPAPAPAMVSALAQAPAPVPVLAPGPPQAVAPPAPKPTQAGEGT

LSEALLQLQFDDEDLGALLGNSTDPAVFTDLASVDNSEFQQLLNQGIPVA

PHTTEPMLMEYPEAITRLVTGAQRPPDPAPAPLGAPGLPNGLLSGDEDFS

SIADMDFSALL

KRAB

DAKSLTAWSRTLVTFKDVFVDFTREEWKLLDTAQQIVYRNVMLENYKNLV

SLGYQLTKPDVILRLEKGEEP

DNMT3A

TYGLLRRREDWPSRLQMFFANNHDQEFDPPKVYPPVPAEKRKPIRVLSLF

DGIATGLLVLKDLGIQVDRYIASEVCEDSITVGMVRHQGKIMYVGDVRSV

TQKHIQEWGPFDLVIGGSPCNDLSIVNPARKGLYEGTGRLFFEFYRLLHD

ARPKEGDDRPFFWLFENVVAMGVSDKRDISRFLESNPVMIDAKEVSAAHR

ARYFWGNLPGMNRPLASTVNDKLELQECLEHGRIAKFSKVRTITTRSNSI

KQGKDQHFPVFMNEKEDILWCTEMERVFGFPVHYTDVSNMSRLARQRLLG

RSWSVPVIRHLFAPLKEYFACV

DNMT3L

MAAIPALDPEAEPSMDVILVGSSELSSSVSPGTGRDLIAYEVKANQRNIE

DICICCGSLQVHTQHPLFEGGICAPCKDKFLDALFLYDDDGYQSYCSICC

SGETLLICGNPDCTRCYCFECVDSLVGPGTSGKVHAMSNWVCYLCLPSSR

SGLLQRRRKWRSQLKAFYDRESENPLEMFETVPVWRRQPVRVLSLFEDIK

KELTSLGFLESGSDPGQLKHVVDVTDTVRKDVEEWGPFDLVYGATPPLGH

TCDRPPSWYLFQFHRLLQYARPKPGSPRPFFWMFVDNLVLNKEDLDVASR

FLEMEPVTIPDVHGGSLQNAVRVWSNIPAIRSRHWALVSEEELSLLAQNK

QSSKLAAKWPTKLVKNCFLPLREYFKYFSTELTSSL

FOG1

MSRRKQSNPRQIKRSLGDMEAREEVQLVGASHMEQKATAPEAPSP

Chapter S2: Supplement to Chapter 3

S2.1 Supplementary Figures

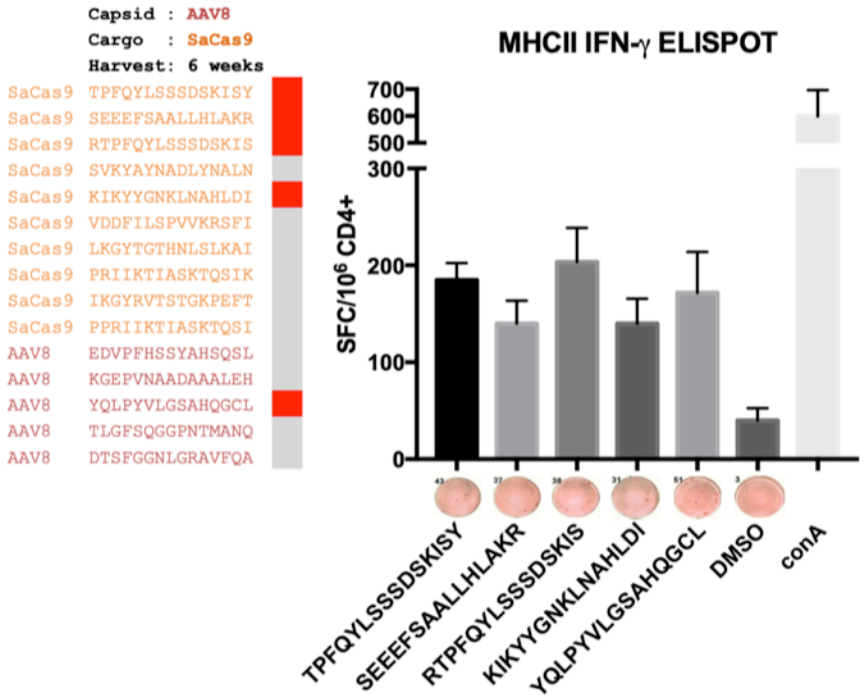

Figure S2.1: Experimental validation of a MHCII peptide predictions via IFN-γ ELISPOT. Mice were injected retro-orbitally with 1012 vg/mouse of AAV8-SaCas9 targeting the PCSK9 gene and were sacrificed after 6 weeks (n=6, error bars are s.e.m.). Purified CD4+ T cells from splenocytes were seeded at 2x105 cells per well in triplicate. 1x105 lipopolysaccharide-activated antigen presenting cells (APCs) from control mice were added to each well. Cells were incubated with highly immunogenic MHC-II predicted peptides for 20h. Spots were developed with biotinylated anti-IFN-γ. A one-way ANOVA with post hoc Dunnett's test was performed to determine statistical differences with DMSO for all peptides (left panel) (TPFQYLSSSDSKISY, p=0.004; SEEEFSAALLHLAKR, p=0.0339; RTPFQYLSSSDSKIS, p=0.0001; KIKYYGNKLNAHLDI, p=0.0339; YQLPYVLGSAHQGCL, p=0.0015). Data for the significant peptides are plotted (right panel).

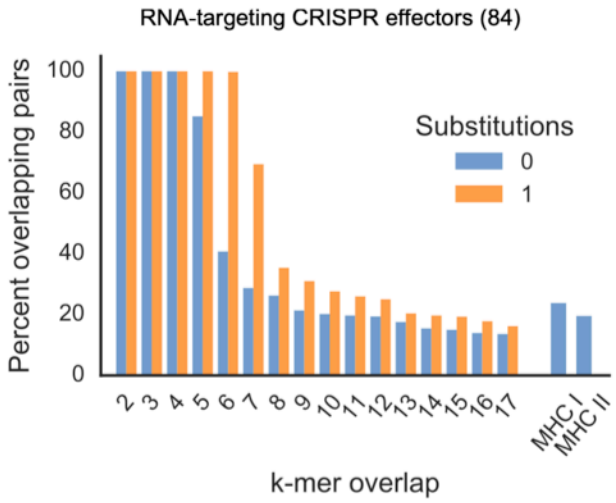

Figure S2.2: Immune orthogonality of RNA-targeting CRISPR effector proteins (Cas13). Immune orthogonality was analyzed using both k-mer comparisons with 0 or 1 substitutions and netMHC binding predictions similar to Figure 1G, but for RNA-targeting CRISPR effectors consisting of 89 Cas13a, b, and c orthologs. Both DNA- and RNA-targeting effectors have a large proportion of immune orthogonal pairs.

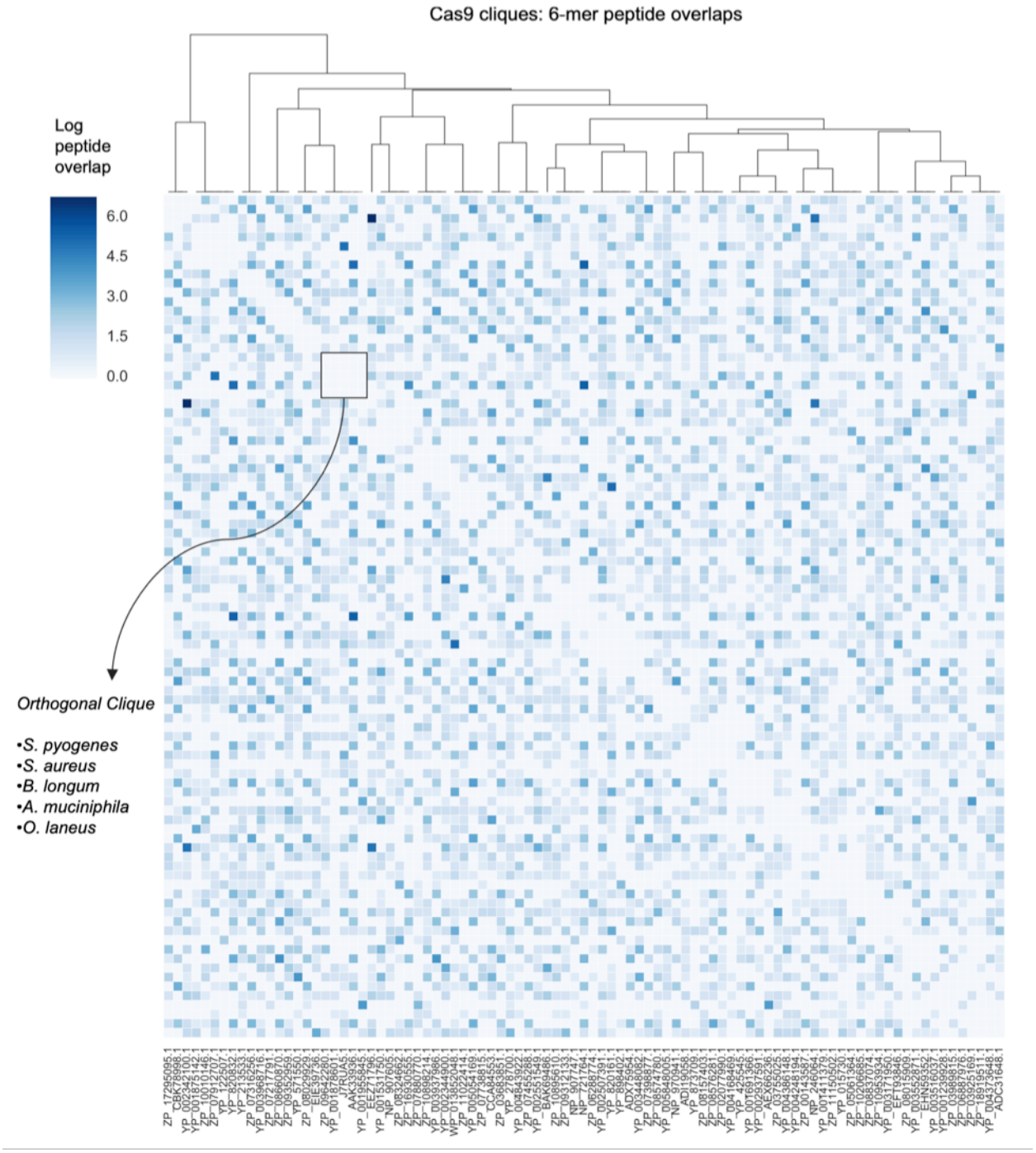

Figure S2.3: Cas9 immune orthogonal cliques. Cliques corresponding to 6-mer overlaps are depicted. An example of an orthogonal clique is highlighted, which includes Cas9s from: *S. pyogenes, S. aureus, B. longum, A. muciniphila,* and *O. laneus.*

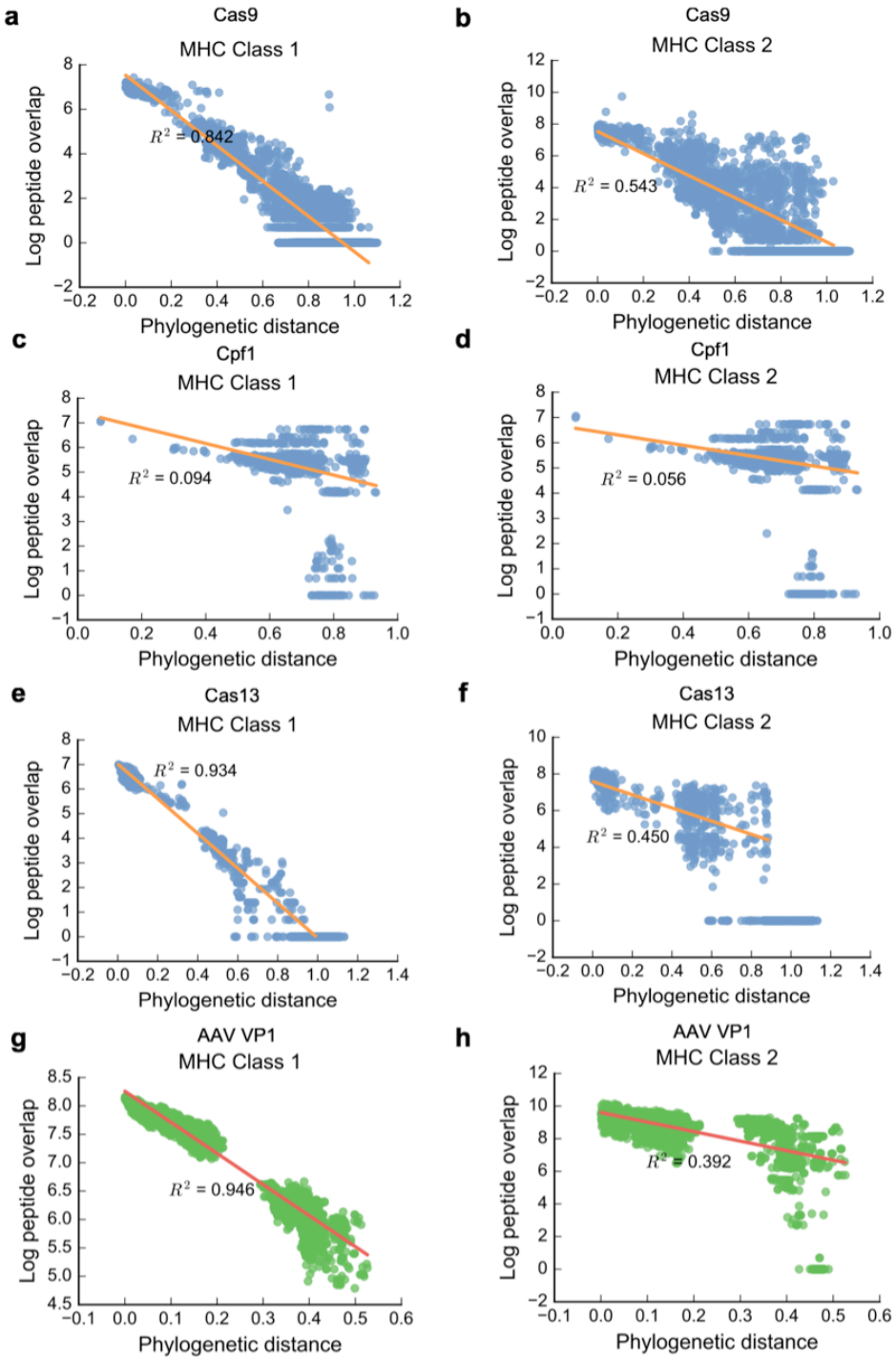

Figure S2.4: ***In silico*** **analyses and comparisons of immunogenicity of Cas9 and AAV orthologs.** Linear regressions exclude pairs of orthologs with no overlap. **(a)** Cas9 MHC class I peptide overlap vs. phylogenetic distance. **(b)** AAV MHC class I peptide overlap vs. phylogenetic distance. **(c)** Cas9 MHC class II peptide overlap vs. phylogenetic distance. **(d)** AAV MHC class II peptide overlap vs. phylogenetic distance.

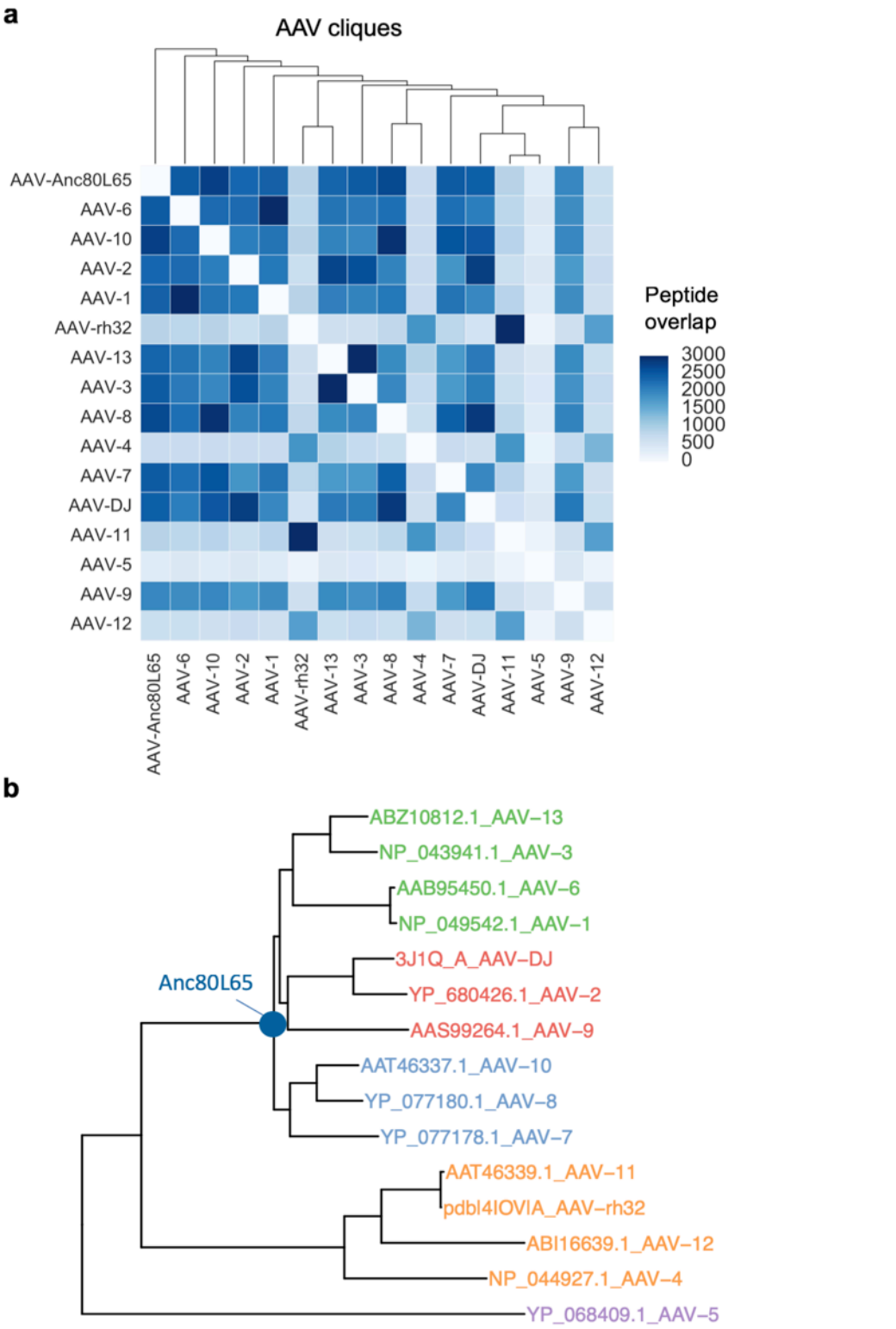

Figure S2.5: Major AAV serotype groups. (a) AAV immune orthogonal cliques over 81 HLA alleles. AAV5 is the most immune-divergent in comparison to the other serotypes. No orthogonal cliques exist. **(b)** AAV phylogeny showing major serotype groupings as well as the position of the reconstructed sequence Anc80L65.

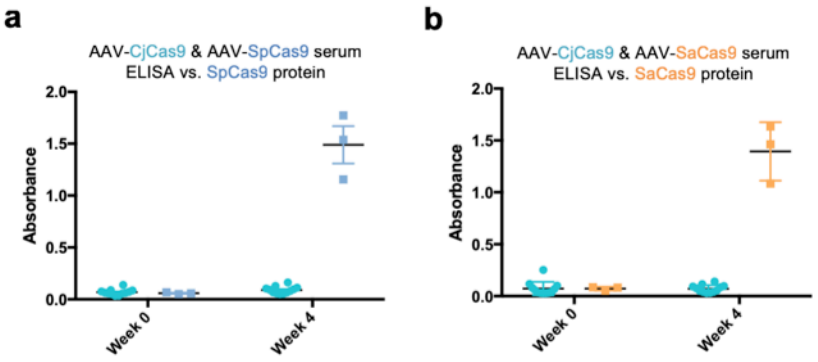

Figure S2.6: Confirming immune orthogonality of *C. jejuni* Cas9 to Sp- and SaCas9. Mice injected retro-orbitally with 10^{12} vg/mouse AAV8-CjCas9 targeting PCSK9 showed no significant response to Sp- or SaCas9.

Figure S2.7: Time course analysis of multiple dosing with immune orthogonal orthologs. (a) Mice were initially immunized (via retro-orbital injections of saline or AAV-CRISPRs at 1012 vg/mouse) with saline, AAV8-mCherry, AAV5-mCherry, AAV5-SaCas9, or AAV5-SpCas9 with no gRNA. At 4 weeks, the mice were given a second dose of saline or AAV8-SaCas9 with a gRNA targeting PCSK9. Serum was harvested prior to the first injection, and weekly thereafter. **(b)** Time course of serum samples taken each week. Shown are ELISAs for antibodies specific to SpCas9, SaCas9, AAV8, and AAV5. For all panels, results are shown as mean ± s.e.m. Each data point represents an individual mouse.

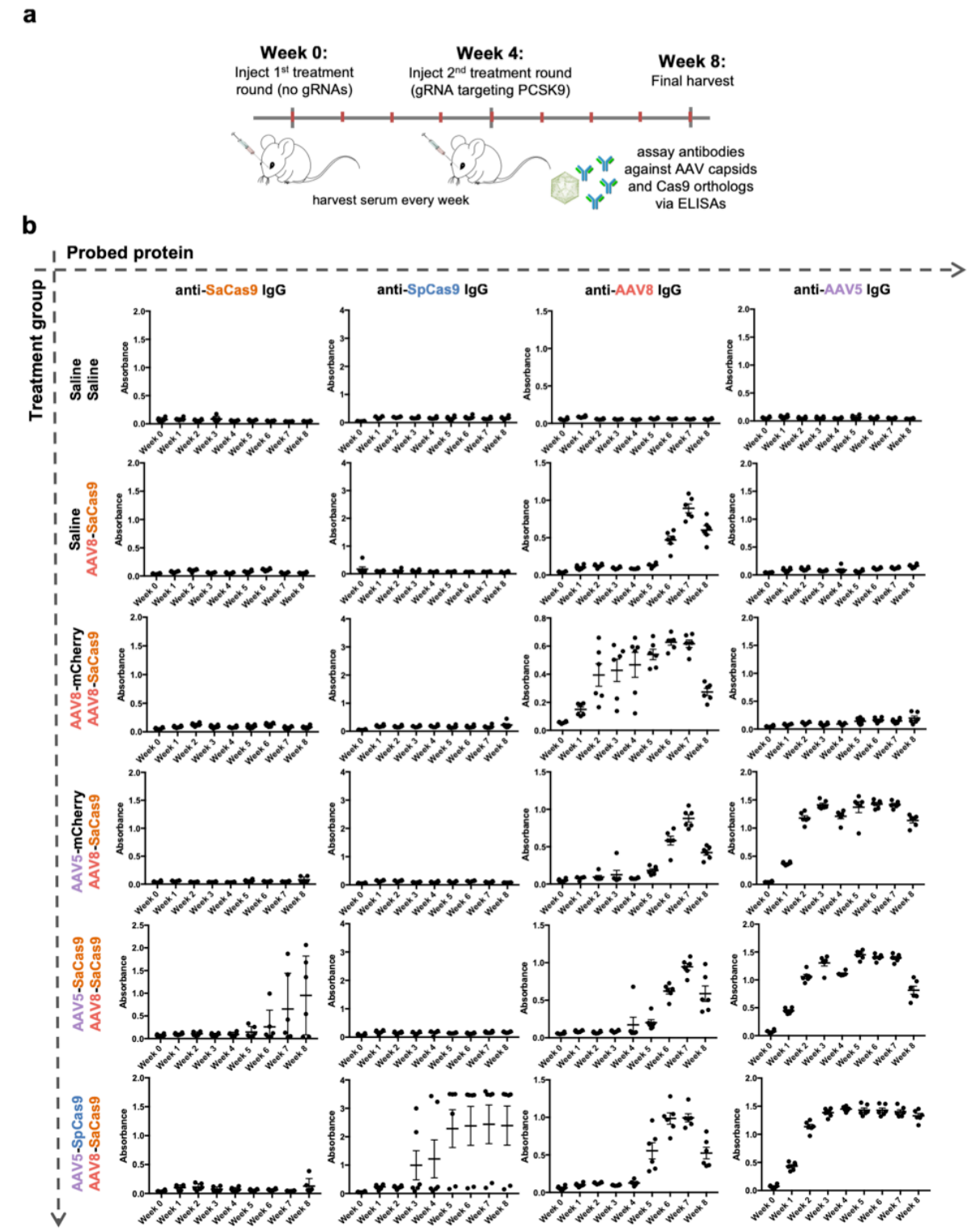
a
Week 0:
Inject 1st treatment round (no gRNAs)
Week 4:
Inject 2nd treatment round (gRNA targeting PCSK9)
Week 8:
Final harvest
harvest serum every week
assay antibodies against AAV capsids and Cas9 orthologs via ELISAs
b
Probed protein
Treatment group
anti-SaCas9 IgG
anti-SpCas9 IgG
anti-AAV8 IgG
anti-AAV5 IgG
Saline
Saline
Saline
AAV8-SaCas9
AAV8-mCherry
AAV8-SaCas9
AAV5-mCherry
AAV8-SaCas9
AAV5-SaCas9
AAV8-SaCas9
AAV5-SpCas9
AAV8-SaCas9
Absorbance
Week 0
Week 1
Week 2
Week 3
Week 4
Week 5
Week 6
Week 7
Week 8

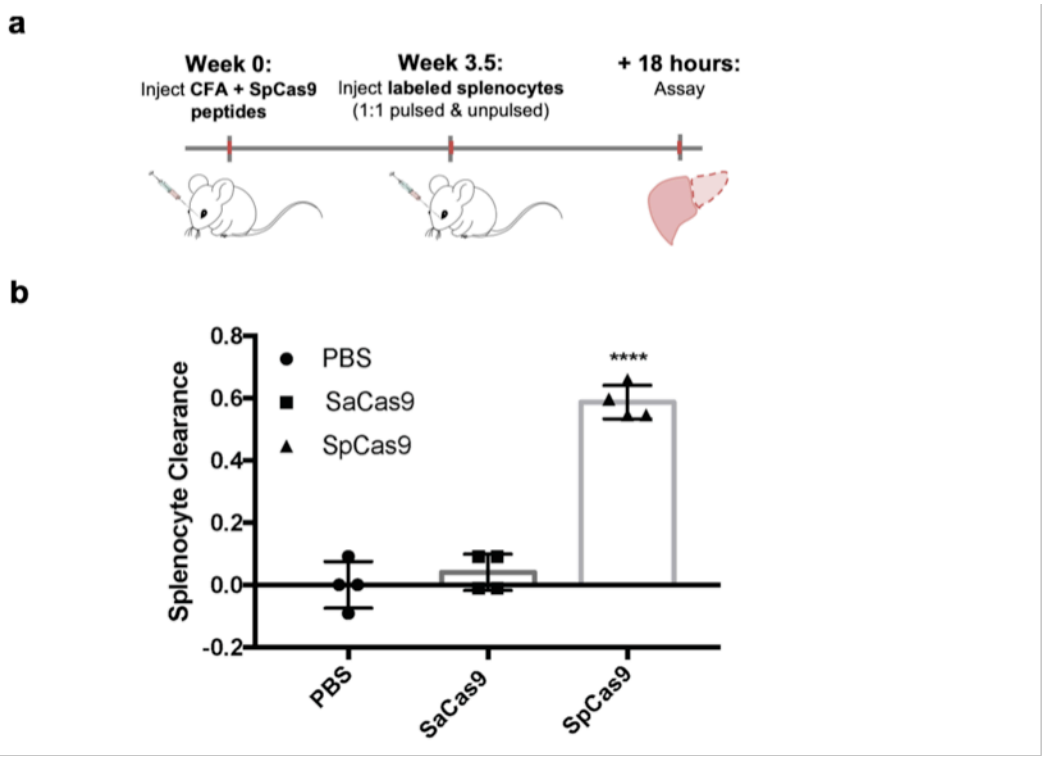

Figure S2.8: Cas9-specific splenocyte clearance *in vivo*. (a) Splenocytes were prepared by labeling with the fluorescent dye CTV or CFSE, and pulsing with either a pool of immunogenic Cas9 epitopes or DMSO. A 1:1 mixture of these cells were injected retro-orbitally at a total of 6 x 10^7 cells per mouse. After 18 hours, splenocytes from these mice were analyzed by flow cytometry to assay for specific clearance of Cas9 epitope pulsed cells. **(b)** At 3.5 weeks post-immunization, Cas9-pulsed splenocytes are specifically cleared at an average rate of ~39%.

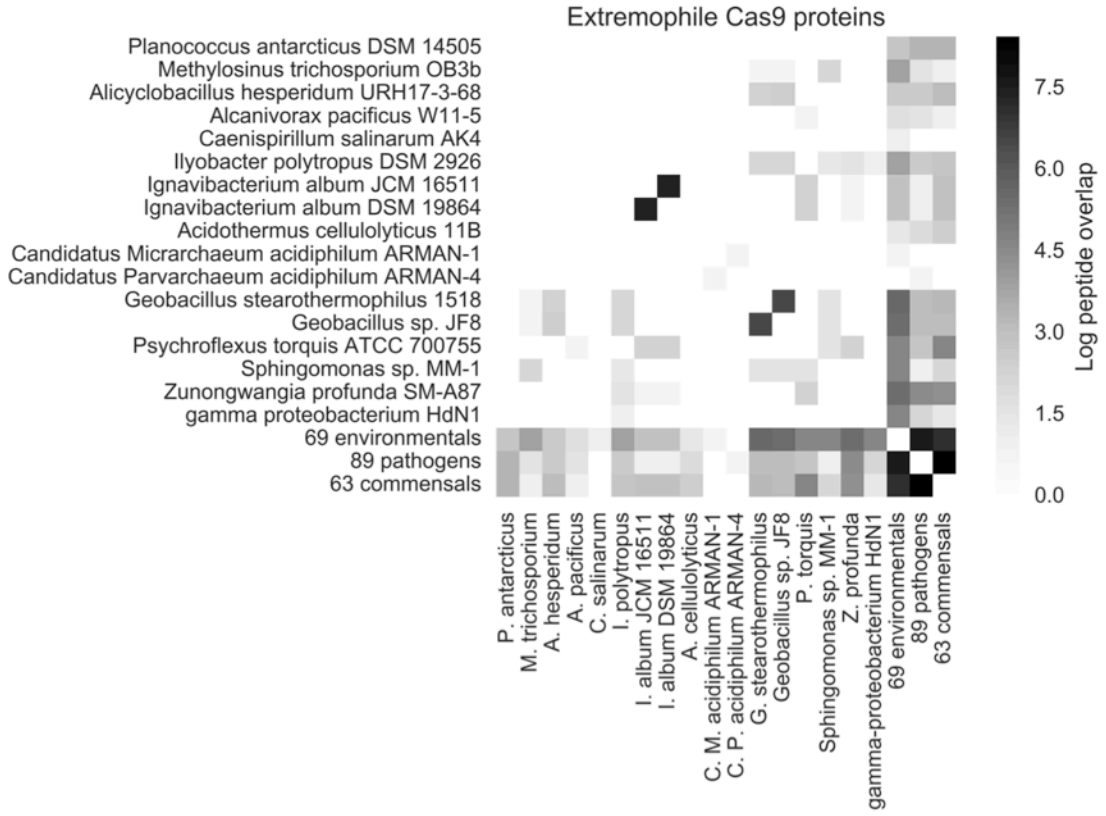

Figure S2.9: Exploring pre-existing CRISPR immunity. Cas9 orthologs were grouped into pathogens, commensals, environmentals, and extremophiles based on their species of origin (see species classification methods). Extremophile orthologs were assayed against pools of all 9-mer peptides originating from Cas9s from pathogenic, commensal, and environmental species. A few orthologs, including some highly divergent sequences from archaeal species, show near complete 9-mer orthogonality to large contingents of possible pre-existing Cas9 immunity.

Chapter S3: Supplement to Chapter 4

S3.1: Supplementary Figures

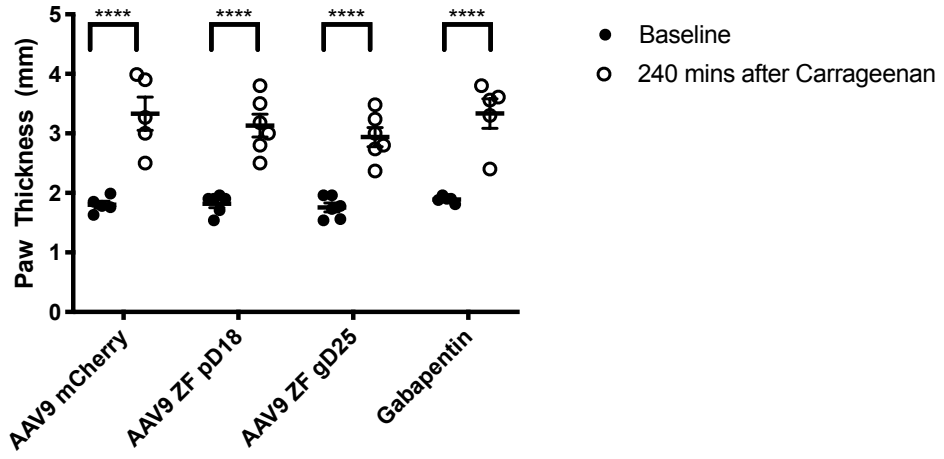

Figure S3.1: Paw Thickness (mm) in the ipsilateral hind paw of mice before and after Carrageenan administration.

S3.2: Supplementary Notes: Sequences and Designs

Table S3.1: Chapter 4 Guide RNA spacer sequences

gRNA	Sequence
SCN9A-1	GACAGTGGGCAGGATTGAAA
SCN9A-2	GGCAGGTGCACTCACCGGGT
SCN9A-3	GAGCTCAGGGAGCATCGAGG
SCN9A-4	GAGAGTCGCAATTGGAGCGC
SCN9A-5	GCCAGACCAGCCTGCACAGT
SCN9A-6	GAGCGCAGGCTAGGCCTGCA
SCN9A-7	GCTAGGAGTCCGGGATACCC
SCN9A-8	GAATCCGCAGGTGCACTCAC
SCN9A-9	GACCAGCCTGCACAGTGGGC
SCN9A-10	GCGACGCGGTTGGCAGCCGA

Table S3.2: Zinc-Finger Target Sequences

ZF Name	ZF Target Location	ZF Target Sequence
pD4	449a	ggGGCGAGGTGATGGAAGGGccttttta
pD18	657a	agGAGGGAGCTAGGGGTGGGgacccgag
gD9	r413a	tcAGTGCTAATGTTTCCGAGaagccact
gD25	r644a	gTAGACGGTGCAGGGCGGAgacctggc

Table S3.3: Chapter 4 qPCR primers

Gene	Forward	Reverse
SCN9A	TGGATTCCCTTCGTTCACAG	GTCGCAGATACATCCTCTTGTTT
GAPDH	TGGCCTTCCGTGTTCCTAC	GAGTTGCTGTTGAAGTCGCA

Zinc-Finger Designs

```
>pD4
mRSMHDYKDHDGDYKDHDIDY
KDDDDKMAPKKKRKVGIHGV
PAAMAERPFQCRICMRNFSR
SAHLSRHIRTHTGEKPFACD
ICGRKFAQSGNLARHTKIHT
GSQKPFQCRICMRNFSRSDA
MSQHIRTHTGEKPFACDICG
RKFARNASRTRHTKIHTGSQ
KPFQCRICMRNFSRSANLAR
HIRTHTGEKPFACDICGRKF
ADRSHLARHTKIHLRQKDAA
RGSRTLVTFKDVFVDFTREE
WKLLDTAQQIVYRNVMLENY
KNLVSLGYQLTKPDVILRLE
KGEEPWLVDYKDDDDKRS

>pD18
mRSMHDYKDHDGDYKDHDIDY
KDDDDKMAPKKKRKVGIHGV
PAAMAERPFQCRICMRNFSR
SANLARHIRTHTGEKPFACD
ICGRKFADSSDRKKHTKIHT
GSQKPFQCRICMRNFSTSGS
LSRHIRTHTGEKPFACDICG
RKFAHSLSLKNHTKIHTGSQ
KPFQCRICMRNFSQSSDLSR
```

HIRTHTGEKPFACDICGRKF
AWKWNLRAHTKIHLRQKDAA
RGSRTLVTFKDVFVDFTREE
WKLLDTAQQIVYRNVMLENY
KNLVSLGYQLTKPDVILRLE
KGEEPWLVDYKDDDDKRS

>gD9
mRSMHDYKDHDGDYKDHDIDY
KDDDDKMAPKKKRKVGIHGV
PAAMAERPFQCRICMRNFSR
SAHLSRHIRTHTGEKPFACD
ICGRKFATSGHLSRHTKIHT
GSQKPFQCRICMRNFSRSDH
LSQHIRTHTGEKPFACDICG
RKFAASSTRTKHTKIHTGSQ
KPFQCRICMRNFSQSSHLTR
HIRTHTGEKPFACDICGRKF
ARSDNLTRHTKIHLRQKDAA
RGSRTLVTFKDVFVDFTREE
WKLLDTAQQIVYRNVMLENY
KNLVSLGYQLTKPDVILRLE
KGEEPWLVDYKDDDDKRS

>gD25
mRSMHDYKDHDGDYKDHDIDY
KDDDDKMAPKKKRKVGIHGV
PAAMAERPFQCRICMRNFSD
RSHLTRHIRTHTGEKPFACD
ICGRKFADRSHLARHTKIHT
GSQKPFQCRICMRNFSRSDN
LSEHIRTHTGEKPFACDICG
RKFARSAALARHTKIHTGSQ
KPFQCRICMRNFSRSDTLSQ
HIRTHTGEKPFACDICGRKF
ATRDHRIKHTKIHLRQKDAA
RGSRTLVTFKDVFVDFTREE
WKLLDTAQQIVYRNVMLENY
KNLVSLGYQLTKPDVILRLE
KGEEPWLVDYKDDDDKRS

>pD4-T2A-pD18
mRSMHDYKDHDGDYKDHDIDY
KDDDDKMAPKKKRKVGIHGV
PAAMAERPFQCRICMRNFSR
SAHLSRHIRTHTGEKPFACD
ICGRKFAQSGNLARHTKIHT
GSQKPFQCRICMRNFSRSDA

MSQHIRTHTGEKPFACDICG
RKFARNASRTRHTKIHTGSQ
KPFQCRICMRNFSRSANLAR
HIRTHTGEKPFACDICGRKF
ADRSHLARHTKIHLRQKDAA
RGSRTLVTFKDVFVDFTREE
WKLLDTAQQIVYRNVMLENY
KNLVSLGYQLTKPDVILRLE
KGEEPWLVDYKDDDDKRS
GSGEGRGSLLTCGDVEENPGP
mRSMHDYKDHDGDYKDHDIDY
KDDDDKMAPKKKRKVGIHGV
PAAMAERPFQCRICMRNFSR
SANLARHIRTHTGEKPFACD
ICGRKFADSSDRKKHTKIHT
GSQKPFQCRICMRNFSTSGS
LSRHIRTHTGEKPFACDICG
RKFAHSLSLKNHTKIHTGSQ
KPFQCRICMRNFSQSSDLSR
HIRTHTGEKPFACDICGRKF
AWKWNLRAHTKIHLRQKDAA
RGSRTLVTFKDVFVDFTREE
WKLLDTAQQIVYRNVMLENY
KNLVSLGYQLTKPDVILRLE
KGEEPWLVDYKDDDDKRS

>gD9-T2A-gD25
mRSMHDYKDHDGDYKDHDIDY
KDDDDKMAPKKKRKVGIHGV
PAAMAERPFQCRICMRNFSR
SAHLSRHIRTHTGEKPFACD
ICGRKFATSGHLSRHTKIHT
GSQKPFQCRICMRNFSRSDH
LSQHIRTHTGEKPFACDICG
RKFAASSTRTKHTKIHTGSQ
KPFQCRICMRNFSQSSHLTR
HIRTHTGEKPFACDICGRKF
ARSDNLTRHTKIHLRQKDAA
RGSRTLVTFKDVFVDFTREE
WKLLDTAQQIVYRNVMLENY
KNLVSLGYQLTKPDVILRLE
KGEEPWLVDYKDDDDKRS
GSGEGRGSLLTCGDVEENPGP
mRSMHDYKDHDGDYKDHDIDY
KDDDDKMAPKKKRKVGIHGV
PAAMAERPFQCRICMRNFSD
RSHLTRHIRTHTGEKPFACD
ICGRKFADRSHLARHTKIHT

GSQKPFQCRICMRNFSRSDN
LSEHIRTHTGEKPFACDICG
RKFARSAALARHTKIHTGSQ
KPFQCRICMRNFSRSDTLSQ
HIRTHTGEKPFACDICGRKF
ATRDHRIKHTKIHLRQKDAA
RGSRTLVTFKDVFVDFTREE
WKLLDTAQQIVYRNVMLENY
KNLVSLGYQLTKPDVILRLE
KGEEPWLVDYKDDDDKRS